A thermo-responsive drug release system for combined chemohyperthermia

Dissertation

to obtain the academic degree
Doctor rerum naturalium (Dr. rer. nat.)

submitted to the
Department of Biology, Chemistry and Pharmacy
of Freie Universität Berlin

by

Fusheng Yan

from Zhejiang, China

March, 2015

The research work for this PhD dissertation was performed from January 2012 to October 2014 in the laboratory of Dr. Jens Peter Fürste, Institute of Chemistry and Biochemistry from Free University of Berlin, Thielallee 63, 14195 Berlin.

Die Forschungsarbeites im Labor für diese Dissertation wurden im Zeitraum von Januar 2012 bis Oktober 2014 unter der Leitung von Dr. Jens Peter Fürste am Institut für Chemie und Biochemie der Freie Universität Berlin, Thielallee 63, 14195 Berlin, durchgeführt.

1st supervisor: Dr. Jens Peter Fürste

2nd supervisor: Prof. Dr. Petra Knaus

Date of the defense: August 13, 2015

"Those who cannot be cured by medicine can be cured by surgery. Those who cannot be cured by surgery can be cured by fire. Those who cannot be cured by fire, they are indeed incurable".

—Hippocrates, pointing to hyperthermia (ca. 460–370 B.C.)

Table of Contents

Table of Contents

1 Introduction

In this chapter, I would like to introduce the concept and history of hyperthermia, as well as its cellular and molecular basis. By doing this, I wish to provide a better understanding of using hyperthermia as a potential treatment for human cancers. Since the aim of this work is to design a novel thermally controlled drug release system for local chemotherapy, basic features of magnetic nanoparticles and magnetic fluid hyperthermia are elaborated. Since I also attempted to isolate a new class of ribozymes from a large pool of random sequences, the relevant information about the *in vitro* selection technology is provided as well. In addition, a brief review on targeted and stimuli-responsive chemotherapy and a summary of the previous developments of thermo-responsive drug release systems are included to indicate the starting point of this work.

1.1 Hyperthermia

The term ‘hyperthermia’ derives from the combination of two Greek words: *hyper* (rise) and *therme* (heat), referring to the escalated temperature of body tissues to achieve a precise therapeutic effect. In oncology, it refers to the treatment of human cancer by administrating heat in various ways (Hildebrandt *et al*., 2002). It was reported that high temperatures can damage and kill cancer cells directly, or sensitize them to the concomitant radiotherapy or chemotherapy (Hildebrandt *et al*., 2002; Van der Zee, 2002).

Hyperthermia treatment can be classified into three different types depending on the applied temperatures. Diathermia is the first type, in which a temperature lower than 41°C is used for the therapy. The treatment of rheumatic diseases in physiotherapy, for example, belongs to diathermia. The second type is moderate

hyperthermia, in which a temperature range from 41°C to 46°C is applied during the treatment. It is the form of hyperthermia commonly used for cancer treatment, which has various effects at both cellular and tissue levels. The third type of hyperthermia treatment is defined as thermoablation, in which the temperature is higher than 46°C (up to 56°C). It can cause widespread necrosis, coagulation or carbonization depending on the applied temperature. Besides, hyperthermia can also be clinically categorized into local, regional and whole-body hyperthermia according to the exposed area of hyperthermia treatment.

Hyperthermia can be achieved by many different techniques, such as ultrasound, infrared radiation, microwave heating, magnetic fluid, infusion of warmed liquids or direct exposure of the body tissue in a hot chamber. Actually, the beneficial effects of using heat to treat diseases had been recognized since ancient times. Nowadays magnetic nanoparticles-based hyperthermia has become the most often used strategy due to its numerous advantages over other methods (Chapter 1.1.1). Moreover, many aspects of its biological effects on the cellular and molecular levels have been unveiled as well (Chapter 1.1.2).

1.1.1 A History of Hyperthermia

The use of heat to halt or treat various diseases including malignant cells was common in various cultures since ancient times. There is evidence shows that the earliest practice of heat treatment was conducted by an Egyptian named Imhotep (2655 – 2600 B.C.). In the *Edwin Smith Papyrus* from about 1700 B.C., which is probably a copy of a thousand year old text, it was recorded that the ancient Egyptians used the so-called “fire drills” (hot blades and sticks) for the treatment of breast cancer. The earliest use of cupping was described in the *Ebers Papyrus* by Egyptians, dating back to 1550 B.C. It is worth noting that various local and systemic hyperthermia treatments were also popular in ancient China and India.

Fever and heat therapy have been appreciated for their beneficial effects on health in ancient Greece and Rome, where many physicians believed that knowing how to control human body temperature will allow them to cure all diseases, including cancer. For example, the Greek physician and philosopher Parmenides (ca. 540 – 470 B.C.), a man who was deeply convinced of the effectiveness of hyperthermia, claimed: “Give me the power to produce fever and I will cure all diseases”.

This opinion was shared by Hippocrates (ca. 460 – 370 B.C.), a Greek physician and philosopher who is referred to as the ‘father of western medicine’. In his opinion, heat treatment was considered as a last resort after unsuccessful trials of surgery and when known drugs and other treatments failed.

Belief in the curative effect of fever was also illustrated in the first systematic treatise on medicine ‘De Medicina’, which was written by a Roman author named Celsus (ca. 25 B.C. – 45 A.D.), who recommended hot bath as a useful tool in the treatment of various diseases.

The first scientific paper on hyperthermia was published in 1866 by a German surgeon Carl D. W. Busch (1826 – 1881), who described regression of sarcoma in a patient who suffered prolonged high fevers due to infectious disease. Inspired by this fundamental discovery that elevated temperature can selectively kill cancerous cells while sparing healthy tissue, a similar attempt was conducted by the young American surgeon William B. Coley (1862 – 1936). In 1891 he developed the so-called Coley’s toxin, a type of bacterial pyrogen, to cause fever in patients on purpose. Because of this achievement, he was remembered as the father of modern use of hyperthermia against cancer. This beneficial treatment against inoperable cancer can improve the five year survival rate up to 64%. However, it had one basic drawback in that every patient responds to the toxin in a different manner. Hence, this method was abandoned over time.

Other attempts were made to achieve therapeutically beneficial hyperthermia. For example, the Swedish doctor Frans J. E. Westermark (1853 – 1941) in 1898 attempted to treat inoperable cancers of the uterine cervix by using high temperature water (42 – 44°C) circulating in a special metal coil. In 1909, the German physician Karl Franz Nagelschmidt (1875 – 1952) commenced practical diathermy to heat up deep tissue by high frequency currents.

The interest in hyperthermia for cancer treatment was distracted with the discovery of X-rays in 1895 and radium in 1898. Since then, the traditional surgical methods as well as radiotherapy and chemotherapy became the preferred methods in cancer treatment. After World War II, the interest in hyperthermia revived and focused on its biological mechanism. It was found that a long-lasting temperature raise to 42 – 50°C can lead to selective destruction of tumors without damaging the surrounding healthy tissues. This discovery inspired the investigations on the effectiveness of hyperthermia in combination with radiotherapy or chemotherapy, which established that the combined therapy was more effective than either therapy alone. Several years later, it was shown that long-lasting exposure (> 30 min) to temperatures higher than 40°C resulted in cell destruction (Dewey *et al*., 1977). Moreover, it was worth noting that 42.5°C seemed to be a critical point, where a slight increase in temperature of the order of tenths of a degree caused a significant increase in cell mortality. These results underscored the importance of accurate control of the temperature during hyperthermia treatment, as well as precise measurement of the real-time temperature within tumors.

A technological revolution in hyperthermia was commenced when the magnetic nanoparticles were developed and applied in medicine. In particular, iron oxide magnetic nanoparticles are currently in the spotlight and being actively investigated to achieve highly efficient cancerous cell destruction under the action of alternating magnetic fields (AMF). Because magnetic nanoparticles-based hyperthermia has a number of advantages compared to conventional hyperthermia, *e.g.*, magnetic

nanoparticles are capable of producing concentrated and homogeneous heat precisely at the site of malignant tissues; the temperature raise can be effectively stimulated and precisely adjusted by the external AMF. Furthermore, magnetic hyperthermia can be further functionalized with other therapeutic agents, *e.g.*, chemotherapy and gene therapy, and directed into local malignant tissues (Timko *et al*., 2010). Therefore, the modern hyperthermia is almost exclusively based on magnetic nanoparticles.

1.1.2 Cellular and Molecular Basis of Hyperthermia

Though hyperthermia had been proven to be therapeutically beneficial for cancer treatment in a number of preclinical and clinical studies, the cellular and molecular basis of hyperthermia remains unclear, and is still controversial. Many aspects of its biological effects, however, had been unveiled.

One of main reason why hyperthermia is beneficial for cancer patients is that the activation energies for protein denaturation and heat-induced cell death are in the temperature range of hyperthermia (Kampinga, 2006). It was reported that nuclear proteins are more sensitive to heat-induced denaturation than other intracellular proteins (Lepock *et al*., 1993 and 2004). In addition, the cell nucleus is the most favorable compartment for protein aggregation to occur (Michels *et al*., 1995 and 1997). More importantly, there are excellent correlations between nuclear protein aggregations and the heat killing effect (Kampinga *et al*., 1989).

It was shown that there is a close connection between hyperthermia and immune system. Hyperthermia seems to imitate fever, triggering the physiological defense mechanisms to strengthen immune activity. It was demonstrated that the number of natural killer (NK) cells started to increase at about 40°C (Shen *et al*., 1994). In animal models, a specific accumulation of adoptively transferred NK-cells at the

tumor site was observed and confirmed that this effect was specifically induced by a long-lasting moderate (fever-like) hyperthermia (Burd *et al*., 1998).

In addition, it is well documented that additional heat treatment can sensitize cancer cells to the concomitant radiotherapy, the so-called thermal radiosensitization. The heat-induced aggregation of nuclear proteins was recognized to play a central role in this process (Lepock, 2004; Kampinga, 2006). Hence, hyperthermia is considered to boost the therapeutic effect of radiotherapy by hindering the repair of radiation-induced, sub-lethal DNA damages (Hildebrandt *et al*., 2002).

The increased cell-killing potential of various cytotoxic agents at elevated temperatures was reviewed by Hildebrandt and Wust (2007). In other investigations, hyperthermia particularly at moderate temperatures was shown to induce various forms of drug resistance under certain conditions (Kampinga, 1995; Li *et al*., 1995). Currently available data concerning hyperthermia and drug resistance, however, indicate that the positive effect (reversal of drug resistance) overweighs the disadvantages (induction of drug resistance) in clinical practices (Hildebrandt *et al*., 2002). Nevertheless, it is recommended to investigate the exact synergic effect of chemotherapy and hyperthermia for each drug applied under different clinical conditions.

1.2 Magnetic Nanoparticles and Hyperthermia

Magnetic nanoparticles, particularly superparamagnetic iron oxide nanoparticles composed of maghemite (γ-Fe_2O_3) or magnetite (Fe_3O_4), are currently preferred for *in vivo* hyperthermia due to their low toxicity and high heating efficiency (Thiesen and Jordan, 2008; Wahajuddin, 2012). Therefore, basic features of magnetic nanoparticles and superparamagnetism are elaborated (Chapter 1.2.1). Magnetic hyperthermia has been widely investigated in different animal experiments (Chapter

1.2.2). Though many encouraging preclinical results were reported, magnetic fluid hyperthermia (MFH) has been confirmed as one of the most prominent procedure for heat-induced destruction of cancer cells by intratumoral instillation of superparamagnetic ferrofluid, supported by many successful clinical trials. A new treatment procedure commercially termed 'NanoTherm® Therapy' was established thereafter by MagForce Nanotechnology AG, Germany (Chapter 1.2.3).

1.2.1 Magnetic Nanoparticles and Superparamagnetism

Magnetic nanoparticles are a class of nanoparticles that commonly consist of magnetic elements such as iron, nickel or cobalt. Therefore, they can be readily manipulated by external magnetic fields. Magnetic nanoparticles can be prepared according to various methods including co-precipitation, thermal decomposition, metal reduction, micelle synthesis and hydrothermal synthesis (Lu *et al*., 2007; Laurent *et al*., 2008). Naked magnetic nanoparticles of small sizes, however, are prone to agglomerate and are thus chemically unstable over an extended period of time. Therefore, it is crucial to develop a protective shell to stabilize them. The protection can be achieved by coating nanoparticle surfaces with organic species, including surfactants or polymers, or coating them with an inorganic layer, such as silica or carbon. More importantly, these protective layers can be further modified with other functionalities for different purposes (Schärtl, 2010).

Typically, superparamagnetism occurs when magnetic particles have a size of 10 – 20 nm. Superparamagnetic nanoparticles can be magnetized up to saturation once they are exposed to an external magnetic field, and they no longer exhibit any residual magnetic interaction upon removal of the magnetic field. These features render superparamagnetic nanoparticles very attractive for various biomedical applications including *in vivo* imaging and drug delivery (Pankhurst *et al*., 2003; Wahajuddin, 2012).

1.2.2 Magnetic Hyperthermia

The first attempt of magnetic hyperthermia commenced in 1957 when magnetic particles of 20 – 100 nm in diameter were employed for inductive heating to destroy the carcinoma in dog's lymph nodes (Gilchrist *et al*., 1957). Inspired by this initial study, numerous animal experiments were carried out to investigate the performance of magnetic hyperthermia with a variety of schemes using different types of magnetic materials, as well as different field strengths and frequencies (Gordon *et al*., 1979; Rand *et al*., 1981; Moroz *et al*., 2001; Ohno *et al.*, 2002).

Though many encouraging preclinical results were reported so far, only one of them has been successfully established in clinical routine, which is the magnetic fluid hyperthermia developed by intratumoral instillation of superparamagnetic nanoparticles.

1.2.3 Magnetic Fluid Hyperthermia

Magnetic fluids are suspensions of superparamagnetic nanoparticles, which can be efficiently heated up under the action of an external alternating magnetic field (AMF) via vigorous rotations leading to the so-called magnetic fluid hyperthermia (MFH). The efficiency of energy transformation from AMF to heat is characterized in terms of specific absorption rate (SAR) that is further characterized by Brownian rotation and Néel relaxation processes. Brownian rotation refers to the physical rotation of the particles themselves within the fluid. It can be characterized by a relaxation time τ_B, which depends on the viscosity of the fluid. The Néel relaxation stands for the rotation of the atomic magnetic moments within each particle. The Néel process can be characterized by a relaxation time τ_N, which is determined by the magnetic anisotropy energy of the superparamagnetic nanoparticles relative to the thermal energy (Rosensweig, 2002; Pankhurst *et al*., 2003). The internal (Néel) and

external (Brownian) sources of friction that lead to a phase lag between applied magnetic field and the direction of the magnetic moments is responsible for heat generation. Generally, SAR values depend on the internal properties of magnetic nanoparticles such as structure (size, shape, composition and coating) and the external parameters such as amplitude (H) and frequency (f) of the applied AMF. The SAR can be determined as:

$$SAR = c(\Delta T/\Delta t)$$

, where c means the specific heat capacity of the sample and $\Delta T/\Delta t$ stands for the initial slope of temperature increase versus the heating duration (Schmid, 2010).

The first comprehensive study of the *in vivo* effect of MFH treatment of tumors was elaborated by Jordan *et al*. (1997). In this study, dextran-coated magnetite nanoparticle fluids with an average particle core size of about 3 nm were directly injected into the tumor tissue and exposed to the subsequent inductive heating by an AMF. The strength and frequency of AMF, tissue conductivity and body cross-section should be taken into account to exclude the harm to healthy tissues (Jordan *et al*., 1993). The AMF with 0.05 – 1.2 MHz frequency and 0 – 15 kA/m field strength was considered to be safe for human application (Schmid, 2010).

Moreover, a number of successful clinical trials of MFH had been conducted by MagForce Nanotechnologies AG (Germany), demonstrating its efficacy for prostate cancer and gliomas without discomfort or serious side effects. A new treatment procedure commercially termed ‘NanoTherm® Therapy’ was established thereafter.

NanoTherm® Therapy is a new clinical procedure for localized treatment of solid tumors. Its principle is to destroy tumor cells by heat generated from the oscillation of intratumoral superparamagnetic nanoparticles by an externally applied AMF. It consists of three components, superparamagnetic fluid, AMF and a cancer imaging

system (Fig. 1). Since the nanoparticles are localized inside the tumor, the heat can be generated in a concentrated and homogeneous manner. In another word, the heat can be selectively targeted to the tumor region while sparing surrounding healthy tissue.

Figure 1: Schematic for NanoTherm® Therapy. This therapy was established by MagForce Nanotechnologies AG (Germany). It consists of three components, NanoTherm®, NanoPlan® and NanoActivator®. NanoTherm® is a superparamagnetic fluid containing iron oxide nanoparticles with an average diameter of 15 nm. An aminosilane-type coating shell endows the particles with fine dispersion in water, forming a colloidal solution that can be introduced to patients via a syringe. After the introduction of nanoparticles into tumor tissue, hyperthermia can be achieved by placing the patient in an AMF applicator, the NanoActivator®. The NanoPlan® is the monitoring system. It can create a simulated heat distribution that is important to determine the optimal magnetic field strength for a desired therapeutic effect. This figure is adopted from Thiesen and Jordan (2008).

One particular advantage of this therapy is that the equipped CT scanner of the NanoPlan® monitoring system can measure density and distribution of implanted nanoparticles. A reliable computer simulation of heat distribution can be generated by the NanoPlan® software. Hence, the whole system enables an accurate control of the temperature to achieve a precise therapeutic effect, such as to destroy tumor cells irreparably or to sensitize them to a concomitant chemotherapy. Another advantage of this therapy is that it is a local and lasting thermotherapy for the reason that the nanoparticles can remain in the tumor site as a stable depot,

enabling repeated treatments after one injection.

The safety and feasibility of the NanoTherm® Therapy have been proven in a number of clinical trials of using magnetic fluid hyperthermia to treat glioblastoma multiforme (Maier-Hauff *et al*, 2007 and 2011; Thiesen and Jordan, 2008) and recurrent prostate cancer (Johannsen *et al*., 2005). Up to now, this novel therapy is available to patients at the NanoTherm® therapy Centers in Germany at the Charité-Universitätsmedizin Berlin, as well as at the University Hospitals in Münster and Kiel.

1.3 Targeted and Stimuli-Responsive Chemotherapy

The major drawback of the traditional chemotherapies is connected to deleterious side effects, since an effective dose of cytotoxic drugs against cancerous cells is usually achieved by intravenous administration and the following systemic distribution. To overcome this impediment, the cytotoxic drugs should be specifically delivered to and accumulated at the target site and thus spare the damage to healthy tissues (Chapter 1.3.1). Moreover, it would be more advantageous if the drugs are released in a stimuli-responsive manner, offering obvious merits of spatial and temporal control (Chapter 1.3.2).

1.3.1 Targeted Chemotherapy

The use of magnetic nanoparticles to achieve targeted *in vivo* drug delivery has come into the picture in the last two decades. Different strategies were applied depending on their unique physical properties and chemically prepared functionalities (Pankhurst *et al*., 2003; Dobson, 2006a; Arruebo *et al*., 2007; Veiseh *et al*., 2010).

Since magnetic nanoparticles can be easily manipulated by an external magnetic field, it would be feasible to administrate drugs via nanoparticle-drug conjugates leading to the concept of magnetically targeted drug delivery. The first report of this development dates back to the beginning of 1980s. Cytotoxic drugs coupled to magnetic microspheres were accumulated in sarcoma tumors in rat tails by an extracorporeal magnet (Widder *et al*., 1981). Encouraged by this initial research, success in magnetically targeted delivery of cytotoxic drugs and tumor remission were reported in different animal models, including swine (Goodwin *et al*., 1999 and 2001), rabbits (Alexiou *et al*., 2000) and rats (Pulfer and Gallo, 1998; Lübbe *et al*., 1999). Clinical trials of magnetically targeted chemotherapy in humans demonstrated the feasibility and safety of applying this method for cancer therapy (Lübbe *et al*., 1996; Lübbe and Bergemann, 1997). In addition, this strategy is compatible for targeted gene delivery (Dobson, 2006b).

The nanometric size of magnetic nanoparticles is a favorable property for drug delivery. On one hand, magnetic nanoparticles of sizes (10 – 100 nm) are small enough to avoid sequestration (100 – 200 nm) by the reticuloendothelial system (Ilium *et al*., 1982), as well as big enough to avoid rapid clearance by the kidneys or through extravasation (Vinogradov *et al*., 2002). Therefore, intravenous injection of magnetic nanoparticles within the sizes of 10 – 100 nm could result in prolonged blood circulation times, offering an effective distribution in targeted tissues (Laurent *et al*., 2008). On the other hand, solid tumors are usually characterized with leaky fenestrations of neovasculature and inefficient lymphatic drainage. This enables the extravasation of certain sized molecules, such as macromolecular drugs and nanoparticles, out of the vasculature leading to the selective accumulation of these molecules in tumor tissues (Lyer *et al.*, 2006; Veiseh *et al*., 2010; Fig. 2). This phenomenon is defined as the enhanced permeability and retention (EPR) effect (Matsumura and Maeda, 1986).

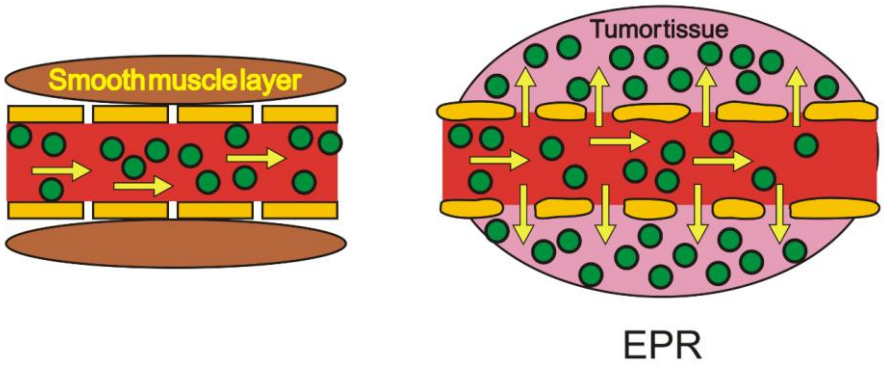

Figure 2: Schematic of the EPR effect. Left: normal blood vessels have regular endothelial cells and tight endothelial gap junctions, preventing the extravasation of macromolecular drugs (in green) through the vessel wall into normal tissues. Right: the vascular leakage will allow macromolecular drugs diffuse into the tumor tissue (in pink) and accumulate in it due to the irregular form of endothelial cells and the absence of a smooth-muscle layer (adopted from Lyer *et al.*, 2006).

To benefit from the EPR effect, the chemotherapeutic drugs coupled to magnetic nanoparticles could be substantially accumulated in tumor tissue, while their localization to healthy tissues is attenuated (Torchilin 2011; Maeda *et al*., 2013). However, there are two disadvantages of this passive targeting strategy. The first reason is that the EPR effect only exists in a certain number of specific metastatic solid tumors. In addition, its effective administration depends on other factors such as the degree of capillary disorder, the blood flow and the lymphatic drainage rate.

To overcome these disadvantages, scientists resorted to functionalized iron oxide nanoparticles equipped with additional targeting ligands to achieve active cell targeting (Zhang *et al*., 2002a; Sinha *et al*., 2006; Veiseh *et al*., 2010; Kievit and Zhang 2011). This targeting will greatly reduce the amount of cytotoxic drugs required for a desired therapeutic effect due the specific accumulation to the desired disease tissues, and thus overcome the adverse side effects of the conventional whole-body chemotherapy. Up to now, antibody (Bhattacharyyaa *et al*., 2010), cell-specific aptamer (Cheng *et al*., 2007; Nair *et al*., 2010) and other small ligands such as folate (Kukowska-Latallo *et al*., 2005) and chlorotoxin (Sun *et al*., 2008) have been conjugated to nanoparticles and verified their competence of delivering drugs to target cells.

1.3.2 Stimuli-Responsive Chemotherapy

A cell targeting nanoparticle can be further functionalized into a stimuli-responsive system that can release the loaded drugs in a controlled manner. Such system can be triggered by externally applied stimuli such as hyperthermia (Lu *et al*., 2005; Brazel, 2009), ultrasound (Liu and Huang, 2011), light (Ma *et al*., 2013) or intracellular stimuli such as reducing conditions (Saito *et al*., 2003) and low pH in the intracellular compartments (Kohler *et al*., 2005).

Generally, nanosystems in response to exogenous stimuli are more advantageous in terms of spatiotemporal control over drug release leading to the possibility of localized cargo release and minimized side effects (Blum *et al.*, 2014). Among the exogenous stimuli that have been used, the core–shell type iron oxide magnetic nanoparticle based thermo-responsive nanosystem holds great promise because magnetic fluid hyperthermia (MFH) alone proved to be clinically effective against solid tumors (Thiesen and Jordan, 2008). Furthermore, it was reported that the local hyperthermia can sensitize cancer cells to the concomitant chemotherapy (Hildebrandt *et al*., 2002), supported by many encouraging clinical results (Issels *et al.*, 2001; Wendtner *et al.*, 2001). Hence, it is conceivable that a thermally controlled drug release system combining magnetic nanoparticles (hyperthermia) and cytotoxic drugs (chemotherapy) may present a seriously improved therapeutic effect agaisnt cancer compared to either hyperthermia or chemotherapy alone.

1.4 Nucleic Acid Technologies

Many different nucleic acid technologies including *in vitro* selection (Chapter 1.4.1), catalytic DNA (Chapter 1.4.2) and mirror-image nucleic acids (Chapter 1.4.3) were used in the pursuit of a thermo-responsive drug release system for combined thermo-chemotherapy. A summary of the previous developments of thermally

controlled drug release systems using nucleic acids as thermosensitive molecules is provided as well (Chapter 1.4.4)

1.4.1 *In vitro* Selection of Functional Nucleic Acids

In vitro selection is a process of molecular artificial evolution using random RNA or DNA sequences as raw material for the development of rare functional molecules that possess desired capability of binding to a specific ligand or catalyze a certain reaction.

The concept of molecular evolution was proposed by Joyce (1989; Fig. 3), who indicated an iterative amplification, mutation and selection of RNA variants may lead to the development of novel ribozymes. Based on this proposal, the pioneering proof-of-concept experiments were commenced by the Szostak lab (Ellington and Szostak, 1990) and the Gold lab (Tuerk and Gold, 1990), who primarily and independently reported the identification of single-stranded RNA molecules with selective ligand binding properties from combinatorial nucleic acid libraries through a defined procedure termed systematic enrichment of ligands by exponential enrichment (SELEX). These ligand-binding nucleic acids are termed ‘aptamers’, from the Latin *aptus*, to fit (Ellington and Szostak, 1990).

A typical *in vitro* selection cycle involves 5 steps (Fig. 3): 1) construction of the starting pool; 2) incubation of molecules under defined conditions or with ligands of interest; 3) separation of desired species from the undesired ones with due criteria; 4) recovery and amplification of the selected individuals; 5) generation of a new pool of single-stranded variants for the next round of selection.

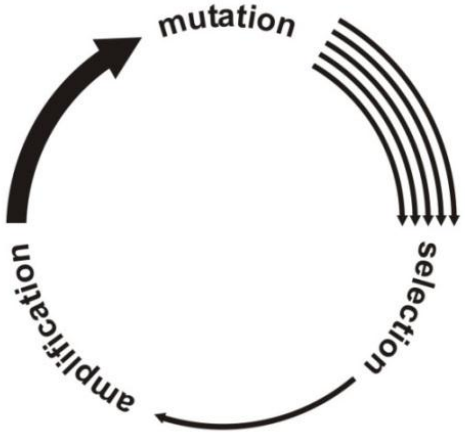

Figure 3: Schematic for directed *in vitro* molecular evolution. It is a process akin to evolution over multiple generations. Arrows represent individual RNA or DNA species. Arrow thickness corresponds to copy number (adopted from Joyce, 1989; kindly provided by Dr. Jens P. Fürste).

Hundreds of DNA or RNA aptamers have been developed against a wide spectrum of targets over the last two decades, including small molecules such as dyes, nucleotides, amino acids, metabolites or short peptides (Bock *et al*., 1992; Davis and Szostak, 2002; Geiger *et al*., 1996), proteins (Ayel and Escude, 2010; Blank *et al*., 2001), bacteria (Bruno and Kiel, 1999; Hamula *et al*., 2008), viruses (Tang *et al*., 2009), cells (Sefah *et al*., 2010) and even whole organisms (Homann and Göringer, 1999; Lorger *et al*., 2003). Inspired by the discovery of natural ribozymes in the early 1980s, many artificial ribozymes and deoxyribozymes have also been identified by *in vitro* selection or evolution, and some of them can catalyze chemical reactions that are non-existent in nature (reviewed by Breaker, 1997 and Silverman, 2008).

The applications of this technology covers basic research, analytical chemistry and medical development, including identification of binding sites between proteins and nucleic acids (He *et al*., 1996; Jolma *et al*., 2010; Liu and Stormo, 2005; Roulet *et al*., 2002), high-throughput aptamer-displacement assays for screening functional small molecules (Hafner *et al*., 2008), targeted drug delivery with cell-specific aptamers (McNamara *et al*., 2006; Shangguan *et al*., 2008; Zhou and Rossi, 2011), bi-specific aptamer-based immunotherapy (Pastor *et al*., 2011), RNA mimics of GFP for *in vivo* imaging (Paige *et al*., 2011) and various kinds of aptamer- or aptazyme-based

biosensors (McCauley *et al*., 2003; Song *et al*., 2008).

In addition, it is worth noting that this nucleic acid technology can be customized for the development of novel enzymes prescribed by the central dogma. For example, novel polymerases with the ability to transcribe and amplify non-natural xeno-nucleic acids (XNAs) were identified by means of *in vitro* evolution (Pinheiro *et al*., 2012). With the creativity of researchers, the scope of application is still ever expanding.

1.4.2 10-23 DNAzyme

Unlike ribozymes, catalytic DNAs have not been observed in nature and all existing DNAzymes were generated by *in vitro* selection from a random pool of DNA sequences. The most well-characterized DNAzyme is the 10-23 subtype capable of efficiently cleaving RNA substrates in a sequence-specific manner. It consists of a catalytic domain of 15 nucleotides (nt) flanked by two binding arms of 6 to 12 nucleotides in length via Watson-Crick hybridization, conferring specificity for the targeted RNA substrates. The 10-23 DNAzyme can cleave RNA substrates at a particular phosphodiester between an unpaired purine residue and a paired pyrimidine residue under near-physiological conditions (Santoro and Joyce, 1997; Fig. 4).

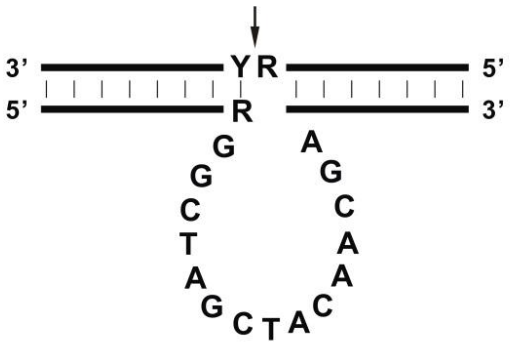

Figure 4: Catalytic motif of 10-23 DNAzyme. The 10-23 DNAzyme (bottom strand) binds the RNA substrate (top strand) through Watson–Crick pairing (adopted from Santoro and Joyce, 1997). Cleavage occurs at the site indicated by the arrow. R = A or G; Y = U or C.

A chemical reaction involving metal-assisted deprotonation of the 2'-hydroxyl group adjacent to the cleavage site was reported to be the most possible mechanism for the cleavage of RNA by 10-23 DNAzymes (Santoro and Joyce, 1998; Fig. 5). The divalent metal ions may participate in the cleavage process either as a metal hydroxide that functions as a general base to assist in deprotonation of the 2'-hydroxyl (Fig. 5a) or as a Lewis acid that coordinates directly to the 2'-hydroxyl and enhances its acidity (Fig. 5b).

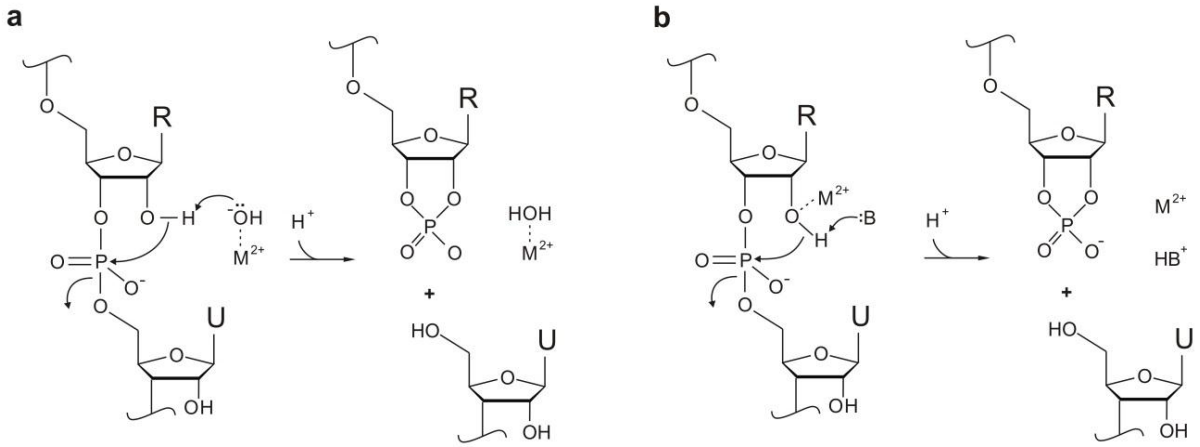

Figure 5: Two hypothetical chemical mechanisms for the catalysis of RNA cleavage by the 10-23 DNAzyme. (a) Mechanism involving a divalent metal hydroxide that functions as a general base. (b) Mechanism involving a divalent metal cation that functions as a Lewis acid (adopted from Santoro and Joyce, 1998).

Despite its small size, the k_{cat} of the 10-23 DNAzyme can reach 0.39 min^{-1} under near-physiological conditions in the presence of 2 mM Mg^{2+} and 150 mM monovalent cation at 37°C and pH 7.5 (Santoro and Joyce, 1998). Moreover, the catalytic efficiency for the 10-23 DNAzyme is reported to be more than an order of magnitude higher than that for the hammerhead ribozyme, measured under similar reaction conditions (Santoro and Joyce, 1998).

Furthermore, these DNAzymes have been utilized for wide applications such as suppressions of a number of viral and endogenous target genes in cell culture studies and *in vivo* involving the sequence-specific cleavage of RNA (Khachigian,

2002). For example, a broad spectrum of genes has been targeted by 10-23 DNAzymes with high specificity, including *EGR1*(Mitchell *et al*., 2004), *Tnf-α* (Iversen *et al*., 2001), *VEGFR2* (Zhang *et al*., 2002b), *c-JUN* (Khachigian *et al*., 2002), *PAI1* (Xiang *et al*., 2004), *Tgf-β1* (Isaka *et al*., 2004), *mPer1* (Liu *et al*., 2005) and *β-Catenin* (Choi *et al*., 2010). Thus, they represent a new class of sequence-specific molecular tools with gene therapeutic potential based on Watson-Crick base-pairing.

1.4.3 Mirror-Image Nucleic Acids

Mirror-image nucleic acids, containing L-ribose or 2'-deoxy-L-ribose, are the enantiomers of natural oligonucleotides (Fig. 6).

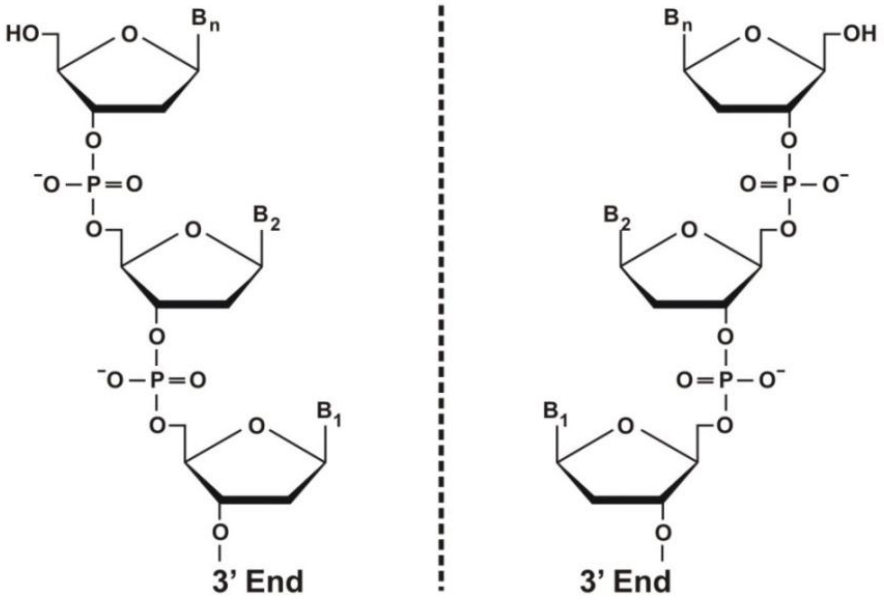

Figure 6: Structures of D-DNA and L-DNA.

These enantiomeric nucleic acids are proven to be substantially stable under simulated *in vivo* conditions due to the absence of nucleases capable of recognizing mirror-image nucleic acids in human serum (Klussmann *et al.*, 1996;

Nolte *et al.*, 1996). In addition, RNA aptamers were shown to possess reciprocal binding specificities of the corresponding D- and L-nucleic acids (Klussmann *et al.*, 1996; Nolte *et al.*, 1996). Moreover, Seelig *et al.* (2000) reported the catalysis of C – C bond forming reactions by an enantioselective ribozyme with identical efficiency. Hence, mirror-image nucleic acids are expected to retain identical properties, such as melting temperature and catalytic efficiency, as the normal D-form nucleic acids.

1.4.4 Thermally Controlled Drug Release Using Nucleic Acids

Generally, the methods used for thermally controlled drug release are either based on bond breaking or enhanced permeability (Kumar and Mohammad, 2011). Following this principle, researchers have used an assortment of nanomaterials for thermally controlled drug release, such as core-shell nanocapsules (Hu *et al.*, 2008 and 2012), porous nanoparticles with various gatekeepers (Guo *et al.*, 2014; Kim *et al.*, 2014; Yu *et al.*, 2014), thermosensitive liposomes (Al-Ahmady *et al.*, 2012; Dicheva *et al.*, 2014), polymeric nanocarriers (Fleige *et al.*, 2012; Yuanpei *et al.*, 2009) and assorted combinations (Hardiansyah *et al.*, 2014; Pradhan *et al.*, 2014).

Instead of going through the grind of developing new thermosensitive nanomaterials, a naturally occurring biological molecule, duplex DNA, can be used as the thermosensitive element for the purpose of thermally controlled drug release. DNA duplex as gatekeeper anchored at the opening of a porous nanoparticle was demonstrated to be feasible for a thermally controlled release of guest molecules (Schlossbauer *et al.*, 2010; Chen *et al.*, 2011; Ruiz-Hernández *et al.*, 2011). The Duplex DNA remains stable and traps the guest molecules inside the channel at 25°C. Increased temperatures, however, render the DNA duplex unstable and trigger its dissociation. The opening becomes uncapped and the trapped guest molecules escape from the channel (Fig. 7).

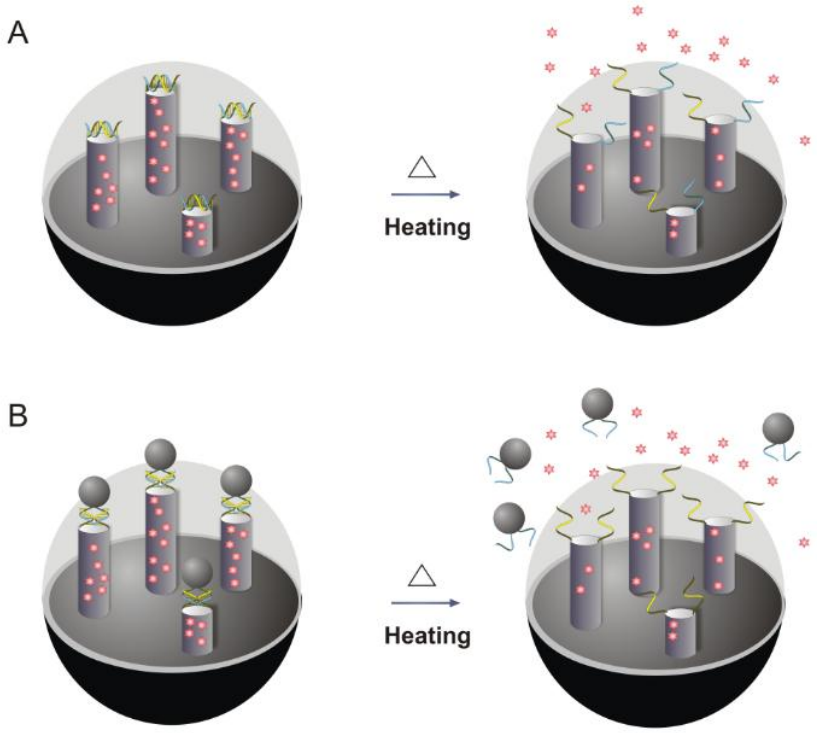

Figure 7: Two examples of a thermally controlled drug release nanosystem using duplex DNA as gatekeeper. (A) DNA duplexes are anchored at the openings of a mesoporous silica nanoparticle to trap the loaded drugs. The dissociation of the duplexes upon heating triggers the release (adopted from Chen *et al.*, 2011). (B) A DNA-nanoparticle conjugate is hybridized to the complementary DNA strands anchored at the openings of a porous nanoparticle to trap the guest molecules. The dissociation of the duplexes upon heating triggers the drug release (adopted from Ruiz-Hernández *et al.*, 2011).

In addition, a state-of-art concept for a thermally controlled release of drugs from magnetic nanoparticles was reported based on the combination of RNA/DNA hybrids and resultant cleavage of drug-carrying substrates by released hammerhead ribozymes (Gao, 2011). In this strategy, minimal hammerhead ribozymes were hybridized to complementary DNA strands that were covalently coupled to nanoparticles, forming the hybrid conjugates. RNA substrate strands, labeled with a fluorescent dye that is used as a substitute for the cytotoxic drug, were coupled to a different nanoparticle leading to substrate conjugates. These coupled hybrids were supposed to be stable at body temperature of 37°C. The increased temperature of 49°C, however, will render them unstable and trigger the dissociation of the annealed ribozymes. The detached ribozymes will then attack substrate conjugates leading to the release of coupled dye or drug. The limited dissociation events were catalytically

amplified by repetitive cleavages of the substrate strands (Gao, 2011).

Release experiments were performed by mixing the two conjugates and incubating them at either 37°C or 49°C, respectively. After 1 h incubation in a reaction buffer (50 mM Tris-HCl; 10 mM $MgCl_2$; pH7.5 at 25°C), the dye release at 49°C was demonstrated to be much higher (4.7%) than the release at 37°C (0.4%). Under a simulated *in vivo* condition of human serum, it was shown that dye release at increased temperature of 49°C is only about 3-fold higher than release at body temperature of 37°C. Thus, the results obtained with hammerhead ribozymes indicate that the concept of thermally controlled drug release requires profound improvement before moving forward to a clinical development.

2 Task

The aim of this work is to develop a thermally controlled nanoparticle-drug delivery system for improved clinical treatment of cancer. The approach depicts a thermally controlled release of cytotoxic drugs from nanoparticles, which can be heated up by an externally applied alternating magnetic field. The successful design could be translated into combined local chemo-hyperthermia that would overcome the severe side effects of traditional whole-body chemotherapy and enhance the killing effect of cytotoxic drugs against cancer cells at the same time.

While a hammerhead ribozyme approach was reported previously (Gao, 2011), its performance in a human serum, however, was not sufficient for clinical applications. Therefore, two new approaches are developed to improve thermosensitive controlled drug release.

In the first approach, a novel single-stranded thermo-responsive self-cleaving ribozyme (termed ‘thermozyme’ in this work) is used as a thermolabile linker between nanoparticle and drug. Since there is no report of a thermozyme yet, the main task of this approach is to develop such a ribozyme through *in vitro* evolution. The isolated thermozymes coupled to nanoparticles would cleave themselves upon heat and hence could trigger drug release in a thermally controlled manner.

In the second approach, DNAzymes and RNA substrate strands are anchored to separate nanoparticles. DNAzymes are immobilized to nanoparticles through hybridizing to complementary inhibitor strands that are covalently linked to nanoparticles, while substrate strands coupled with drugs are directly bound to nanoparticles. DNAzymes are designed to dissociate from DNAzyme/inhibitor duplexes in a thermally controlled manner, triggering the release of coupled drugs through repetitive catalytic RNA cleavages under increased temperatures.

3 Methods

3.1 Chemical Synthesis of Oligonucleotides

The chemical synthesis of oligonucleotides proceeds in 3’ to 5’ direction, the opposite of the biosynthesis of nucleic acids. The phosphoramidite method, pioneered by Marvin Caruthers in the early 1980s and facilitated by the invention of automatic solid-phase synthesizers, is now established as the method of choice to produce oligonucleotides (Caruthers, 2013). The synthesis is carried out by a stepwise addition of nucleotide residues to the 5'-terminus of the growing chain that is attached onto a controlled pore glass (CPG) support. The key steps of solid-phase phosphoramidite DNA synthesis cycle is outlined in Figure 8.

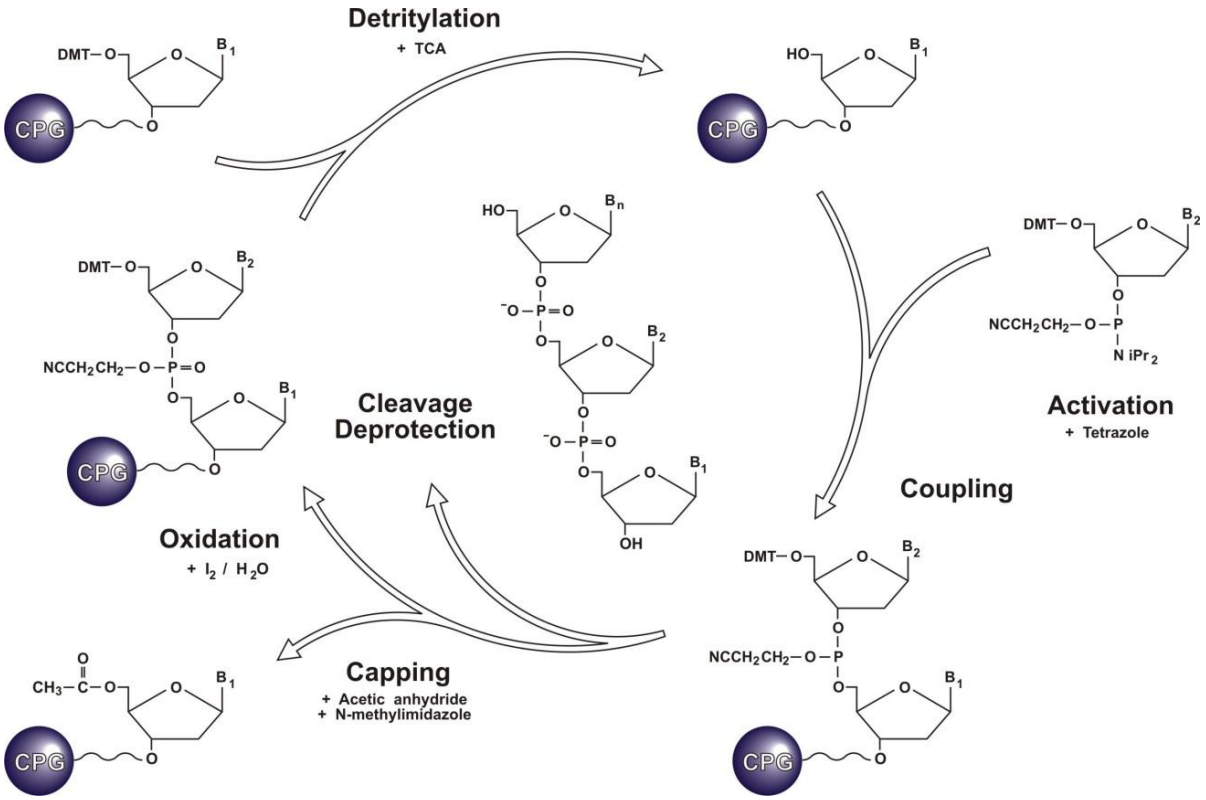

Figure 8: Solid-phase DNA phosphoramidite synthesis cycle. CPG means controlled pore glass, DMT stands for 4,4’-dimethoxytrityl, TCA denotes trichloroacetic acid and B refers to base (kindly provided by Dr. Jens P. Fürste).

The RNA synthesis cycle is basically identical except for the requirement of the

additional protection of 2'-hydroxyl group by a tert-Butyldimethylsilyl group. This spacious protection group imposes steric hindrance for the deprotected 5'-hydroxyl from one nucleotide to attack the activated phosphate atom from the other nucleotide. Hence, the coupling efficiency of RNA synthesis (98%) is lower than that of DNA synthesis (99.8%). In addition it requires an extended time for the coupling reaction to occur as compared to DNA synthesis.

The mirror-image oligonucleotides were also prepared by the phosphoramidite synthesis cycle using L-phosphoramidites as the building blocks. The 5'-terminal thiol group was incorporated through a thiol-modifier phosphoramidite. The 3'-terminal fluorescent reporter group was coupled to RNA via post-synthesis conjugation. All oligonucleotides used in this work were purchased from IBA GmbH (Göttingen, Germany).

3.2 Nucleic Acid Technology

3.2.1 Polymerase Chain Reaction (PCR)

Developed in 1983 by Kary Mullis (Bartlett and Stirling, 2003), the polymerase chain reaction (PCR) is now a common and often indispensable biochemical method used in medical and biological research labs. PCR is used to amplify a few copies of DNA to generate millions of copies of a particular DNA sequence with Taq DNA polymerases. Generally, 10 –100 ng template DNA was used per PCR reaction in this work. PCR reactions were carried out in a volume of 100 µl (Tab. 1). An initial denaturing step of 4 min at 95°C was used to ensure the complete denaturation of the template DNA. The number of PCR cycles was optimized for each selection round to ensure a specific amplification of target sequences, with a denaturing step for 30 s at 95°C, an elongation step for 30 s at 54 – 60°C depending on different

primer-pairs and an extension step for 30 s at 72°C. A final extension step was performed for 2 min at 72°C.

Table 1: Conditions for PCR.

stock	volume	final concentration
template DNA	0.5 – 1 µl	10 – 100 ng
PCR buffer, 10 x	10 µl	1 x
dNTPs, 10 mM each	2 µl	0.2 mM each
forward primer, 100 µM	2 µl	2 µM
reverse primer, 100 µM	2 µl	2 µM
Taq, 5 U/µl	0.5 µl	0.025 U/µl
H_2O	add to100 µl	

3.2.2 Mutagenic PCR

Mutagenic PCR is a variation of conventional PCR, where random mutations are introduced into any position of amplified DNA at an increased rate on purpose. In a mutagenic PCR, the fidelity of the Taq DNA polymerase is decreased through altering the composition of the reaction buffer. It was reported that the addition of Mn^{2+} and increased concentrations of Mg^{2+}, enzyme and the pyrimidine deoxynucleotides can lead to a raised mutation rate of about 0.66% in 10 doublings (done in 30 PCR cycles), with very little bias in the types of mutations generated (Cadwell and Joyce, 1992).

In this work, the following changes were made to enhance the mutation rate: 1) 7 mM $MgCl_2$ was used to stabilize non-complementary base pairs; 2) $MnCl_2$ with final concentration up to 0.5 mM was added to diminish the template specificity of the Taq DNA polymerases; 3) the concentration of dCTP and TTP was increased to 1 mM each to promote misincorporation; 4) A high concentration of Taq DNA polymerase (0.05 U/µl) was used to promote chain extension beyond mismatched positions.

The mutagenic PCR procedure was essentially performed as described by Bartel and Szostak (1993). Reactions were carried out in a volume of 30 µl (Tab. 2) in a 1 x Mut-PCR buffer [10 mM Tris-HCl, pH 8.3 at 25°C; 7 mM $MgCl_2$, 50 mM KC1 and 0.01% (w/v) gelatin] in the presence of 1 x Mut-dNTPs (0.2 mM dGTP, 0.2 mM dATP, 1 mM dCTP, and 1 mM TTP). An initial denaturing step for 4 min of 95°C was used to ensure the complete denaturation of the template DNA. Each PCR reaction was carried out for 6 – 7 cycles (2 doublings) to ensure a specific amplification of target sequence, with a denaturing step for 30 s at 95°C, an elongation step for 30 s at 60°C and an extension step for 30 s at 72°C. The mutagenic PCR was conducted without a 'hot start' procedure. After each PCR reaction, 3 µl of PCR product was brought up to 30 µl and subjected to another 6 – 7 cycles of amplification until 30, 60 and 90 doublings were reached, with respect to 2%, 4% and 6% mutation rates.

Table 2: Conditions for a mutagenic PCR reaction.

stock	volume	final concentration
template DNA	3 µl	~17 fmol
Mut-PCR buffer, 10 x	3 µl	1 x
Mut-dNTPs, 10 x	3 µl	1 x
forward primer, 10 µM	0.9 µl	0.3 µM
reverse primer, 10 µM	0.9 µl	0.3 µM
$MnCl_2$, 5 mM	3 µl	0.5 mM
Taq, 5 U/µl	0.3 µl	0.05 U/µl
H_2O	add to 30 µl	

3.2.3 Cleavage of DNA with Restriction Endonucleases

Restriction endonucleases are used to perform highly specific DNA-cleavage reactions within or near recognition sites. The recognition sites are usually 4 – 8 base pairs in length. The enzyme makes two incisions at each strand of a target DNA duplex, resulting in blunt ends or cohesive ends of 5'- or 3'-overhangs.

In this work, two restriction enzymes, BanI and StyI-HF, were used to process double-stranded DNAs. The cleavage reactions were performed according to the manufacturer's specifications (New England Biolab, USA).

3.2.4 DNA Ligation

T4 DNA ligase covalently attaches the 5'-phosphate to the 3'-hydroxyl in duplex DNA or RNA leading to the formation of a phosphodiester bond. In this work, T4 DNA ligase was used to ligate the cohesive DNA fragments cleaved by restriction enzymes. The reactions were performed according to the manufacturer's specifications (New England Biolab, USA).

3.2.5 T7 *In vitro* Transcription

T7 *in vitro* transcription is an efficient technique for high yield RNA synthesis from double-stranded DNA embedded with a T7 promoter sequence (5'-TAATACGACT-CACTATA-3') with T7 RNA polymerases. In this work, the radioactively labeled RNAs were prepared basically as described by Tang and Breaker (1997; Tab. 3).

Table 3: RNA synthesis by T7 *in vitro* transcription.

stock	volume	final concentration
5 x transcription buffer	4 µl	1 x
NTPs, 20 mM each	0.2 µl	0.2 mM each
DNA template	3 µl	0.1 µM
ribonuclease inhibitor, 40 U/µl	0.5 µl	1 U/µl
T7 RNA polymerase, 20 U/µl	2 µl	2 U/µl
[α-^{32}P]GTP, (10 µCi/µl)	3 µl	30 µCi
DEPC-H_2O	add to 20 µl	

The reaction was incubated for 2 h at 37°C. The DNA templates were degraded by an addition of 3 µl DNase I after incubation for another 30 min at 37°C. The

transcribed RNAs were recovered from 8% denaturing polyacrylamide gels by a crush-soaking procedure in 50 mM Tris-HCl (pH 7.5 at 25°C) and 1 mM EDTA. RNA molecules in the elution were then either concentrated by microcon centrifugal filter devices (Millipore, USA) or purified by ethanol precipitation.

3.2.6 Reverse Transcription

Reverse transcription is used for the synthesis of single-stranded complementary DNA (cDNA) from a single-stranded RNA template in the presence of reverse transcriptases and a short primer complementary to the 3' end of the RNA. The resultant cDNA can be used as a template for amplification by PCR. In this work, the reverse transcription was combined with PCR, allowing the amplification of the enriched thermo-responsive self-cleaving ribozyme motifs. SuperScript™ III reverse transcriptase with reduced RNase H activity (Life Technologies), which is thermostable up to 50°C, was chosen for this purpose. The reverse transcription was performed basically according to the instruction of the manufacturer (Tab. 4).

Table 4: cDNA synthesis by reverse transcription.

stock	volume	final concentration
RNA template	40 µl	
dNTPs, 20 mM each	0.8 µl	0.2 mM each
N60-Rev primer, 100 µM	1.6 µl	2 µM
DEPC-H_2O	18.8 µl	
First-Strand buffer, 5 x	16 µl	1 x
SuperScript™ III, 200 U/µl	0.8 µl	2 U/µl
RiboLock RNase Inhibitor, 40 U/µl	2 µl	1 U/µl

The mixture of RNA templates, dNTPs and primers was heated for 5 min at 95°C and then cooled on ice for 2 min leading to the annealing of primers onto RNA molecules. The reverse transcription was initiated by the addition of reverse transcriptases followed by incubating for 1 h at 50°C and 30 min at 55°C. The reaction was inactivated by heating for 15 min at 70°C.

3.3 Analysis of Nucleic Acids

3.3.1 Gel Electrophoresis

Gel electrophoresis was performed to the analysis and purification of nucleic acids. A gel made from agarose or polyacrylamide acts like a molecular sieve to separate oligonucleotides on the basis of their length under an applied current. The nucleic acids migrate from cathode to anode due to the negatively charged phosphate groups in their sugar-phosphate backbone.

3.3.1.1 Agarose Gel Electrophoresis

Agarose is a linear polysaccharide composed of neutrally charged, alternating isomers of the sugar galactose (D- and L-galactose). Agarose electrophoresis is widely used for separating and analyzing nucleic acids. The recommended agarose gel percentages for resolution of linear double-strand nucleic acids are indicated (Tab. 5).

Table 5: Separating range by agarose gels.

Agarose (%, w/v)	0.5	0.7	1.0	1.5	2.0	3.0
Seperating range (bp)	1000-30000	800-12000	500-10000	200-3000	50-2000	< 50

In this work, agarose gels were prepared by suspending dry agarose (Roth, Germany) in a 50 ml 1 x TAE buffer, boiling in a microwave oven until the solution becomes clear, cooling down and then pouring it into a casting plate and allowing it gelation for 15 min under room temperature. The DNA samples were mixed with 6 x Loading buffer (containing bromophenol blue and xylene cyanol) before loading into the gel pockets. The gels were then run in 1 x TAE buffer for 40 min under a

voltage of 100 V. The position of nucleic acids was visualized under UV light after soaking the gel in 1 µg/ml ethidium bromide solution for 10 min (Sambrook *et al.*, 1989).

3.3.1.2 Polyacrylamide Gel Electrophoresis (PAGE)

Polyacrylamide gels afford a precise separation of nucleic acids with high resolution due to their three-dimensional mesh structure. The formation of a polyacrylamide gel is commenced by the addition of ammonium persulfate (APS) that generates free radicals and *N*,*N*,*N*',*N*'-tetramethylethylene diamine (TEMED) that acts as a catalyst into the mixture of acrylamide/bis-acrylamide, which are nonreactive by themselves or when mixed together. Then the complicate three-dimensional mesh structure is formed by the polymerization of the acrylamide that is crosslinked by *N*,*N*'-methylene-bis-acrylamide.

3.3.1.2.1 Denaturing PAGE

Various concentrations of polyacrylamide gels can be prepared (Tab. 6). Denaturing PAGE employs 6 – 8 M urea to denature secondary structures of nucleic acids leading to the separation of oligonucleotides merely on the basis of molecular weight.

Table 6: Preparation of the denaturing polyacrylamide gels.

Acrylamide concentration	6%	8%	10%	12%	15%	20%
Acrylamide/Bisacrylamide (40%/2%) (ml)	3.75	5	6.25	7.5	9.38	12.5
5 xTBE (ml)	5	5	5	5	5	5
Urea (g)	10.5	10.5	10.5	10.5	10.5	10.5
10% (w/v) APS (µl)	300	300	300	300	300	300
TEMED (µl)	30	30	30	30	30	30
Add H_2O to (ml)	25	25	25	25	25	25

In this work, 8 – 20% polyacrylamide gels containing 7 M urea were prepared for the analysis of single-stranded oligonucleotides according to the instructions of the supplier (Carl Roth, Karlsruhe). The nucleic acid samples were mixed with an equal volume of 2 x Loading buffer containing 7 M urea and denatured for 2 min at 95°C before loading to the gel that was preheated for 40 min under 450 V. The loaded gels were then run at 400 – 500 V (18 – 30 mA) in 1 x TBE buffer.

3.3.1.2.2 Native PAGE

Native PAGE was carried out under non-denaturing conditions in the absence of urea or other denaturants. It separates nucleic acids with higher resolution and capacity compared to agarose gels. The protocol for the preparation of native polyacrylamide gels with different concentrations is outlined (Tab. 7).

Table 7: Protocol for native polyacrylamide gels.

Acrylamide concentration	6%	8%	10%	12%	15%	20%
acrylamide/bisacrylamide (40%/2%) (ml)	3.75	5	6.25	7.5	9.38	12.5
5 x TBE (ml)	5	5	5	5	5	5
10% APS (w/v) (µl)	300	300	300	300	300	300
TEMED (µl)	30	30	30	30	30	30
Add H_2O to (ml)	25	25	25	25	25	25

In this work, native PAGE was performed for the gel purification of restriction enzymes processed dsDNA. A low electric field strength (5 V/cm) was applied to avoid excessive heating of the gel to prevent loaded samples from denaturing. Alternatively, a higher voltage (10 V/cm) was applied to shorten the duration of electrophoresis in a 4°C cold room.

3.3.2 Detection of Nucleic Acids on a Gel

3.3.2.1 Ethidium Bromide Staining

Ethidium bromide (EtBr) is the most commonly used fluorescent stain for detecting DNA/RNA from electrophoretic gels under UV light. It can intercalate between the base pairs of the double helixes and the resultant complex leads to a 20-fold increased fluorescence compared to the equal amount of free EtBr in aqueous solution under UV light. The detection limit of EtBr staining is about 10 ng per band. In this work, the position of nucleic acids in the gels was visualized under an ultraviolet transilluminator at 302 nm (GelDoc 2000, Bio Rad) or a Typhoon FLA 7000 multi-purpose laser scanner (GE Healthcare, Sweden) after soaking the gels in 1 µg/ml EtBr solution for 10 min.

3.3.2.2 UV Shadowing

UV shadowing is used as a low sensitive method for detecting nucleic acids in gels, with a detection limit of about 0.3 µg per band. This method is based on the UV-absorbing ability of nucleic acids. It requires a shortwave UV light (254 nm) source and a fluor-coated thin layer chromatography (TLC) plate that can be excited by 254 nm UV light. The plastic-wrapped gels after electrophoresis are placed on the TLC plate and exposed to the UV light. The nucleic acid bands are visualized as dark shadows against a light background. In this work, this technology was used to recover the desired fragments of restriction enzymes processed dsDNA from native polyacrylamide gels.

3.3.2.3 Phosphor Imaging

Phosphor imaging is an accurate method to detect and quantify radioactively labeled nucleic acids in electrophoretic gels. It requires shorter exposure time in contrast with standard autoradiography. Moreover, it provides a more accurate way of quantification as well. In this work, plastic-wrapped gels were placed in a film cassette and covered with a phosphorimager plate. Different durations of exposure (30 – 60 min) were applied according to the radioactive strength presented in samples. The phosphorimager plate was then scanned by a Phosphor-imager Storm 840 (Molecular Dynamics, USA) or a Typhoon FLA 7000 multi-purpose laser scanner (GE Healthcare, Sweden) followed by image analysis using the supplemented quantification software.

3.3.3 Determination of Nucleic Acids Concentration

3.3.3.1 UV Spectrophotometry

UV spectrophotometry is the mostly used method to quantify the concentration of nucleic acids in solution. Direct measurements of nucleic acid samples at 260 nm can be converted to concentrations using the Beer-Lambert law that relates absorbance to concentration using the light pathlength and an extinction coefficient.

$$Beer\text{–}Lambert\ law \qquad A = \varepsilon c l$$

Where A = absorbance, ε = molar extinction coefficient, c = concentration (in the units corresponding to ε) and l = light pathlength. If a 1 cm quartz cuvette is used for the UV spectrum, the conversion of absorbance to concentration is as follow (Sambrook *et al.*, 1989):

dsDNA: 1 A_{260} = 50 ng/µl

ssDNA: 1 A_{260} = 33 ng/µl

RNA: 1 A_{260} = 40 ng/µl

The maximum UV absorption of proteins is at 280 nm due to their aromatic residues. The ratio of the absorbance at 260 nm over the absorbance at 280 nm (A_{260}/A_{280}) of a pure nucleic acids sample ranges from 1.65 to 1.85.

3.3.3.2 Fluorescent Labeling

Fluorescent labeling offers another way to determine the concentration of nucleic acids in solution. The labels can be incorporated into nucleic acids by solid-phase synthesis or by post-synthesis conjugation. In this work, Alexa Flour® 647 modified with an amine-reactive N-hydroxysuccinimidyl ester (NHS ester) group was conjugated to a 3'-terminus of amino modified RNA by post-synthesis conjugation. Standard calibration curves between relative fluorescence unit (RFU) and concentration of fluorescent RNA were plotted to determine the concentration of fluorescently labeled RNA. The commercially available RNA labeled with Alexa Flour® 647 (0.1 nmol/µl) was diluted either in reaction buffer (50 mM Tris-HCl, pH 7.5 at 23°C; 10 mM $MgCl_2$) or 90% human serum buffered by 1 x DPBS buffer (155.17 mM NaCl, 2.71 mM Na_2HPO_4, 1.54 mM KH_2PO_4, final pH 7.2 at 25°C) from 0 to 3 µM. The RFU of each dilution was measured by a NanoDrop 3300 Fluorospectrometer (excitation at 650 nm, emission at 670 nm) and the standard calibration curves were plotted. Moreover, fitting equations were generated by linear regression. The concentration can then be converted from the RFU value of a RNA sample by interpolation.

3.3.4 Purification of Nucleic Acids

3.3.4.1 Purification by Silica-Based Resin

StrataClean™ resin (Agilent Technologies, USA) is a phenol-free technique for the purification of nucleic acids. The solid phase silica-based resin has an abundant supply of hydroxyl groups that react with proteins in a similar manner like the hydroxyl group of phenol. A broad spectrum of proteins can be rapidly and efficiently removed from the nucleic acid samples by a simple incubation and centrifugation procedure. In this work, the resin was used to remove T4 polynucleotide kinases from the reaction of 5'-terminal radioactive labeling of RNA. For a 20 µl labeling reaction, 5 µl resin slurry was added to sequestrate the enzymes. The reaction was mixed thoroughly by vortexing for 15 s and then left to stand for 1 min under room temperature. The solid-phase resin bound with proteins was collected by a short centrifugation at 2,000 x g for 1 min. The supernatant was carefully transferred into a new tube. The resin treatment was repeated twice to ensure a sufficient removal of proteins according to the instruction of the supplier (Agilent Technologies, USA).

3.3.4.2 Purification by Silica-Based Spin Column

Silica-based spin column is a solid phase extraction method to quickly purify nucleic acids. This method relies on the fact that nucleic acid will bind to the solid phase of silica in the presence of chaotropic agents, such as guanidinium thiocyanate or guanidinium hydrochloride.

In this work, NucleoSpin® Gel and PCR Clean-up (Macherey-Nagel, Germany) was used for the purification of conventional and mutagenic PCR products, dsDNA

cleaved by restriction enzymes (BanI and StyI) and ligation reactions with T4 DNA ligase. The purification procedure was composed of binding, washing and elution according to the instruction of the manufacturer (Macherey-Nagel, Germany).

3.3.4.3 Microcon Centrifugal Filter Devices

Microcon centrifugal filter devices provide another simple and efficient way for concentrating and desalting nucleic acid solutions. Low-binding ultracel-YM regenerated cellulose membranes are available with different molecular weight cut-offs. Nucleic acids with length below the indicated cut-off will pass through the filter, while the larger ones are retained on the filter. In this work, Microcon YM-3 and YM-30 were used to purify and concentrate nucleic acid preparations according to the specification of the manufacturer (Millipore, USA).

3.3.4.4 Phenol-Chloroform Extraction

Phenol-chloroform extractions were performed to purify nucleic acids from a solution that contains proteins. The nucleic acid sample was extracted with an equal volume of a mixture of phenol:chloroform:isoamylalcohol (25:24:1) saturated with 10 mM Tris, pH 8.0 and 1 mM EDTA. An additional extraction step with chloroform can remove the phenol.

3.3.4.5 Ethanol Precipitation

Ethanol precipitation was performed to concentrate or desalt nucleic acids from aqueous solution. Ethanol precipitates nucleic acids in the presence of monovalent cations such as Na^+. Nucleic acid sample was first mixed with a 1/10 volume of 3 M

sodium acetate solution (pH 5.2). Then, 2.5 x volume of ice cold 100% ethanol was added into the sample. 10 ng of glycogen (Life Technologies, USA) was added to maximize the yield when there were only low copies of nucleic acids presented in the sample. The mixture was placed for 30 min at -20°C and was then centrifuged for 30 min at 16,000 x g in a microfuge (Biofuge Fresco, Heraeus) at 4°C. The pellet was rinsed with 1 ml 70% ethanol and centrifuged for 5 min at 16,000 x g (Biofuge Fresco, Heraeus). After removal of the supernatant, the pellet was dried for 1 min at 37°C and dissolved in nuclease-free water.

3.4 Nucleic Acids 5´-End Labeling

The 5'-hydroxyl group of nucleic acids can be phosphorylated by T4 polynucleotide kinase in the presence of ATP. The enzyme catalyzes the transfer and exchange of an organic phosphate from the gamma position of ATP to the 5'-hydroxyl group of polynucleotides. Thus, it can be used for labeling the 5'-ends of polynucleotides with radioactive phosphate from isotope-modified ATP.

This labeling reaction was performed according to the instruction of the manufacturer (NEB, England). In this work, the radioactive labeling of oligonucleotides was carried out as indicated (Tab. 8). The reaction mixture was incubated for 30 min at 37°C and inactivated by heating for 10 min at 80°C.

Table 8: 5'-end radioactive labeling of polynucleotides.

stock	volume	final concentration
polynucleotides, 100 µM	10 µl	50 µM
reaction buffer, 10 x	2 µl	1 x
[γ-^{32}P]ATP, 10 µCi/µl	1 µl	10 µCi
T4 polynucleotide kinase, 10 U/µl	1 µl	0.5 U/µl
H_2O	6 µl	

3.5 Coupling of Oligonucleotides to Nanoparticles with Sulfo-SMCC

Sulfosuccinimidyl-4-(N-maleimidomethyl)cyclohexane-1-carboxylate (sulfo-SMCC) is a well-established amine-to-sulfhydryl crosslinker that contains NHS-ester and maleimide reactive groups at opposite ends of a medium-length cyclohexane spacer arm (0.83 nm). In this work, it was used as the crosslinker for coupling 5'-thiol modified oligonucleotides to amino-modified nanoparticles (NP). The principle of this sulfo-SMCC-based amine-to-sulfhydryl cross-linking reaction is illustrated (Fig. 9).

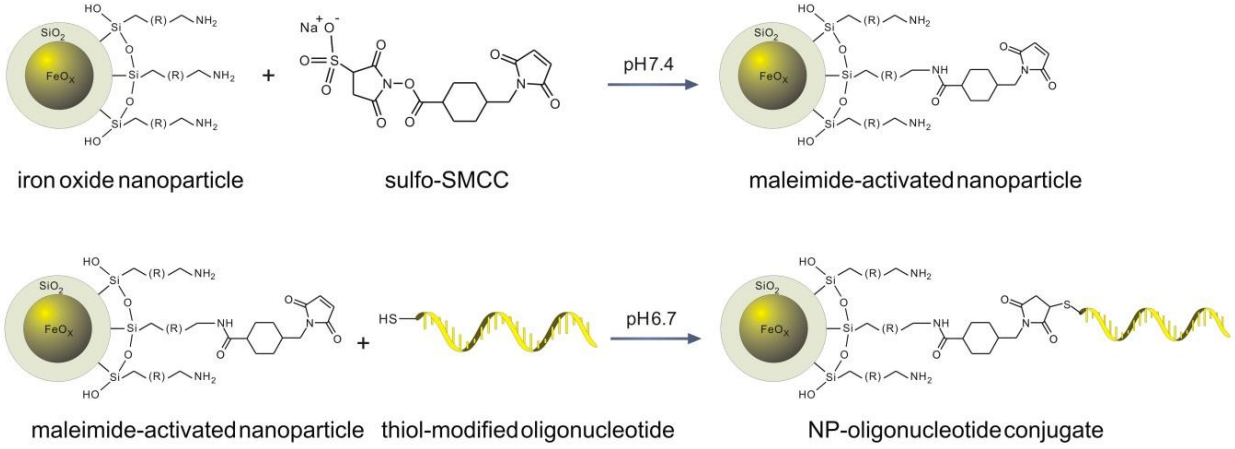

Figure 9: Coupling of oligonucleotides to nanoparticles with sulfo-SMCC. The sulfo-SMCC coupling is a two-step pH-dependent reaction. First, the aminosilane-coated nanoparticle is reacted with the amine reactive sulfo-NHS ester of sulfo-SMCC at pH 7.4, resulting in the maleimide-activated nanoparticle. Second, the maleimide group is reacted with thiol-modified oligonucleotide at pH 6.7 leading to the formation of a stable thioester linkage and the resultant NP-oligonucleotide conjugate.

The 15 nm aminosilane-coated superparamagnetic iron oxide nanoparticles (NanoTherm®) were synthesized by MagForce Nanotechnologies AG (Germany). It was reported that each nanoparticle carries about 550 amino groups on its surface confirmed by a previous nitrobenzaldehyde assay (Gao, 2011). The 5'-thiol modified oligonucleotides were purchased from IBA GmbH (Göttingen, Germany) and are listed in Table 9.

Table 9: The 5'-thiol modified oligonucleotides for coupling.

oligonucleotide	sequence in 5' to 3'	type
inhibitor1	SH-GGAGAGAGTCGTTGTAGCTAGCCTGG	D-DNA
inhibitor2	SH-GGAGAGAGTCGTTGTAGCTAGC	D-DNA
substrate	SH-GGAGAGAGGUGGGUGCG-Alexa 647	D-RNA
L-inhibitor2	SH-GGAGAGAGTCGTTGTAGCTAGC	L-DNA
L-substrate	SH-GGAGAGAGGUGGGUGCG-Alexa 647	L-RNA

The coupling reactions were essentially performed as described by Gao (2011). The thiol-modified oligonucleotides were efficiently reduced for 3 h under room temperature in the presence of 3 mM freshly prepared TCEP. The reduced fluorescent RNA substrate strands were directly reacted with the maleimide activated nanoparticles. The reduced inhibitor strands were hybridized with DNAzymes at different molar ratios in PBS (pH 6.7) before coupling to nanoparticles.

Nanoparticles were reacted with 6.7 mM sulfo-SMCC in PBS (pH 7.4) for 40 min at 20°C in a thermomixer with 1200 rpm shaking. The activated nanoparticles were collected by a magnet to remove the unreacted crosslinkers and resuspended in PBS (pH 6.7) to reach a final concentration of about 1 µM. The reduced oligonucleotides were reacted with activated nanoparticles at a molar ratio of 20:1 between oligonucleotide and nanoparticle in PBS (pH 6.7) for 1.5 h under room temperature. The resultant NP-oligonucleotide conjugates were collected by a magnet to remove the uncoupled oligonucleotides. The amount of uncoupled oligonucleotides was quantified either by a NanoDrop 3300 Fluorospectrometer or a UV Spectrophotometer.

An additional step of treatment with reduced L-Glutathione (GSH) was initially performed to block the unreacted maleimide groups after the coupling reactions. The NP-oligonucleotide conjugates obtained were further incubated for 1 h with 10 mM GSH that was buffered by PBS (pH 6.7). After removal of the supernatant and washing, the resultant NP-oligonucleotide conjugates were resuspended in

reaction buffer (50 mM Tris-HCl, pH 7.5 at 23°C; 10 mM $MgCl_2$) or 90% human serum buffered by 1 x DPBS buffer (155.17 mM NaCl, 2.71 mM Na_2HPO_4, 1.54 mM KH_2PO_4, final pH 7.2 at 25°C) to reach a final concentration of 1 µM.

3.6 Serum Stability Assay

The serum stability assay was performed to evaluate the stability of nucleic acids of the thermally controlled drug release system under a simulated *in vivo* condition. The assay was essentially performed as previously described (Klussmann *et al*., 1996). Human serum H4522 was purchased from Sigma (USA). The D-DNAzyme and L-DNAzyme were incubated at a concentration of 10 µM in a 90% human serum buffered by 1 x DPBS (155.17 mM NaCl, 2.71 mM Na_2HPO_4, 1.54 mM KH_2PO_4, final pH 7.2 at 25°C) in an incubator at 37°C with 95% humidity and 5% carbon dioxide. Aliquots were taken at different durations and mixed with an equal volume of stop solution (8 M Urea, 50 mM EDTA and 2% SDS, pH 7.2 at 25°C). The samples were further purified by phenol/chloroform extraction followed with DNA ethanol precipitation. The purified DNA samples (60 pmol each) were separated on a denaturing 20% polyacrylamide gel. The result was recorded by a Typhoon FLA 7000 multi-purpose laser scanner (GE Healthcare, Sweden) after staining the gel in 1 µg/ml ethidium bromide for 10 min.

3.7 Nucleic Acids Dependent Nanoparticle-Drug Release System

3.7.1 Thermozyme-based Nanoparticle-Drug Release System

This approach is dependent on the isolation of a thermo-responsive self-cleaving ribozyme (thermozyme) from a large pool of random RNA sequences using an iterative *in vitro* selection and amplification procedure.

The RNA population was created by generating a double-stranded (ds) DNA pool for *in vitro* transcription. The construction of the dsDNA pool with a large random region was achieved by joining two smaller random pools, essentially following the protocol described by Bartel and Szostak (1993). The library and the primers were purchased from IBA GmbH (Göttingen) and are listed in Table 10. The mixture of phosphoramidites used for the random positions in the oligonucleotides of N64 and N60 were under a molar ratio of dA:dG:dC:dT=3:2.5:2.5:2 to uniform the inhabitation of the four different phosphoramidites.

Table 10: Synthetic DNAs for the selection of thermozymes. The T7 promotor is italicized and the schemed cleavage region is underlined. The randomized positions are bolded.

oligonucleotides	sequences, 5' -> 3'
Sub	TTC*TAATACGACTCACTATA*GGAACATTTCTGTTGAGGTTGA CCAATGTAAACACTATCCGACTGGCACCGTAGACTA
Sub-For	TTCTAATACGACTCACTATAGG
Sub-Rev	TAGTCTACGGTGCCAGTC
N64	AACACTATCCGACTGGCACC-**N_{64}**-CCTTGGTCATTACGAGTCG
N64-For	AACACTATCCGACTGGCACC
N64-Rev	CGACTCGTAATGACCAAGG
N60	CGGGACTGTCACCTTGG-**N_{60}**-CCTGACTTGTCCACGCTC
N60-For	CGGGACTGTCACCTTGG
N60-Rev	GAGCGTGGACAAGTCAGG

To prepare the two smaller DNA pools, 0.23 nmol of the single-stranded N64 and N60 were amplified in 10 ml PCR reactions both for 10 cycles. The double-stranded fragments of Sub were also prepared by PCR. After phenol/chloroform extraction

and ethanol precipitation, the purified dsSub was cleaved with restriction endonuclease BanI, while dsN64 was cleaved with both, BanI and StyI, and dsN60 was digested with StyI. All three processed fragments (dsSub-BanI, dsN64-BanI-StyI and dsN60-StyI) were then purified from 8% native polyacrylamide gels. Finally, the full-length dsDNA pool was created by ligating these three fragments.

The starting population of RNA variants was transcribed from 200 pmol of the dsDNA pool as described in chapter 3.2.5. Purified RNAs (300 pmol) were denatured for 5 min at 85°C and cooled slowly to room temperature. The renatured RNAs were then incubated in 500 µl reaction buffer (50 mM HEPES, pH 7.3 at 37°C; 150 mM NaCl and 10 mM $MgCl_2$) for 2.5 h at 37°C. The reaction was quenched by the addition of an equal volume of 50 mM EDTA. The uncleaved RNA precursors were recovered by 8% denaturing PAGE, resuspended in the reaction buffer at a final RNA concentration of 0.6 µM and incubated for 18 h under increased temperatures (8 h at 40°C, 8 h at 50°C and 2 h at 45°C). The reaction was stopped by adding an equal volume of 50 mM EDTA, concentrated by spin-filter YM-30 (Millipore) and subjected to 8% denaturing PAGE. Cleaved 3'-fragments about 10 – 30 nucleotides shorter in length were recovered, amplified by RT-PCR and digested by BanI. The enriched full-length dsDNA pool was generated by ligation of the two digested fragments. The new RNA pool was transcribed *in vitro* and submitted to the next round of selection.

3.7.2 DNAzyme-based Nanoparticle-Drug Release System

The DNAzyme-based nanoparticle-drug release system was at first investigated in reaction buffer to evaluate its ability for release in a thermally controlled manner. L-DNAzyme/inhibitor-NP conjugates and L-substrate-NP conjugates were prepared as described (Chapter 3.5). The two different conjugates were then mixed in

reaction buffer (50 mM Tris-HCl, pH 7.5 at 23°C; 10 mM $MgCl_2$) at a molar ratio of 1:1. Two equal aliquots of the mixture were transferred into new tubes. One aliquot was incubated for 1 h at 37°C, while the other was incubated for 1 h at 49°C. Samples were taken and centrifuged immediately at 16,000 x g for 5 min to give rise to clean supernatants. The RFU values of the supernatants were determined by a NanoDrop 3300 Fluorospectrometer (Thermo Scientific).

To evaluate its efficacy under simulated *in vivo* conditions, the same release assay of the L-oligonucleotides-NP conjugates was performed in human serum. The assay was conducted in a 90% human serum (#H4522, Sigma) that was buffered by 1 x DPBS (155.17 mM NaCl, 2.71 mM Na_2HPO_4, 1.54 mM KH_2PO_4, final pH 7.2 at 25°C) in a water bath at 37°C or 49°C. Aliquots were taken at durations of 20 min, 40 min, 60 min, 120 min and 180 min. After centrifugation at 16,000 x g for 5 min, RFU values of the supernatants were determined by a NanoDrop 3300 Fluorospectrometer and plotted at the indicated durations.

4 Results

The initial strategy aimed to develop a thermal-responsive self-cleaving ribozyme (thermozyme) as a thermolabile linker between nanoparticle and cytotoxic drug. The thermozyme should remain inactive at body temperature, but should transform into an active conformation at elevated temperature and cleave itself. A temperature range of 40 – 50°C was chosen to establish a proof of concept for hyperthermia conditions. Since there is no report of a thermal-responsive ribozyme yet, the first task was to develop a thermozyme through *in vitro* selection (Chapter 4.1). Due to unsatisfactory results of this subtask, a second project was pursued to develop a novel DNAzyme-based strategy (Chapter 4.2).

4.1 Thermozyme-based Nanoparticle-Drug Release System

An iterative *in vitro* selection and amplification procedure was used to isolate a thermozyme from a large pool of RNA random sequences. A potential candidate should undergo efficient self-cleavage under escalated temperatures (40 – 50°C), while it should remain inactive at body temperature (37°C). After successful identification of a thermozyme candidate, it would be transformed into mirror-image RNA to ensure its *in vivo* stability and coupled to a nanoparticle. After attaching a cytotoxic drug to the free terminus of the candidate, the NP-thermozyme conjugates may undergo thermally controlled self-cleavages leading to hyperthermia induced drug release.

4.1.1 Pool Construction and Preparation

A large random region was considered to be superior to a smaller one, since

broader regions are more likely to contain interacted sets of sequence elements that can form a complex RNA structure (Bartel and Szostak, 1993). A large random pool was preferred in view of that this project is aimed to isolate novel thermozymes that would require complex structures to respond to a small temperature change. The chemical synthesis of long oligonucleotides, however, is difficult due to the fact that both yield and quality of synthetic DNA decline substantially with increasing length. This problem was circumvented by joining smaller pools to generate a larger pool, following the protocol of Bartel and Szostak (1993), who successfully identified novel functional ribozymes from a large random pool. The scheme for DNA pool construction is outlined in Figure 10.

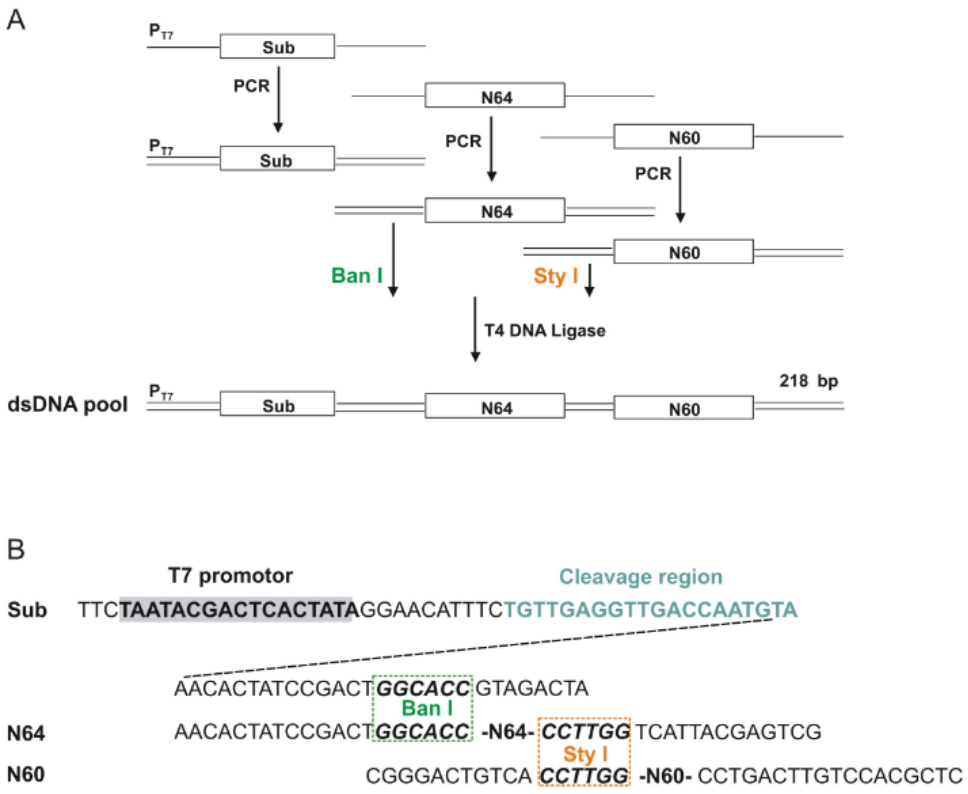

Figure 10: DNA pool construction. (A) Generation of full-length dsDNA pool. Three synthetic oligodeoxynucleotides (Sub, N64 and N60) were amplified by PCR and the double stranded products were cleaved by restriction endonucleases as indicated. The processed fragments were then ligated to form the full-length dsDNA pool. N64 and N60 define the 64 and 60 randomized nucleotides. (B) Sequences of the synthetic DNAs. The dashed line indicates adjacent nucleotides.

To prepare the starting dsDNA pool, 0.23 nmol of each single-stranded

oligodeoxynucleotide (Sub, N64 and N60) were amplified by PCR. After phenol/chloroform extraction and ethanol precipitation, the purified dsSub was cleaved with restriction endonuclease BanI, while dsN64 was cleaved with both, BanI and StyI, and dsN60 was digested with StyI. All three processed fragments (dsSub-BanI, dsN64-BanI-StyI and dsN60-StyI) were then purified from 8% native polyacrylamide gels. Finally, the full-length dsDNA pool was created by ligating the three fragments (Fig. 11). The fragment ligation (500 pmol each) yielded 200 pmol full-length starting dsDNA after gel purification.

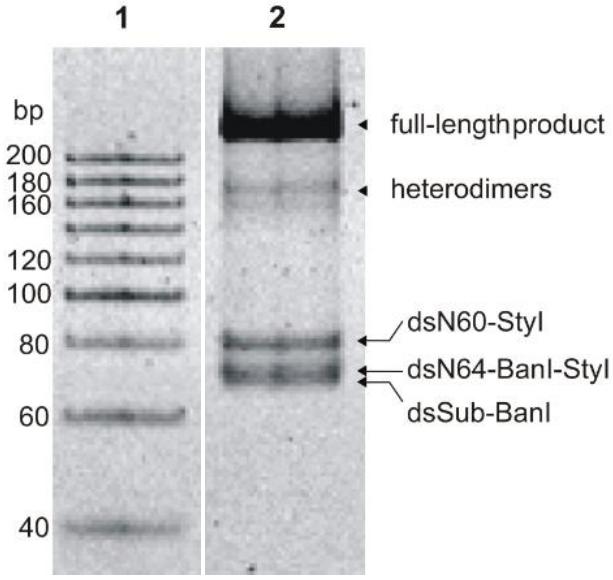

Figure 11: Ligation for DNA pool construction. Lane 1 is a 20-bp DNA ladder. Lane 2 is the ligation of three processed fragments (dsSub-BanI, dsN64-BanI-StyI and dsN60-StyI). The two bands at ~70 bp and ~83 bp denote the unreacted fragments. The band region marked 'heterodimer' contains ligation products between dsSub-BanI and dsN64-BanI-StyI or between dsN64-BanI-StyI and dsN60-StyI, respectively. The band marked as full-length product represents the 218-bp full-length dsDNA pool.

The starting RNA pool was transcribed from 200 pmol of full-length dsDNA pool. The RNA variants for the selection of thermozymes are outlined (Fig. 12). Each RNA variant contains two random regions joined by a 6-nt defined sequence. A schemed cleavage region providing 12 possible neighboring combinations was designed to avoid the formation of localized stable secondary structures within the 5'-fixed region (analyzed by RNA Mfold). Two flanking domains around the N64 and N60 random regions serve as primer-binding sites for RT-PCR amplification of

enriched variants.

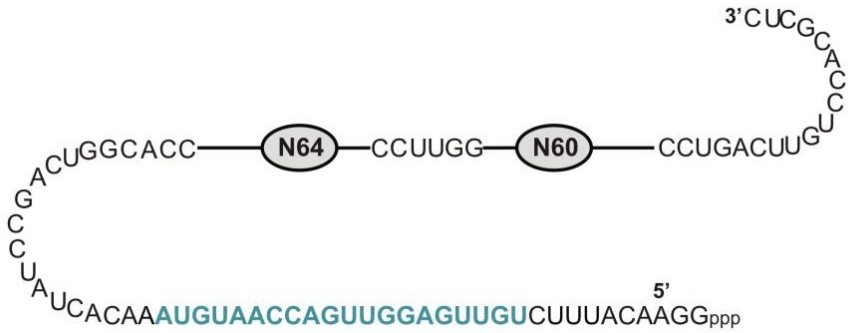

Figure 12: RNA variants for the selection of thermozymes. The cleavage region is colored in blue. N64 and N60 denote the 64 and the 60 randomized nucleotides.

4.1.2 *In vitro* Selection

The schematic procedure for thermozyme selection is outlined in Figure 13. Purified RNA variants (300 pmol) from *in vitro* transcription were subjected into the first round of selection as described in chapter 3.7.1. The undesired variants that could self-cleave at body temperature were removed through incubation at 37°C followed by denaturing gel recovery. The purified intact RNA precursors were then incubated at increased temperatures of 40 – 50°C. The cleaved 3'-fragments were recovered from denaturing gel, reverse transcribed and amplified by PCR. The enriched full-length dsDNA pool was generated by ligation of the two digested fragments. A new population of RNA variants was created through *in vitro* transcription and submitted to the next round of selection. The stringency of selection was steadily increased in later rounds, *i.e.*, Mg^{2+} concentrations and incubation times at 40 – 50°C were declined gradually, while incubation times at 37°C were increased (Tab. 11).

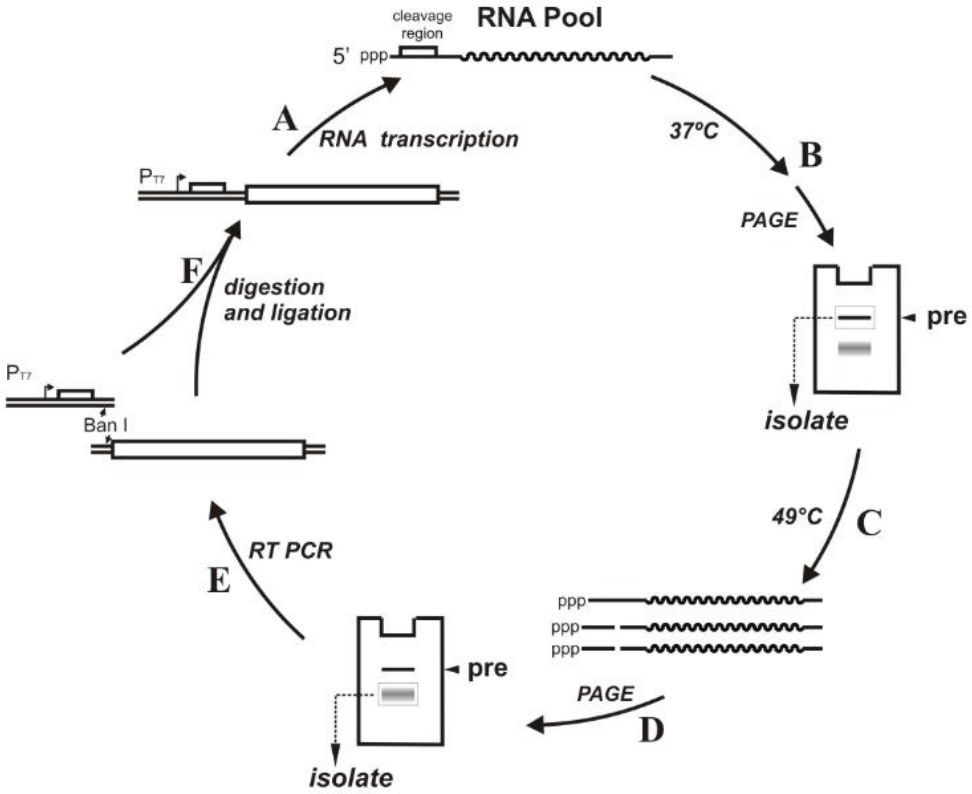

Figure 13: Selection of thermozymes from a random pool of RNA. (A) RNAs are transcribed from the full-length double-stranded DNAs and (B) are incubated at 37°C. The uncleaved RNA precursors are recovered by PAGE and (C) are incubated at 40°C to 50°C. (D) The 3' fragments of cleaved RNAs are separated from uncleaved precursors by PAGE and (E) are amplified by RT-PCR. (F) The RT-PCR products are cleaved by BanI and ligated with another processed fragments that include a T7 promotor and a schemed cleavage region. The resulting double-stranded DNAs are transcribed into the subsequent population of RNAs.

Table 11: Conditions for thermozyme selection. Asterisks denote that mutagenic PCR was performed during the round.

Round	Incubation Duration		$MgCl_2$	NaCl
	37°C	40 – 50°C	(mM)	(mM)
1	2 h	18 h	10	150
2	2 h	6 h	5	150
3	2 h	3 h	5	150
4	2 h	3 h	2	150
5	2 h	3 h	2	150
6	2 h	3 h	2	150
7*	18 h	3 h	2	150
8*	16 h	3 h	2	150
9*	16 h	3 h	2	150
10*	16 h	3 h	2	150
11*	16 h	3 h	2	150
12	16 h	3 h	2	150
13	16 h	3 h	2	150
14	16 h	3 h	2	150
15	16 h	3 h	2	150

Mutagenic PCR was reported to enhance the activity of the selected pool of ribozymes through generating a broader spectrum of RNA variants (Bartel and Szostak, 1993). It was found that addition of Mn^{2+}, high concentrations of Mg^{2+}, pyrimidine deoxynucleotides and enzyme lead to a mutation rate during PCR of about 0.66 percent in 10 doublings (done in 30 PCR cycles) with very little bias in the types of mutations generated (Cadwell and Joyce, 1992). Therefore, the RT-PCR products from round 6 were subjected to mutagenic PCR for 0, 30, 60, and 90 doublings corresponding to expected mutation rates of about 0, 2, 4, and 6 percent per residue, respectively. Equal amounts of mutagenic PCR products at four different mutation rates were pooled together, cleaved by BanI and ligated with dsSub-BanI, which introduces a T7 promoter sequence and restores the nucleotides that were lost upon self-cleavage. The resulting full-length dsDNAs of round 7 were transcribed into a new pool of RNA variants. Initially, the RNA variants from round 7 were incubated for an extended time at 37°C to remove the undesired RNA motifs. PCR mutagenesis was included during rounds 8 to 11. The fractions of self-cleaved RNAs from rounds 8 to 15 are outlined (Fig. 14).

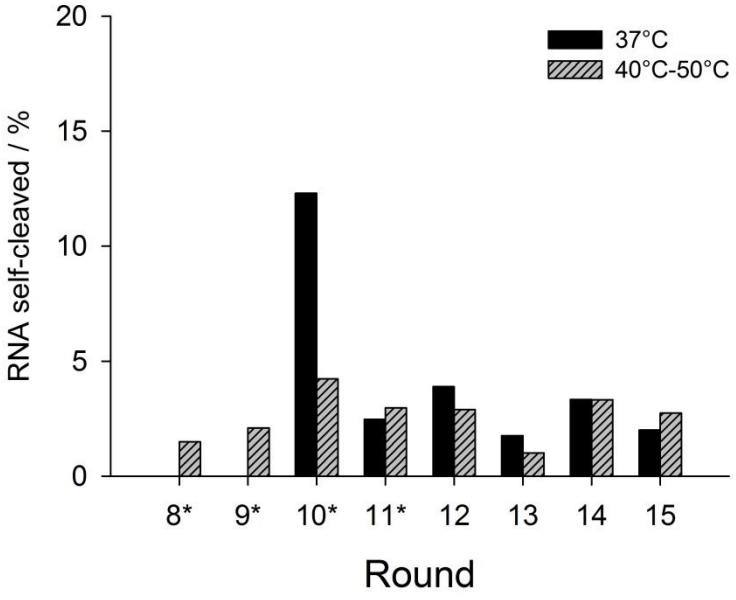

Figure 14: Fractions of RNA in different selection rounds. Asterisks denote that mutagenic PCR was performed during the round.

A significant self-cleavage of RNA variants at 37°C was observed at round 10. The RNA variants from the same round, however, failed to undergo an efficient cleavage at increased temperatures of 40 – 50°C. Further enrichment of the thermo-responsive self-cleaving RNA variants was unobservable after five additional rounds of selection, indicating that the currently applied selection procedure was unable to yield the desired thermozyme candidates.

4.2 DNAzyme-based Nanoparticle-Drug Release System

Since the first approach depending on the successful isolation of a novel thermo-responsive self-cleaving thermozyme remained unsuccessful (chapter 4.1), a DNAzyme-based nanoparticle-drug release system was developed to achieve an efficient thermally controlled drug release. This concept requires a significant release of drugs at hyperthermic temperatures from nanoparticles (49°C was used for a proof of concept), while no drug should be released at the body temperature of 37°C. Therefore, this thermally controlled system may overcome the adverse side effects of traditional whole-body chemotherapy that relies on intravenous administration and systemic distribution. The schematic for the DNAzyme-based nanoparticle-drug release system is presented (Fig. 15). It consists of two different NP-oligonucleotide conjugates. In the first conjugate, a RNA-cleaving DNAzyme (blue strand) is hybridized to an inhibitor strand that is covalently bound to the surface of an iron oxide nanoparticle. In the second conjugate, the RNA substrate labeled with a fluorescent dye is attached to a different nanoparticle. The fluorescent dye will be replaced by a cytotoxic drug in the future development of the project.

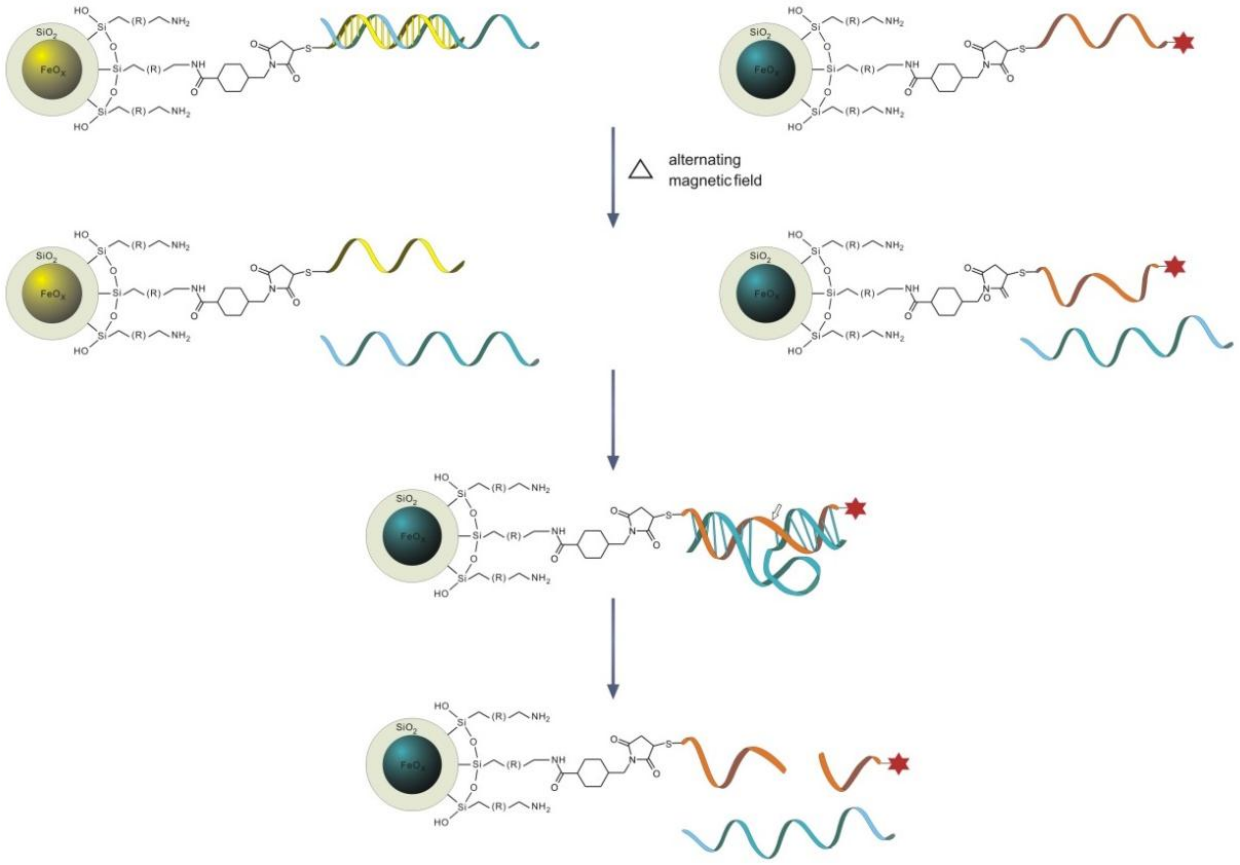

Figure 15: DNAzyme-based nanoparticle-drug release system. The yellow nanoparticle carries a RNA-cleaving DNAzyme by hybridizing to an inhibitor strand. The blue nanoparticle carries a RNA substrate coupled with a fluorescent reporter group that will be replaced by a cytotoxic drug in human applications. Upon heat, the DNAzyme will dissociate from the inhibitor strand, associate with the substrate strand and cleave it.

Depending on the base pair interactions and the optimal molar ratio between DNAzyme and inhibitor strand, a release of DNAzyme should be prohibited at 37°C leading to the absence of undesired drug release. Once the magnetic nanoparticles are heated up in an external alternating magnetic field, the raised temperature will render the complex of the first conjugate unstable and a portion of single-stranded DNAzymes will be released from nanoparticles. The free DNAzymes can then attack the NP-substrate conjugates. Upon specific cleavage of the substrates by DNAzymes, the covalently attached drugs at the end of the substrates will be released into the surrounding tissue. The DNAzyme after cleavage will dissociate from the cleaved fragments and attack another substrate.

4.2.1 Choice of DNAzyme, Substrate and Inhibitors

The success of the DNAzyme-based thermally controlled drug release system requires that hybrids of DNAzyme and inhibitor strand are stable at 37°C, while a part of annealed DNAzymes will be released at elevated temperature of 49°C. These released DNAzymes will yield a significant release of drugs due to repeated RNA-cleaving events. All the oligonucleotides used in this part of the project are listed in Table 12.

Table 12: Sequences of the DNAzyme, substrate and inhibitors. The arrow marks the cleavage site by DNAzyme.

Oligonucleotide	Type	Length	Sequence, 5' to 3'
DNAzyme	DNA	31 nt	CGCACCCAGGCTAGCTACAACGACTCTCTCC
substrate	RNA	17 nt	GGAGAGAGG↓UGGGUGCG
inhibitor1	DNA	26 nt	GGAGAGAGTCGTTGTAGCTAGCCTGG
inhibitor2	DNA	22 nt	GGAGAGAGTCGTTGTAGCTAGC

The two inhibitor candidates (inhibitor1 and inhibitor2) were screened by their ability to deliver a thermally controlled release of DNAzyme and concomitant cleavage of RNA substrates. DNAzyme and inhibitor strands were hybridized in reaction buffer (50 mM Tris-HCl, pH 7.5 at 23°C; 10 mM $MgCl_2$) at different molar ratios. Equal amounts of 5'-end radioactively labeled RNA substrates were added to these hybrids. Each mixture was divided into two equal parts and simultaneously incubated for 50 min at 37°C or 49°C. The reactions were quenched by addition of 2X Gel loading buffer containing 8 M Urea, analyzed by 20% denaturing PAGE and visualized by phosphorimaging. The best results of thermally controlled cleavage of RNA substrate was achieved by the hybrids of DNAzyme and inhibitor2 at molar ratios between 0.9:1 and 1.01:1 (Fig. 16, lanes 3 – 6). Hence, the hybrids of DNAzyme/inhibitor2 were further investigated after coupling the oligonucleotides to nanoparticles. The optimum of thermally controlled RNA cleavage should be located in between these two ratios. Moreover, it is worth noting that the DNAzyme cleaved substrates more efficiently at 49°C than at 37°C (Fig. 16, Lanes 12 and 13).

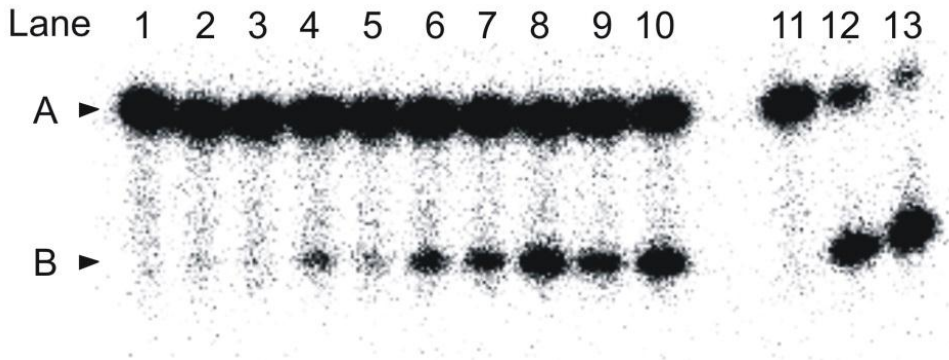

Figure 16: Optimization of the DNAzyme cleavage reaction. Phosphorimage of a 20% denaturing gel was used to analyze the effect of five different hybridization ratios of DNAzyme and inhibitor2 on the cleavage of substrates. A indicates the position of the substrate precursors of 17 nucleotides in length. B marks the position of 5' cleaved RNA fragments of 9 nucleotides in length. The molar ratio of DNAzyme to inhibitor2 in lanes 1 and 2 was 0.81:1, in 3 and 4 was 0.9:1, in 5 and 6 was 1.01:1, in 7 and 8 was 1.12:1 and in 9 and 10 was 1.18:1. Samples 1, 3, 5, 7, 9, 11 and 12 were incubated at 37°C for 50 min, while samples 2, 4, 6, 8, 10 and 13 were incubated at 49°C for 50 min. Lane 11 shows the negative control without inhibitor and DNAzyme. Lanes 12 and 13 were positive controls without inhibitors.

4.2.2 Coupling of Oligonucleotides to Nanoparticles

After confirming the feasibility of using the hybrids of DNAzyme and inhibitor2 for thermally controlled release of DNAzymes in solution, the system was further tested after coupling the oligonucleotides to nanoparticles. The thiol-modified inhibitor2 and substrate are listed (Tab. 13).

Table 13: Thiol-modified substrate and inhibitor2 strand. The arrow marks the cleavage site by DNAzyme.

Oligonucleotide	Type	Length	Sequence, 5' to 3'
substrate	RNA	17 nt	HS-GGAGAGAGG↓UGGGUGCG-Alexa 647
inhibitor2	DNA	22 nt	HS-GGAGAGAGTCGTTGTAGCTAGC

Sulfo-SMCC was used as the crosslinker for coupling thiol-modified oligonucleotides to aminosilane-coated iron oxide nanoparticles (provided by the cooperation partner MagForce AG, Germany). First, the aminosilane-coated iron oxide nanoparticles were reacted with the amino-reactive sulfo-NHS ester of

sulfo-SMCC at pH 7.4, resulting in maleimide-activated nanoparticles. Thiol-modified oligonucleotides were then coupled to the maleimide groups at pH 6.7. In consequence, a stable covalent thioester linkage is formed. The coupling results indicated that each nanoparticle can be coupled with an average 16 substrates.

An additional GSH treatment was performed to improve the stability of the NP-oligonucleotide conjugates after two steps of sulfo-SMCC coupling reactions. The unreacted hydrophobic maleimide groups on the surface of NP-oligonucleotide conjugates were blocked by incubation with 10 mM reduced L-GSH for 1 h under room temperature. The stability of the NP-substrate conjugates was substantially improved by GSH-treatment (Fig. 17).

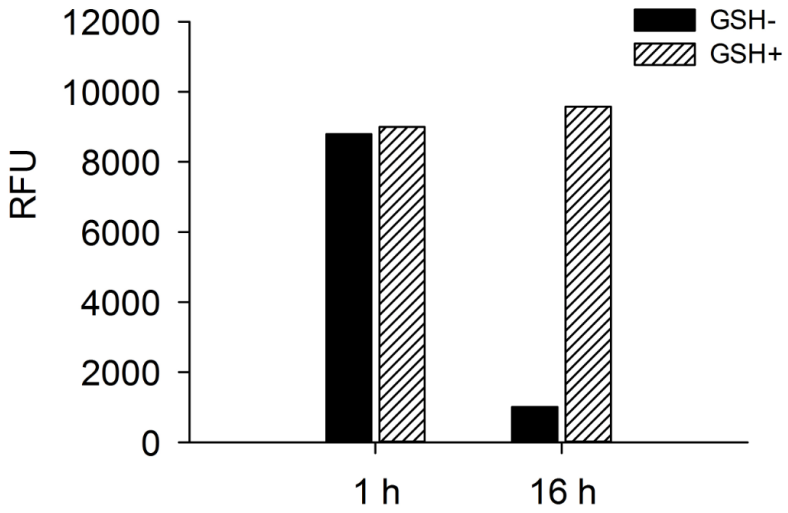

Figure 17: Effect of GSH-treatment on fluorescent dye release from NP-substrate conjugates. NP-substrate conjugates with or without GSH-treatment were reacted with 0.8 µM DNAzymes at 49°C for 1 h after incubating the conjugates in a PBS buffer (137.9 mM NaCl, 8.06 mM Na_2HPO_4, 2.67 mM KCl, 1.47 mM KH_2PO4; pH 6.7) for 1 h or 16 h. After centrifugation at 16,000 x g for 5 min, the relative fluorescence unit (RFU) values in the supernatants were measured by a NanoDrop 3300 Fluorospectrometer and plotted.

The stability of the conjugates was evaluated by monitoring the dye release through co-incubation of NP-substrate conjugates with DNAzymes in a reaction buffer (50 mM Tris-HCl, pH 7.5 at 23°C; 10 mM $MgCl_2$) at 49°C for 1 h. The dye release

was efficient after incubating in a PBS buffer (137.9 mM NaCl, 8.06 mM Na_2HPO_4, 2.67 mM KCl, 1.47 mM KH_2PO4; pH 6.7) for 1 h, whether the conjugates were GSH treated or not. The dye release from the conjugates without GSH-treatment was, however, greatly prohibited after incubating in the PBS buffer for 16 h, while the dye release remained almost unchanged over the time period investigated for the GSH-treated NP-substrate conjugates. To my knowledge, this additional GSH-treatment was firstly reported by this work. In addition, the solubility of the conjugates was slightly improved due to the blocking of unreacted hydrophobic maleimide groups.

Therefore, the two different NP-oligonucleotide conjugates used in this work, NP-DNAzyme/inhibitor2 conjugates and NP-substrate conjugates, were both treated with 10 mM GSH after the two-step sulfo-SMCC coupling reaction to ensure their stability.

4.2.3 Release Experiments of NP-Oligonucleotide Conjugates

After preparation of the NP-oligonucleotide conjugates, release experiments were performed to evaluate their ability to achieve thermally controlled dye release. The schematic for the release experiment is depicted (Fig. 18). First, DNAzyme/inhibitor2 hybrids at different molar ratios were coupled to nanoparticles, forming the NP-DNAzyme/inhibitor2 conjugates. The NP-substrate conjugates were produced by direct coupling of thiol-modified substrate strands to nanoparticles. Upon heating, the DNAzymes dissociated from the inhibitor2 strands and attacked the NP-substrate conjugates leading to dye release.

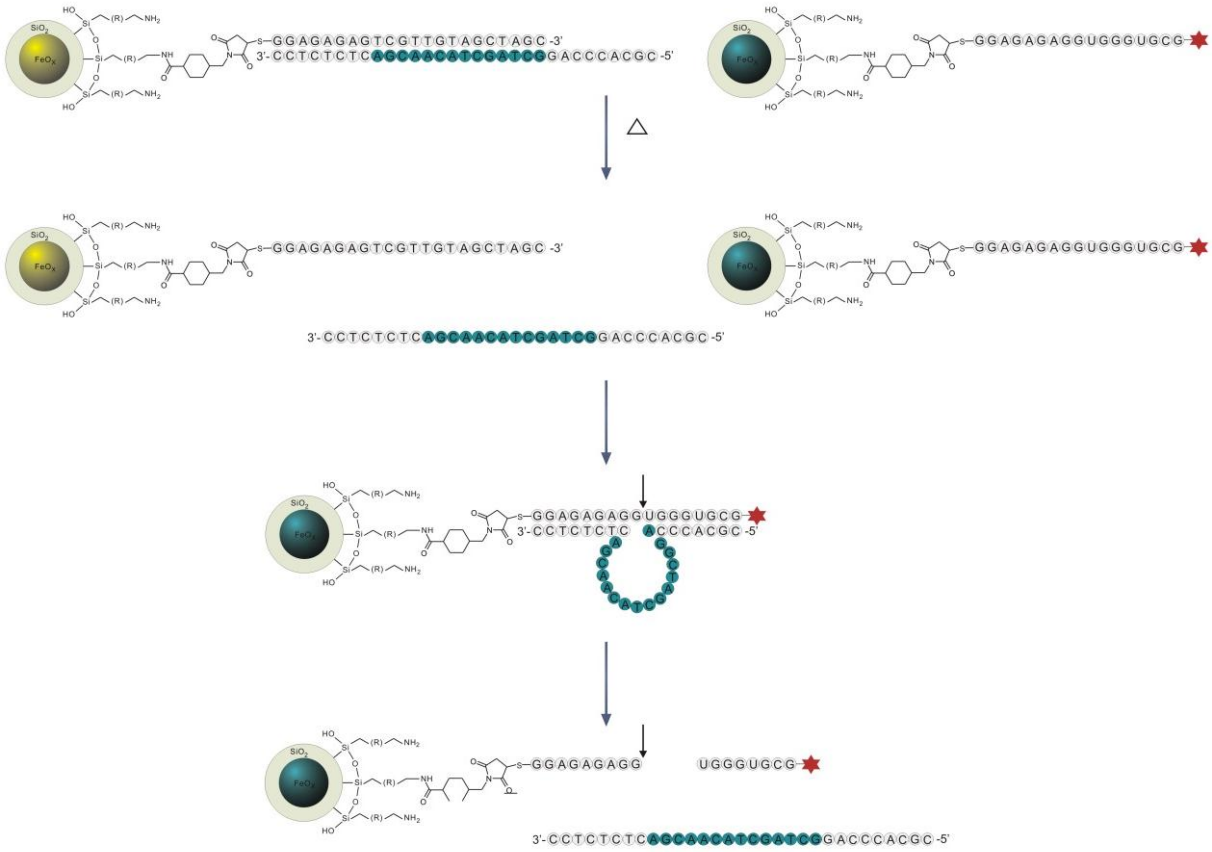

Figure 18: DNAzyme-based nanoparticle-drug release system. NP-DNAzyme/inhibitor conjugate (yellow particle) and NP-substrate conjugate (blue particle) were mixed at 1:1 molar ratio in reaction buffer (50 mM Tris-HCl, pH 7.5 at 23°C; 10 mM $MgCl_2$) and divided into two equal parts. One part was incubated at 37°C, while the other was incubated at 49°C. Upon heating in a thermomixer at 49°C, the hybridized DNAzymes detached from the inhibitor strands, cleaved the substrates and triggered dye release.

Prior to release experiments, a linear range of relative fluorescence unit (RFU) vs. concentration of the 3'-Alexa Flour® 647–labeled substrates in reaction buffer (50 mM Tris-HCl, pH 7.5 at 23°C; 10 mM $MgCl_2$) was plotted (Fig. 19), which can be used to quantify the amount of released dyes by interpolation. The values of RFU were measured by a NanoDrop 3300 Fluorospectrometer (Thermo Scientific, USA). The standard calibration curve indicated a strong linear correlation (R^2=0.9986) between RFU and concentration of fluorescent substrates in the range of 10 nM to 3 µM.

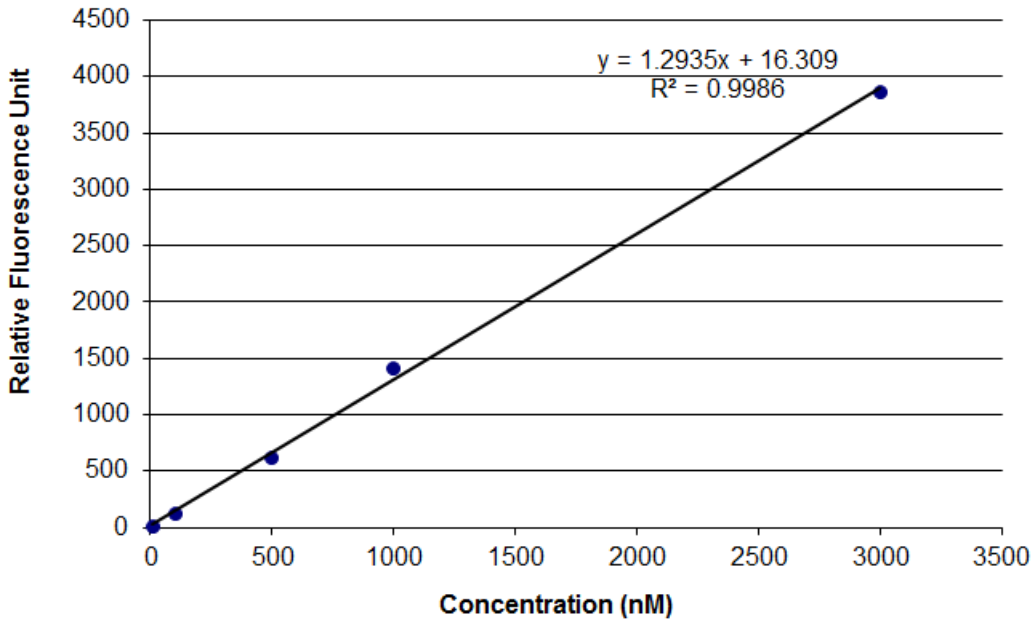

Figure 19: Standard calibration curve for substrate in reaction buffer. The relative fluorescent units (RFU) were plotted against the concentrations (nM) of Alexa Fluor® 647–labeled RNA substrate in reaction buffer (50 mM Tris-HCl, pH 7.5 at 23°C; 10 mM $MgCl_2$).

The result of the cleavage optimization using a mixture of radioactively labeled substrate and DNAzyme/inhibitor2 duplex prepared under different molar ratios in reaction buffer suggested that a certain molar ratio between 0.9 and 1 could yield a thermally controlled cleavage of substrate. Therefore, two molar ratios (0.9:1 and 1:1) were initially investigated for their ability to deliver a thermally controlled dye release from NP-substrate conjugates through the cleavages of dye-labeled substrate strands by DNAzymes. The dye release, however, was insufficient (Fig. 20), yielding a thermosensitivity (dye release at 49°C over dye release at 37°C) of 3.4 – 4.6. A higher molar ratio of 2:1 between DNAzyme and inhibitor2 strand was then explored, revealing a thermosensitivity of 6.7 (Fig. 20), *i.e.*, the release at 49°C is 6.7-fold higher than at body temperature.

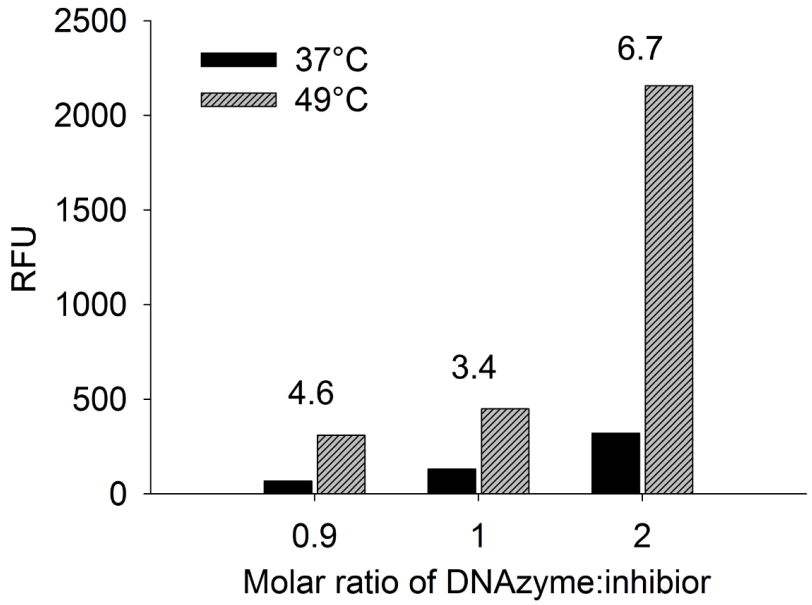

Figure 20: Release experiments with three different molar ratios between DNAzyme and inhibitor. The hybrids of DNAzyme/inhibitor2 with the indicated molar ratios were coupled to nanoparticles, forming the NP-DNAzymes/inhibitor2 conjugates. The NP-hybrid conjugates were then mixed with equal amount of NP-substrate conjugates in reaction buffer. The mixture was divided into two equal parts and incubated for 1 h at 37°C or 49°C. The RFU values in the supernatants were determined by a NanoDrop 3300 Fluorospectrometer. The numbers above the bar-sets are the defined thermosensitivity.

Consequently, the thermally controlled dye release in reaction buffer (50 mM Tris-HCl, pH 7.5 at 23°C; 10 mM $MgCl_2$) was further investigated using the molar ratio of 2:1 for the preparation of NP-DNAzyme/inhibitor2 conjugates (Fig. 21). The positive control shows about 85% release of coupled dyes after incubation of NP-substrate conjugates with 0.5 µM free DNAzymes for 1 h at 37°C, while the negative control including NP-substrate conjugates alone in reaction buffer for 1 h at 37°C exhibits 0.7% release. The dye release at 49°C was demonstrated to be significantly higher (21.8%) than at 37°C (1.1%), suggesting that this DNAzyme-based approach is feasible for an efficient thermally controlled drug release.

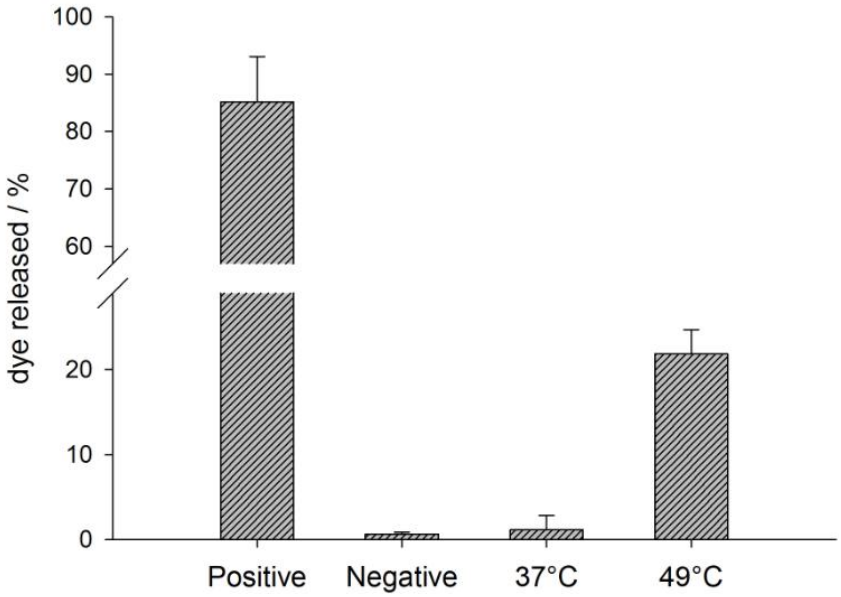

Figure 21: Thermally controlled dye release from NP-substrate conjugates in reaction buffer. Positive refers to the control, in which free DNAzyme (0.5 µM) was added to the NP-substrate conjugates in reaction buffer and incubated at 37°C for 1 h. Negative refers to the control, in which the NP-substrate conjugates were incubated merely in reaction buffer and incubated for 1 h at 37°C. The bars marked with 37°C and 49°C denote the mixture of NP-DNAzyme/inhibitor2 and NP-substrate conjugates that were incubated in reaction buffer for 1 h at the indicated temperatures. Error bars indicate standard deviations (n = 3).

4.2.4 Stability and Activity of Mirror-Image Nucleic Acids

After confirming the feasibility of using this DNAzyme-based two-conjugate system (NP-DNAzyme/inhibitor2 and NP-substrate) for thermally controlled drug release, all the D-oligonucleotides were transformed into mirror-image L-oligonucleotides. This change was made to ensure the stability of all oligonucleotides used in the drug release system under human cellular environments. The activity of the system would be maintained due to the reported chiral specificities (Klussmann *et al.*, 1996; Nolte *et al.*, 1996). The mirror-image oligonucleotides are listed as follow (Tab. 14).

Table 14: Mirror-image oligonucleotides. The arrow marks the cleavage site.

Oligonucleotide	Type	Sequence, 5’ to 3’
DNAzyme	L-DNA	CGCACCCAGGCTAGCTACAACGACTCTCTCC
substrate	L-RNA	SH-GGAGAGAGG↓UGGGUGCG-Alexa 647
inhibitor2	L-DNA	HS-GGAGAGAGTCGTTGTAGCTAGC

A comparative stability assay of D- and L-form DNAzymes was performed to assess their resistance against nuclease degradation. Human serum was used as a natural source of nucleases. It was reported that the *in vitro* half-life of a typical oligodeoxynucleotide in plasma is 30 to 60 minutes (White *et al.*, 2000). Therefore, the lengthy incubation of both D-form and L-form DNAzymes in human serum was performed in an incubator with 95% humidity and 5% carbon dioxide to stabilize the pH value of the serum. Samples were taken at indicated durations and analyzed by 20% denaturing PAGE. The result was recorded by a Typhoon FLA 7000 multi-purpose laser scanner (GE Healthcare, Sweden) after staining the gel in 1 µg/ml ethidium bromide for 15 min as illustrated (Fig. 22). The D-DNAzymes were almost completely degraded after 24 h, while the degradation of their mirror-image counterparts was undetectable even after 48 h.

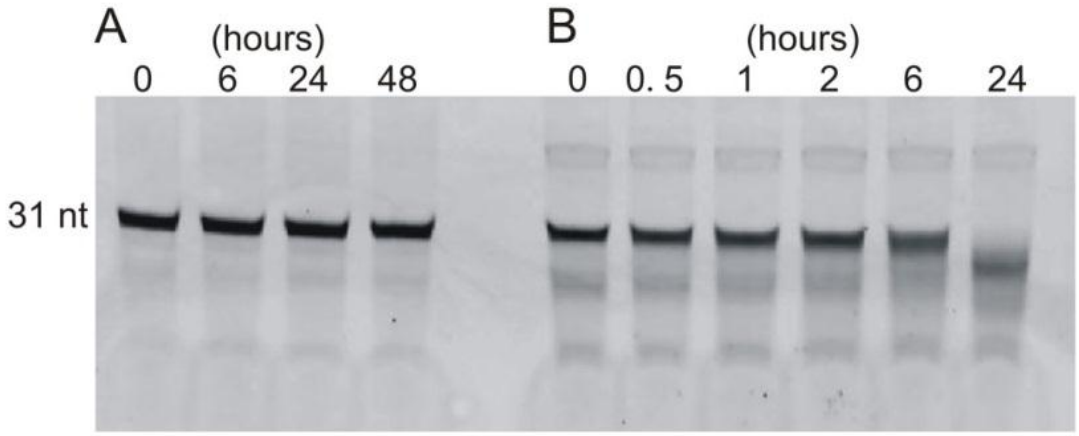

Figure 22: Stability of D- and L-DNAzyme in human serum. Aliquots of DNAzymes (each 60 pmol) were taken from the incubation solution at indicated durations and recorded on a 20% denaturing polyacrylamide gel. Part A refers to the L-DNAzymes in human serum, while part B shows the natural D-DNAzymes in human serum.

Though mirror-image nucleic acids were proven to possess chiral specificities (Klussmann *et al*., 1996; Nolte *et al*., 1996), it remains necessary to confirm whether the L-DNAzymes are able to cleave the L-substrates with the same catalytic activity. Since the substrate strands were functionalized with 5'-terminal thiol groups for the covalent immobilization to nanoparticles, dimerization of oligonucleotides posed experimental problems due to formation of disulfide bonds

through oxidation. Thus, the thiol-modified L-substrate strands were reduced by reaction with 3 mM TCEP for 3 h at room temperature (Fig. 23).

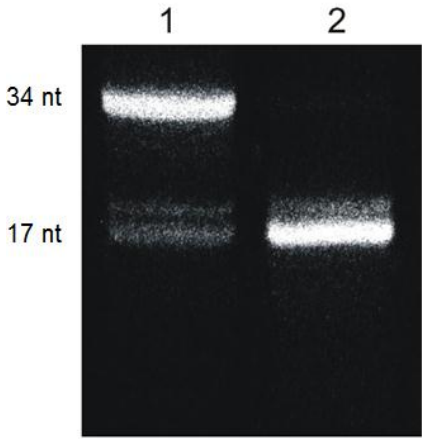

Figure 23: Reduction of thiol-modified L-substrates with TCEP. Lane 1 was the L-substrates without TCEP-treatment, showing a strong band for dimers (34 nt) and a weak band for monomers (17 nt). Lane 2 was L-substrates after TCEP-treatment.

To investigate the chiral specificity of L-DNAzymes towards L-substrates, reduced L-substrates were incubated with L-DNAzymes or D-DNAzymes, respectively. As can be seen from the gel, only the combination of identical chirality displays a new product band (Fig. 24, lanes 2 and 3), while the reciprocal combination of chiralities remained inactive, hence announcing the strict chiral specificity between DNAzyme and substrate.

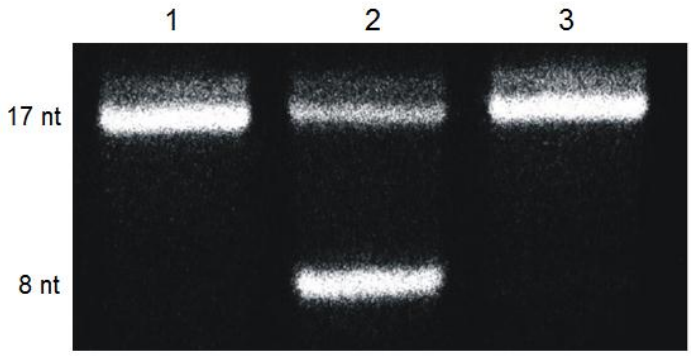

Figure 24: Chiral specificity of DNAzymes towards substrates. Lane 1 was the reduced L-substrates with length of 17 nucleotides. Lane 2 was the reduced L-substrates after incubating with 0.5 µM L-DNAzymes for 1 h at 37°C, where a product band appeared with a size of 8 nucleotides. Lane 3 was the reduced L-substrates after incubating with 0.5 µM D-DNAzymes for 1 h at 37°C, where cleavage was unobservable.

In addition, the stability of L-substrate-NP conjugates was further investigated to determine whether the coupled dyes could be efficiently released after an extended period of incubation in human serum in view of using the conjugates as depots during anti-tumor treatment. L-substrate-NP conjugates (1 µM) were kept in human serum for 3 days at 37°C in an incubator with 95% humidity and 5% carbon dioxide. Afterwards, the conjugates were treated with L-DNAzymes (0.1 nmol in 1 µl) in human serum for 1 h at 37°C, while the negative control was merely the L-substrate-NP conjugates in human serum. RFU values of the supernatants were determined and plotted after centrifugation at 16,000 x g for 5 min (Fig. 25). The result suggested that the L-substrate-NP conjugates can still be cleaved by L-DNAzymes after an extended incubation in human serum leading to an efficient release of the coupled dyes.

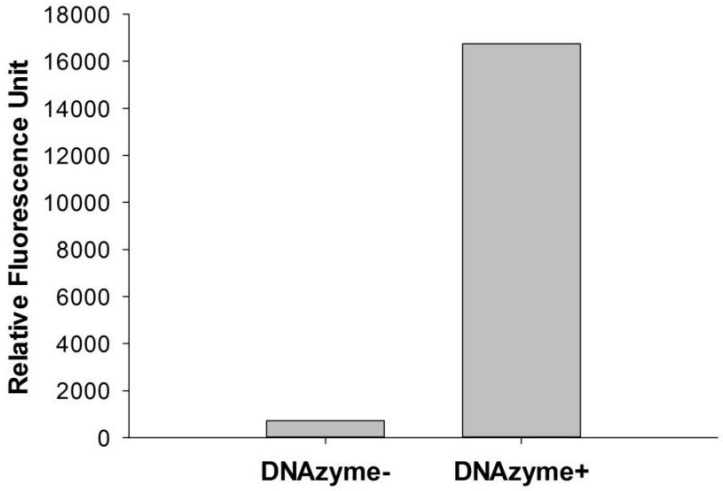

Figure 25: Stability of L-substrate-NP conjugates in human serum. The RFU values of the supernatants were determined by a NanoDrop 3300. The bars marked with DNAzyme- and DNAzyme+ refer to the absence and presence of L-DNAzymes during the incubation of L-substrate-NP conjugates for 1 h at 37°C.

4.2.5 Release Assay in Reaction Buffer

The mirror-image system of the two NP-oligonucleotide conjugates was further examined to determine whether it can achieve a thermally controlled dye release in

reaction buffer like its natural chiral counterparts. The release assay of the L-form system was performed under identical conditions as for the D-form system. The L-DNAzyme/inhibitor-NP conjugates were prepared by employing the established molar ratio of 2:1 between L-DNAzymes and inhibitor2 strands. Again, a standard calibration curve for fluorescently labeled L-substrate in reaction buffer was plotted as RFU vs. concentration (Fig. 26), so that the amount of fluorescent oligonucleotides in the supernatants can be calculated by interpolation during release assays.

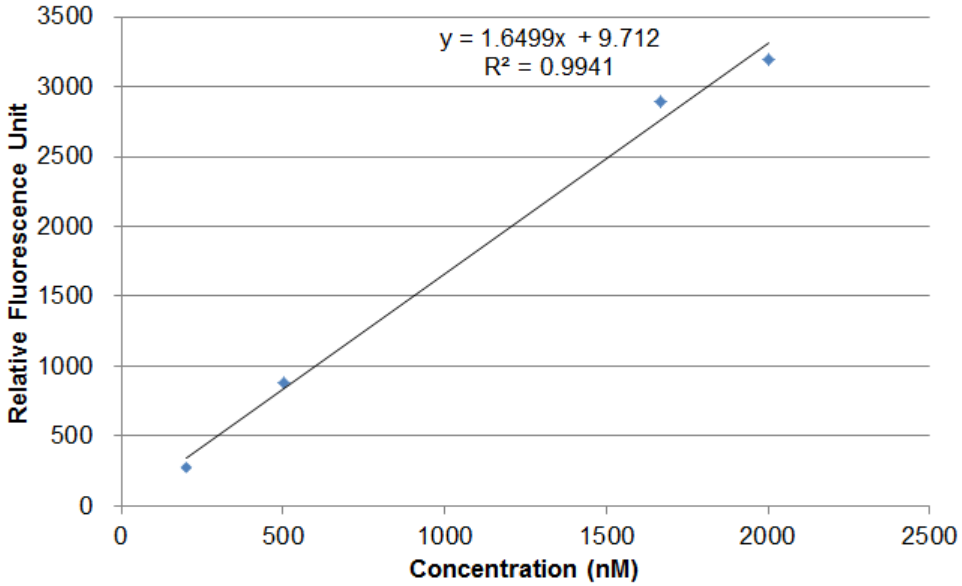

Figure 26: Standard calibration curve for L-substrate in reaction buffer. The relative fluorescence units (RFU) were plotted against the concentrations (nM) of Alexa Fluor® 647–labeled L-substrates in reaction buffer (50 mM Tris-HCl, pH 7.5 at 23°C; 10 mM $MgCl_2$).

A thermally controlled dye release from L-substrate conjugates was observed as expected from the experiments with D-oligonucleotide-NP conjugates (Fig. 27). The positive control shows about 70% release of all coupled dyes when incubating NP-substrate conjugates with 0.5 µM free DNAzymes for 1 h at 37°C, while the negative control shows 0.54% dye release. The dye release at 49°C was demonstrated to be significantly higher (21%) than at 37°C (0.47%). Therefore, the thermally controlled dye release was reproducible between the two chiral forms of oligonucleotide-NP conjugates.

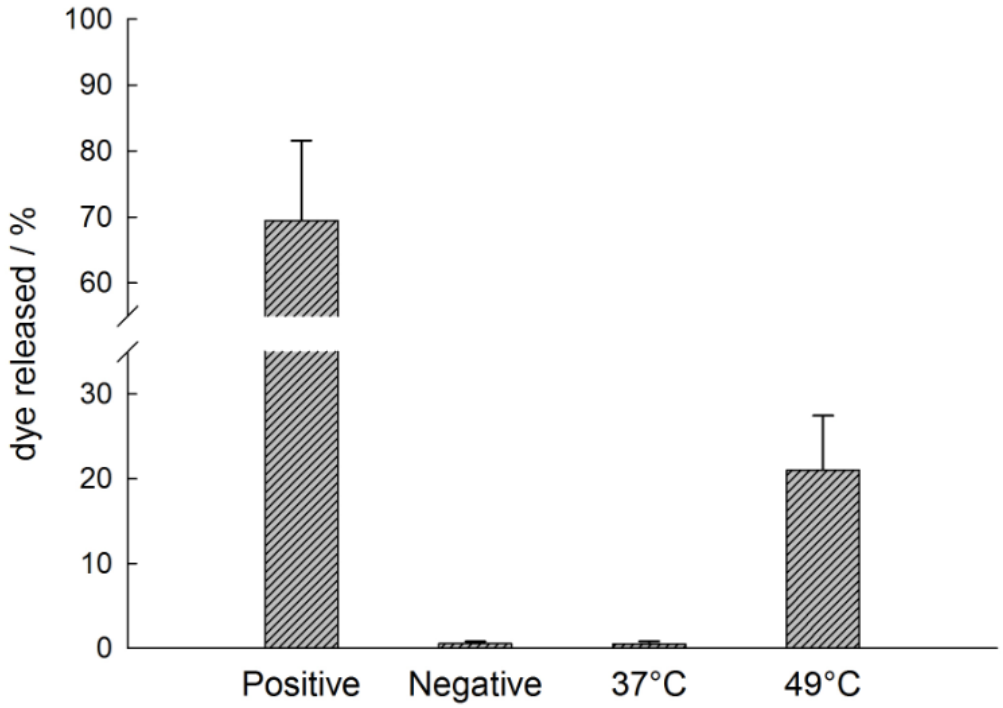

Figure 27: Thermally controlled dye release from L-substrate-NP conjugates in reaction buffer. Positive refers to the control, in which free L-DNAzyme (0.5 µM) was added to the L-substrate-NP conjugates in reaction buffer and incubated for 1 h at 37°C. Negative refers to the control, in which the L-substrate-NP conjugates were incubated merely in reaction buffer and incubated for 1 h at 37°C. The bars marked with 37°C and 49°C refer to the mixture of L-DNAzyme/inhibitor2-NP and L-substrate-NP conjugates that were incubated in reaction buffer for 1 h at the indicated temperatures. Error bars indicate standard deviations (n = 3).

4.2.6 Release Assay in Human Serum

To evaluate the efficacy of this two-conjugate system under a simulated *in vivo* condition, release assays were performed in human serum. A standard calibration curve for fluorescently labeled L-substrate in human serum was plotted as RFU vs. concentration (Fig. 28), so that the amount of released dye can be quantified during the assays.

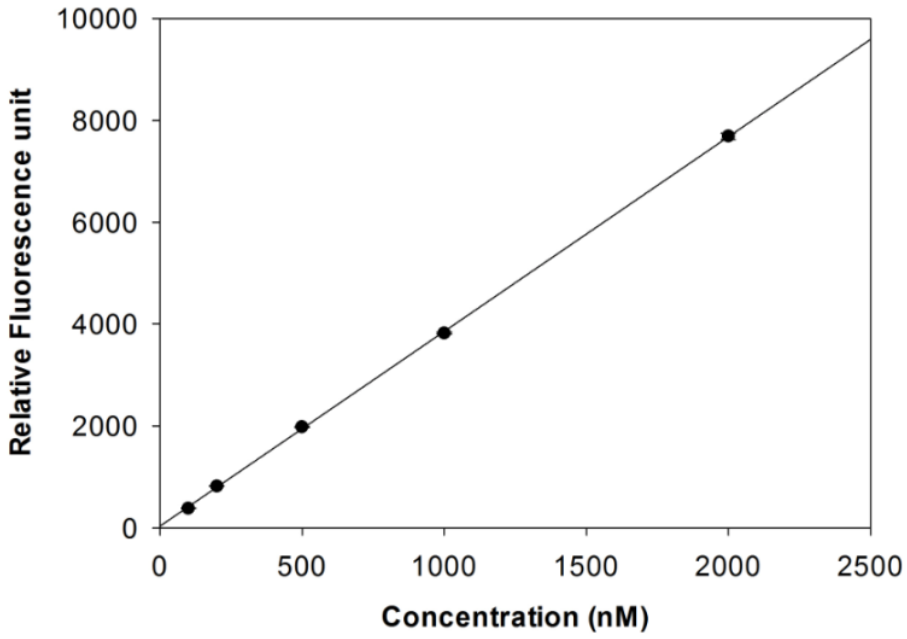

Figure 28: Standard calibration curve for L-substrate in human serum. The relative fluorescent units (RFU) were plotted against the concentrations (nM) of Alexa Fluor® 647–labeled L-substrate in 90% human serum that was buffered by 1 x DPBS (155.17 mM NaCl, 2.71 mM Na_2HPO_4, 1.54 mM KH_2PO_4, final pH 7.2 at 25°C). The linear regression equation is y = 3.8245x + 31.072 (R^2 = 0.9999). Error bars indicate standard deviations (n = 4).

The mixed conjugates (L-DNAzyme/inhibitor-NP and L-substrate-NP) were suspended in 90% human serum that was buffered by 1 x DPBS (155.17 mM NaCl, 2.71 mM Na_2HPO_4, 1.54 mM KH_2PO_4, pH 7.2 at 25°C) at a concentration of 1 µM and incubated in a water bath at 37°C or 49°C. Aliquots were taken at indicated durations and the RFU values were determined and plotted (Fig. 29). The positive control and the 49°C sample release fluorescent dyes quickly and efficiently over the course of time investigated. The 37°C sample also shows an increasing dye release, however, the values remain as low as the negative control. The positive control released about 42% of all coupled dyes after incubating NP-substrate conjugates with 0.5 µM free L-DNAzymes for 3 h at 37°C. The dye release at 49°C was demonstrated to be significantly higher (25.2%) than at 37°C (1.2%), suggesting that this two-conjugate DNAzyme-based approach is feasible for an efficient thermally controlled drug release.

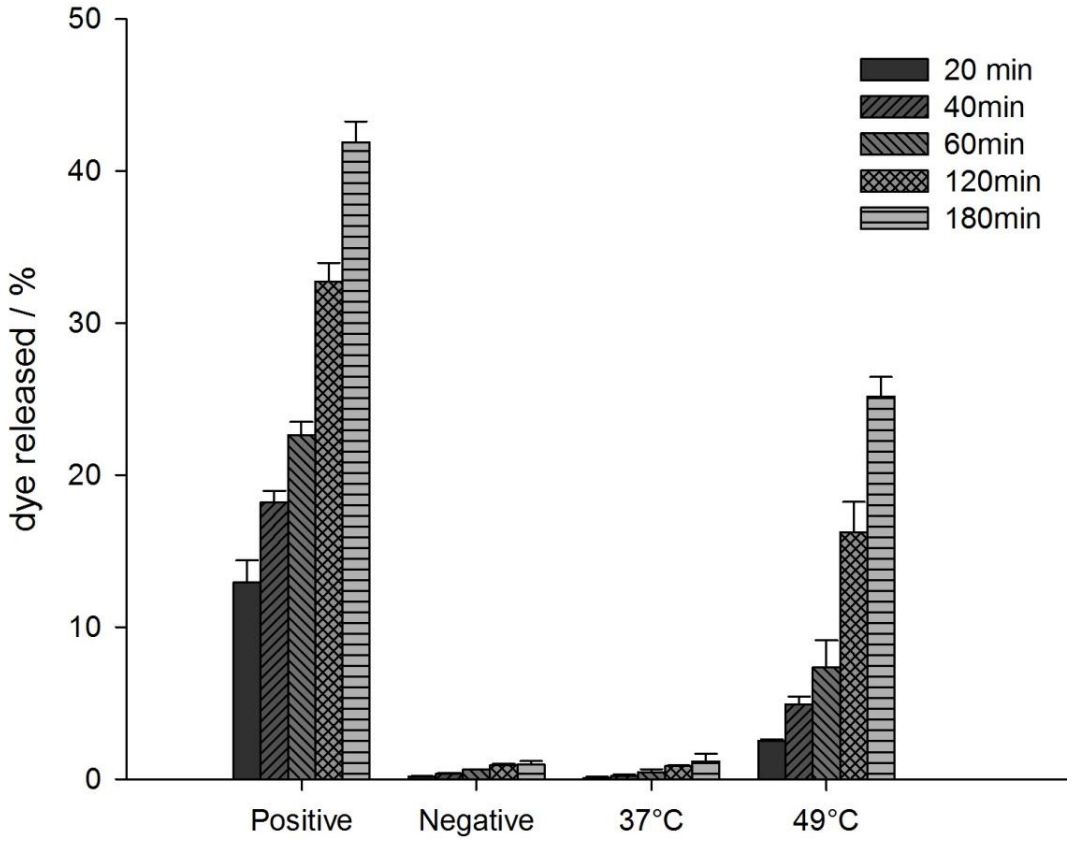

Figure 29: Thermally controlled dye release from L-substrate-NP conjugates in human serum. Positive refers to the control, in which L-substrate-NP conjugates were incubated with L-DNAzymes (0.5 µM) in 90% human serum for 1 h at 37°C. Negative refers to the incubation of L-substrate-NP conjugates in 90% human serum for 1 h at 37°C. The bar-sets marked with 37°C and 49°C defines the mixture of L-DNAzyme/inhibitor2-NP and L-substrate-NP conjugates that were incubated in 90% human serum for 3 h at the indicated temperatures. Error bars indicate standard deviations (n = 3).

4.2.7 One-Conjugate DNAzyme Approach

The established DNAzyme approach is based on a strategy involving two different kinds of conjugates, *i.e.* L-DNAzyme/inhibitor-NP and L-substrate-NP. It is possible, however, to immobilize both, DNAzyme/inhibitor duplex and L-substrate to identical nanoparticles in a one-conjugate system (Fig. 30). The experiments of this section, however, could only be conducted once due to the limited amount of mirror-image oligonucleotides. Thus, the results are mere indicative rather than conclusive.

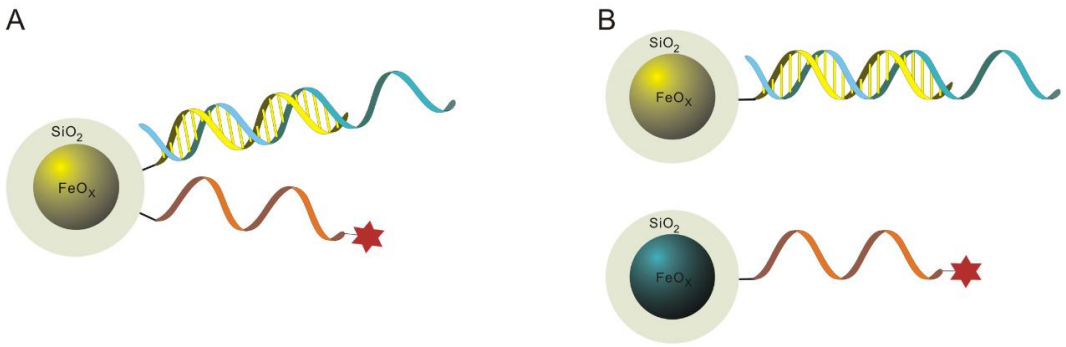

Figure 30: Schematic for the one-conjugate and the two-conjugate DNAzyme approach. Part A shows the one-conjugate system, in which DNAzyme/inhibitor duplex and substrate strand are bound to an identical nanoparticle. Part B is the established two-conjugate system, in which the DNA duplex and substrate strand are separately coupled to nanoparticles.

Again, the one-conjugate system was investigated by varying the molar ratios between DNAzyme and inhibitor strand. The L-DNAzyme/inhibitor2 duplex, prepared under different molar ratios between DNAzyme and inhibitor strand, was coupled to nanoparticle with a two-step sulfo-SMCC reaction. Uncoupled oligonucleotides were removed from L-DNAzyme/inhibitor2-NP conjugates. The NP-duplex conjugates were further reacted with the L-substrate strands leading to the formation of nanoparticles carrying both, DNAzyme/inhibitor duplexes and fluorescently labeled substrate strands. This one-conjugate system, prepared under different molar ratios between DNAzyme and inhibitor strand, was then investigated for its ability to deliver a thermosensitive controlled dye release (Fig. 31). The highest thermosensitivity (dye release at 49°C over dye release at 37°C; see above) was obtained, when the DNA duplexes were prepared at a molar ratio of 1:1. Again, the highest dye release was achieved at a molar ratio of 2:1.

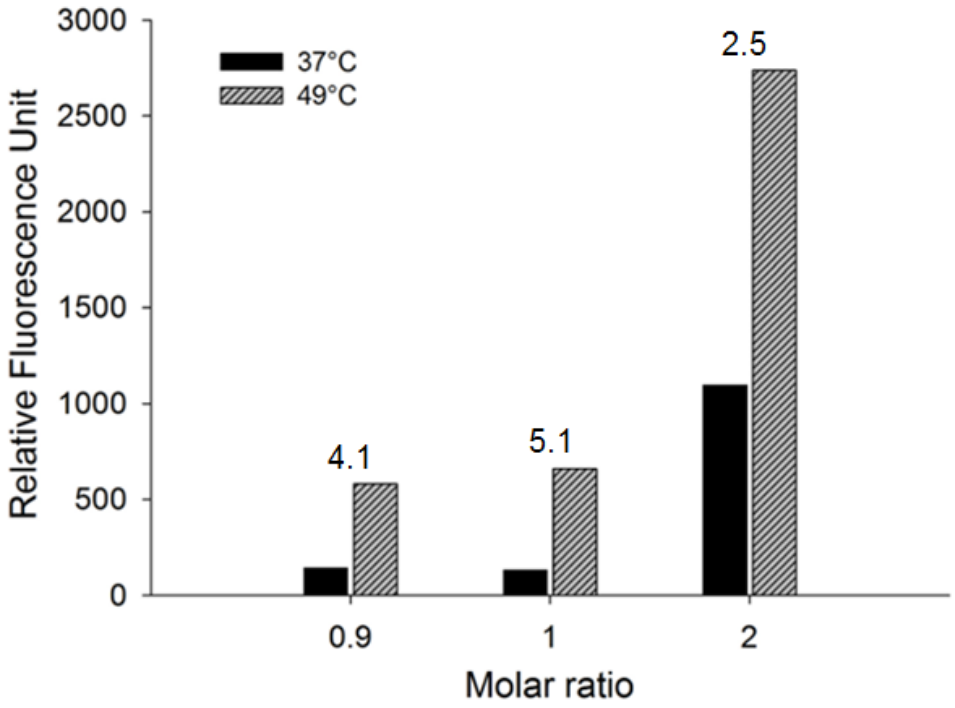

Figure 31: Release experiments of the one-conjugate DNAzyme approach. The duplexes of DNAzyme/inhibitor2 with different molar ratios were coupled to nanoparticles, forming the NP-DNAzymes/inhibitor2 conjugates. After removal of the uncoupled oligonucleotides, the NP-duplex conjugates were further coupled with L-substrate strands. The prepared one-conjugate system with different molar ratios was incubated for 1 h at 37°C or 49°C. The RFU values in the supernatants were determined by a NanoDrop 3300 Fluorospectrometer. The numbers above the bar-sets are the defined thermosensitivity.

Due to the limited materials, the results were obtained from a single experiment with mirror-image oligonucleotides. However, it may indicate the potential problem of undesired drug release at body temperature in contrast with the two-conjugate system (Fig. 32). Both two systems achieved an efficient dye release at 49°C (21%). The dye release at 37°C of the one-conjugate system was higher (8.35%) than that of the two-conjugate system (0.47%). Therefore, the two-conjugate system was demonstrated to be advantageous in the term of reducing drug release at body temperature.

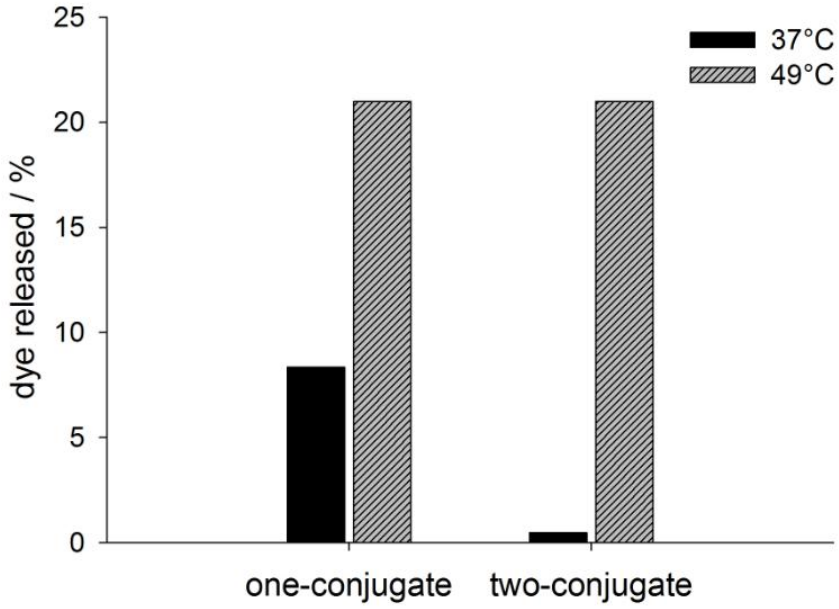

Figure 32: Thermally controlled dye release of one-conjugate and two-conjugate system. The DNA duplexes in both systems were prepared with molar ratio of 2 between L-DNAzyme and L-inhibitor2 strand. After preparation of conjugates for both systems, the L-DNAzyme/inhibitor2-substrate-NP conjugates and the mixture of L-DNAzyme/inhibitor2-NP and L-substrate-NP conjugates were both incubated for 1 h at 37°C or 49°C, respectively.

5 Discussion

Two approaches were developed and investigated for thermosensitive controlled drug release. In the thermozyme approach, a thermo-responsive self-cleaving ribozyme (thermozyme) was intended to be used as a thermolabile linker between nanoparticle and drug. Since there was no reported thermozyme yet, an *in vitro* selection experiment was performed to obtain such thermozymes from random RNA sequences (Chapter 5.1). Due to the unsatisfying results of thermozyme selection, a DNAzyme approach was developed for an efficient thermally controlled drug release from nanoparticles by taking advantage of dsDNA thermosensitivity and DNAzyme catalysis. The nucleic acid components in this system were turned into mirror image counterparts to attain substantial stability under *in vivo* conditions (Chapter 5.2). Finally, a clinical prospect of this novel DNAzyme-based nanoparticle-drug release system was envisaged for the combined chemo-hyperthermia treatment of human cancers (Chapter 5.3).

5.1 The Thermozyme Approach

An iterative *in vitro* selection and amplification procedure was used to isolate thermozymes from a starting pool of random RNA sequences. The thermozyme candidates should be able to cleave themselves efficiently under hyperthermic temperatures (40 – 50°C), while they should remain inactive under body temperature (37°C). Thus, the selected candidates would be used as a thermolabile linker between nanoparticles and cytotoxic drugs for a thermally controlled drug release.

A pool of about 10^{14} RNA variants was used for the selection of thermozymes that can distinguish a small temperature change. The RNA molecules were at first

incubated at body temperature of 37°C to remove undesired variants that would self-cleave under these conditions. The intact RNA precursors were recovered from denaturing gels and incubated at increased temperatures of 40 – 50°C. The variants able to self-cleave were recovered from denaturing gels and amplified by RT-PCR. An enriched full-length dsDNA pool was then prepared by ligation and transcribed to yield a new pool of RNA variants for the next round of selection. The stringency of selection was steadily increased in later rounds, *i.e.*, Mg^{2+}concentrations and incubation times at increased temperatures were declined gradually, while incubation times at body temperature were increased. Finally, a near-physiological condition with 2 mM Mg^{2+} was used to ensure the activity of thermozymes under *in vivo* conditions. An increased temperature range from 40°C to 50°C was used to mimic hyperthermia, as well as to encourage individual variants to explore alternate conformations, so that fewer thermozyme candidates might be locked in inactive metastable conformations (Bartel and Szostak, 1993).

In addition, mutagenic PCR was performed to introduce random mutations from rounds 7 to 11 on the purpose of generating more active variants. It is worth noting that a strong self-cleavage (12.5%) at 37°C was observed at round 10, while less than 5% self-cleavage was obtained at increased temperatures of 40 – 50°C from the uncleaved RNA precursors. Further enrichment of thermozyme was, however, unobserved after four additional rounds of selection. Hence, the currently applied selection procedure was shown to be unable to yield enriched thermozyme candidates.

To my knowledge, there have been no previous reports of the isolation of thermo-responsive self-cleaving ribozymes. It is conceivable that there may be no variant in the starting RNA pool that would be able to cleave itself in the desired thermally controlled manner. This assumption is supported by the fact that the RNA variants from round 10 showed a significant cleavage at 37°C even after three rounds of stringent negative selection that were supposed to remove any RNA motif

active at body temperature. Hence, it is conceivable that the self-cleaving ribozymes active under increased temperatures of 40°– 50°C are also prone to cleave themselves at body temperature of 37°C.

Alternatively, there may have been thermozyme candidates in the starting pool, but the applied selection procedure failed to sufficiently enrich them. The selection procedure imposes additional selection criteria besides the pursued property of thermo-responsive self-cleavage. The potential thermozyme motifs are required to be reverse-transcribed into cDNA and then efficiently amplified via PCR to be preserved and enriched during each selection cycle.

The thermozyme candidates need to be active during the selective step. This implies that they maintain a complex and stable structure at 40 – 50°C. The active candidates, however, are required to offer an accessible structure for reverse transcriptases at 50°C, since the enzymes employed will be inactivated at higher temperatures. Obviously, there is a structural conflict between self-cleavage and cDNA synthesis in the experimental strategy. This conflict may be solved by the use of reverse transcriptases that are active at temperatures above 50°C. Baranauskas and his colleagues (2012) designed a mutant reverse transcriptase through compartmentalized ribosome display evolution that is thermostable up to 62°C and is now distributed by Life Technologies (USA). Moreover, Life Technologies offers a Thermo-X™ reverse transcriptase that is thermostable up to even 70°C. These novel enzymes might allow efficient cDNA synthesis from thermozyme candidates that maintain a complex structure at 50°C and could thus enable the successful identification of a thermozyme.

In addition, an amplification bias might also impose problems on the efficient amplification of potential motifs, which is considered to be common for the conventional one-compartment PCR. Templates with simple structures are preferentially amplified over variants with a more complex structure. This bias is

able to be significantly reduced through emulsion PCR by separating the templates into individual reaction compartments. The template oligonucleotides can only be amplified at the expense of the resources contained within each emulsion cell. Hence, it could be worth trying to repeat the selection process by using a highly thermostable reverse transcriptase in combination with emulsion PCR.

5.2 The DNAzyme Approach

A DNAzyme approach was developed due to unsatisfying results of the thermozyme selection. In this project, the DNAzyme and the RNA substrate were separately immobilized to iron oxide nanoparticles. The substrate strand functions as linker between nanoparticle and cytotoxic drug. The DNAzyme strand was immobilized indirectly through hybridizing it to a complementary strand that is covalently coupled to a nanoparticle. Thus, the complementary strand, termed as inhibitor strand, prevents the cleavage of the RNA substrate by the DNAzyme. The DNAzyme/inhibitor duplex remains intact under body temperature, while DNAzyme strands will dissociate from the inhibitor strands upon heat. Released DNAzymes will attack the substrate strands, resulting in drug release. Moreover, the cleavage reaction is not stoichiometric, but catalytic, which means multiple cleavages can be achieved by each released DNAzyme strand.

A RNA-cleaving DNAzyme, 10-23 DNAzyme, was chosen due to its small size and reported high tolerance of low Mg^{2+} concentrations (Santoro and Joyce, 1998; Kurreck *et al*., 2002). The 10-23 DNAzyme, isolated by *in vitro* selection from a pool of random DNA sequences (Santoro and Joyce, 1997), is one of the best-studied and most widely used RNA-cleaving DNAzymes. The catalytic core of the 10-23 DNAzyme is composed of an unstructured loop formed by 15 nucleotides. Moreover, 10-23 DNAzymes have been widely utilized to suppress a number of viral and endogenous target genes in cell culture studies and also *in vivo* via

sequence-specific cleavage of RNA.

The sequence of the RNA substrate was designed by referring to a previous publication from Santoro and Joyce (1998), in which 5'-GU-3' was proven to be a better cleavage site than others. Two binding arms each in length of 8 nucleotides were chosen instead of 7 nucleotides due to its higher catalytic efficiency.

Two inhibitor strands that vary in length by 4 nucleotides were designed and screened by their ability to deliver a thermally controlled release of the hybridized DNAzymes through monitoring the concomitant cleavage of radioactively labeled RNA substrates. The hybrids between DNAzymes and the shorter inhibitor strands at molar ratios between 0.9:1 and 1.01:1 were able to cleave the substrates in a thermally controlled manner (Fig. 16). It is worth noting that the DNAzymes cleaved the substrates more efficiently at 49°C than at 37°C. The decreased activity of DNAzyme under body temperature might be due to the slower recycling of the DNAzymes, since the dissociation of the DNAzyme from the cleaved fragments may become a reaction limiting step. Under hyperthermic temperatures, however, the DNAzymes would dissociate quickly from the cleaved fragments and attack the next substrate. Therefore, the enhanced temperature, necessary to release DNAzyme from the inhibitor strand, was beneficial for the purpose of this project.

Sulfo-SMCC was reported to be superior to other commonly used crosslinkers such as sulfo-GMBS, EDC and PDITC, in terms of binding efficiency and specificity for coupling oligonucleotides to amino-functionalized iron oxide nanoparticles (Gao, 2011). Consequently, after investigating the DNAzyme cleavage with unbound substrates and inhibitors, the thiol-modified oligonucleotides were coupled to nanoparticles by using sulfo-SMCC as a linker. The results indicated that on average 16 substrate strands can be efficiently coupled to one nanoparticle. This result is in accord with the work of Gao (2011), who coupled about 15 RNA strands per nanoparticle. The NP-substrate conjugates would have about 2.3×10^{12}

substrates per cm^2 assuming that the superparamagnetic iron oxide nanoparticles of 15 nm in size were perfect spheres. This density also concur with another reported immobilization efficiency of approximately 5×10^{12} molecules per cm^2 using sulfo-SMCC to link thiol-DNA to an amine-surface (reviewed by Pirrung, 2002).

The 16 coupled substrates are few in contrast with the previously reported 550 primary amino groups on each nanoparticle, which was revealed by a colorimetric NBA assay (Gao, 2011). The low immobilization efficiency is likely due to steric hindrances, since the RNA substrate with 17 nucleotides is a large molecule compared to the nitrobenzaldehyde used in the colorimetric assay. In addition, repulsive electrostatic forces between the polyanionic RNA strands might also account for the low density of coupled substrates per nanoparticle.

Initially, the NP-substrate conjugates prepared by the two-step sulfo-SMCC coupling reaction were unstable. The coupled dyes can not be released efficiently from the NP-substrate conjugates after extended storage in PBS (pH 6.7) when treated with free DNAzymes. The blocked dye release may be due to the undesired interaction between nanoparticle and substrate. The large number of unreacted maleimide groups, as mentioned above, might react with the primary amino groups from adenine, guanine or cytosine via a nucleophilic addition mechanism resulting in the formation of a stable secondary amine linkage. Based on this assumption, a small thiol-carrying molecule GSH was chosen to block the unreacted maleimide groups. The GSH-treated NP-substrate conjugates exhibited an efficient dye release after extended incubation in PBS (pH 6.7). Therefore, the blocking of the unreacted maleimide groups by GSH may prevent the formation of undesired covalent bonds that would anchor the single-stranded substrate strands tightly to the nanoparticle surface and impede the approximation of DNAzyme to substrate strand.

The task of the pursued system is the thermally controlled dissociation of DNAzyme/inhibitor duplexes, which was achieved by varying the molar ratio between DNAzyme and inhibitor strand during duplex preparation. After coupling the duplex to nanoparticle, the amount of released DNAzyme was indirectly quantified by its ability to cleave the immobilized substrate strand from another nanoparticle. A fluorescent dye at the 3'-terminus of the substrate strand was used as reporter group to monitor the cleavages. By defining the thermosensitivity as dye release at increased temperature over release at body temperature, it was found that a sufficient thermosensitivity was obtained when DNAzymes/inhibitor duplexes were prepared at a molar ratio of 2:1. Under this ratio each inhibitor strand is likely to form a duplex with a DNAzyme. The dye release at 49°C was demonstrated to be significantly higher (21.8%) than at 37°C (1.1%), suggesting that this DNAzyme-based approach is feasible for an efficient thermally controlled drug release. Hence, the DNAzyme/inhibitor duplex is rather stable at body temperature, while the dissociation of the duplex is triggered at increased temperature.

The successful translation of this DNAzyme approach for a thermally controlled drug release in humans would rely on the stability of all components involved. The nucleic acids, however, are easily degraded by abundant nucleases present under *in vivo* conditions leading to the annihilation of the drug release system. Apart from the stability of the conjugates, the *in vivo* stability of the oligonucleotides was guaranteed by transforming them into mirror-image forms that are virtually undegradable by all kinds of nucleases present under *in vivo* conditions due to their chiral specificities (Klussmann *et al.*, 1996; Nolte *et al.*, 1996).

Initially, a comparative stability assay of D- and L-form DNAzymes in human serum was performed to assess their resistance against nuclease degradation. The result demonstrated that the D-DNAzymes were almost completely degraded after 24 h, while the degradation of the L-DNAzymes was undetectable even after 48 h. Thus, the transformation of D-DNAzymes to mirror-image L-DNAzymes is sufficient for their

stability *in vivo*.

The assay of the cleavage of L-substrate strands by either D-DNAzymes or L-DNAzymes was carried out to confirm whether the mirror-image L-DNAzymes could still cleave the L-substrate strands. The result showed that the L-substrate can only be cleaved by the L-DNAzymes rather than through reciprocal cleavage by D-DNAzymes, approving the strict chiral specificities between DNAzyme and substrate.

After preparation of the conjugates (L-DNAzyme/inhibitor2-NP and L-substrate-NP), release experiments in reaction buffer were performed to investigate, whether the L-form system can inherit the ability of thermally controlled drug release from the D-form system. The dye release at 49°C was demonstrated to be significantly higher (21%) than at 37°C (0.47%), suggesting that the DNAzyme-based approach in its mirror-image L-form is feasible for an efficient thermally controlled drug release, which is in accord with the earlier result obtained from the natural D-form system.

To evaluate the efficacy of this two-conjugate system under simulated *in vivo* conditions in view of future clinical applications, release assays were performed in human serum. The dye release at 49°C was demonstrated to be significantly higher (25.2%) than at 37°C (1.2%) after 3 h incubation in human serum. In addition, the release at 37°C remains as low as the negative control (1%). A more than 20-fold higher dye release was triggered at increased temperature than at body temperature.

This established DNAzyme approach could be turned into a thermally controlled drug release system, when the coupled dyes are replaced by chemotherapeutic drugs. In addition, the DNAzyme-based system is inherently compatible with the reported magnetic fluid hyperthermia (MFH), since the oligonucleotides were immobilized to superparamagnetic iron oxide nanoparticles that can be efficiently heated up by an alternating magnetic field (AMF). Thus, the two-conjugate DNAzyme-based

nanoparticle-drug release system could present a new application for combined chemo-hyperthermia against solid tumors.

Apart from the thermosensitivity and release efficiency, the established two-conjugate DNAzyme approach may be advantageous in comparison to a one-conjugate drug release system in terms of reducing undesired side effects. To test this assumption, the two-conjugate system was rendered into a one-conjugate system, in which the L-DNAzyme/inhibitor duplex and the L-substrate strand are both bound to the same nanoparticle. Due to the limited amount of mirror-image oligonucleotides, the release experiments of the one-conjugate system were only performed once in reaction buffer. Thus, the results are mere indicative rather than conclusive.

The data from the release experiments showed that the one-conjugate system can achieve an efficient dye release (21%) at increased temperature like the two-conjugate system. The dye release at body temperature of the one-conjugate system, however, is much higher (8.35%) than that of the two-conjugate system (0.47%). It is conceivable that a released DNAzyme is likely to associate with substrate strands in the one-conjugate system due to their proximity. In contrast, a released DNAzyme in the two-conjugate system is more likely to reanneal to an adjacent inhibitor strand as compared to hybridize with a substrate on a distant nanoparticle. Hence, it is conceivable that the two-conjugate system may be superior to the one-conjugate system in terms of reducing undesired drug release at body temperature.

How do these results compare with the performance of other reported strategies in which nucleic acid duplexes were used as thermosensitive molecules? Double-stranded DNAs, as naturally occurring biological molecules, were reported to be used as gatekeepers for a thermally controlled release of drugs that were preloaded inside a mesoporous silica nanoparticle (Schlossbauer *et al.*, 2010; Chen

et al., 2011; Ruiz-Hernández *et al.*, 2011). Duplex DNA was anchored to the openings of the nanoparticle and was utilized as a cap for trapping the guest cytotoxic drugs within the porous channels. It is worth noting, however, that the release experiments in all three dsDNA-gatekeeping strategies were conducted under buffer conditions rather than in human serum.

Biotin-labeled DNA duplex was attached to the opening pore of the nanoparticle in the work of Schlossbauer *et al.* (2010), allowing a subsequent closing of the pores by the protein avidin. DNA duplexes of two different lengths (15 bp and 25 bp) with melting temperatures (Tm) of 56°C and 76°C were used as gatekeepers and investigated for their thermo-responsive release of guest fluorescein molecules, respectively. When all intensity values were normalized to the highest obtained fluorescent count of the respective sample, the 15 bp duplex system achieved 3% relative release after 1 h incubation at 25°C, while 100% relative release was observed after 30 min incubation at 45°C. The 25 bp duplex system achieved 3% relative release after 1 h incubation at 25°C, 3.6% relative release after 1 h incubation at 45°C and 100% relative release after 30 min incubation at 65°C. It would be more appropriate, however, to investigate the background release at body temperature (37°C) rather than at 25°C in view of a potential clinical application.

In the work from Chen *et al.* (2011), a self-complementary duplex DNA of 14 nucleotides with a melting temperature (Tm) of 41°C was anchored to the openings of the nanoparticle and was utilized as a cap for trapping the guest cytotoxic drugs within the porous channels. An efficient release of guest molecules (78%) was reported after 2 h incubation at an elevated temperature (50°C), while the release at 25°C was about 3.6%. Here again, this system is unable to be applied directly in the clinical context, since the study addressed the background release at 25°C rather than at body temperature of 37°C.

It is conceivable that a high amount of drug release at body temperature may occur

since the melting temperature of this duplex DNA is about 40°C. This assumption is confirmed by another dsDNA-based gatekeeping strategy where a 15 bp DNA duplex with a melting temperature of 49°C was used to trap the guest molecules. Ruiz-Hernández *et al.* (2011) reported that 40% of the guest molecules were released after incubation for 40 min at 37°C. Hence, a strategy based on mere dissociation of DNA duplexes may be unable to achieve the desired thermally controlled drug release.

In my thesis, the predicament of how to avoid undesired drug release under body temperature while maintaining a sufficient release under elevated temperatures was circumvented by the introduction of a catalytic DNAzyme. Here, the dissociation of DNA duplexes is combined with a multiple cleavage of substrate strands by released DNAzymes. A DNA duplex of 22 bp with a melting temperature of about 66°C was applied as the thermosensitive molecule. Unlike the gatekeeping strategies requiring a sufficient dissociation of dsDNA molecules to achieve the desired drug release, this approach requires only a small amount of dissociated DNAzymes under hyperthermic temperatures. The limited dissociation events are then catalytically amplified by repetitive cleavage of substrate strands leading to a sufficient drug release in a thermally controlled manner.

Gao (2011) reported a similar strategy for thermally controlled drug release from nanoparticles, which relies on a thermally controlled dissociation of RNA/DNA hybrids and resultant cleavage of drug-carrying substrates by released hammerhead ribozymes. A fluorescent dye was used as a substitute for the cytotoxic drug. In reaction buffer, the dye release at increased temperature of 49°C was shown to be about 12-fold higher than the release at 37°C. To simulate its efficacy under *in vivo* conditions, release experiments were performed in human serum. The result showed that dye release at increased temperature of 49°C is about 3-fold higher than release at the body temperature of 37°C. Hence, the ribozyme-based system may be insufficient for future clinical developments.

The hammerhead ribozyme used in this strategy was in its minimal form, which was reported to be suboptimal for *in vivo* function due to its limited tolerance of a low concentration of Mg^{2+} (Khvorova *et al*., 2003; Uhlenbeck, 2003). The minimal hammerhead ribozyme is fully active in the presence of at least 10 mM Mg^{2+}. Its activity would decline quickly along the decreasing concentration of Mg^{2+}. Since the concentration of Mg^{2+} in human serum is about 0.46 – 0.6 mM (Ising *et al*., 1995), it is predictable that a system based on hammerhead ribozymes will display a low drug release in human serum.

Hence, a small 10-23 DNAzyme with both higher catalytic activity and tolerance of low concentrations of Mg^{2+} was chosen for this project, demonstrating a substantial improvement of thermally controlled dye release in human serum. The dye release at increased temperature of 49°C was 20-fold higher than the release at the body temperature of 37°C, presenting a promising strategy for combined thermo-chemotherapy.

In addition, the current development of a DNAzyme-based strategy has a further advantage over a ribozyme-based approach, since the chemical synthesis of DNA is more cost-effective than the preparation RNA. In contrast to the DNA synthesis, the phosphoramidite-based RNA synthesis requires an extra protection of the 2'-hydroxyl group. The protective group used for 2'-protection should be neither acid-labile nor alkali-labile due to the course of the synthesis scheme. The established solid-phase synthesis of RNA employs silyl groups for this purpose leading to significant loss of materials in the preparation of RNA phosphoramidites. In addition, even trace impurities of the phosphoramidite building blocks will result in a significant amount of full-length by-products. Furthermore, the spacious silyl groups impose steric hindrance for the coupling reaction leading to an extended reaction time and a decreased yield of desired products. Hence, the coupling efficiency of RNA synthesis is lower (98%) than that of DNA synthesis (99.8%). This small difference in cycle leads to a serious loss in yields over the course of multiple couplings needed to

synthesize a full-length oligonucleotide. Moreover, a large-scale (up to 1 kg) chemical synthesis of oligonucleotides is required in clinical settings, which means huge volumes and amounts of expensive solvents and reagents would be wasted due to the inherent problem of 2'-hydroxyl groups. Thus, the DNAzyme-based strategy can greatly reduce the production cost compared to the ribozyme-based approach in a clinical context.

In conclusion, an efficient thermally controlled drug release system was established by taking advantage of the thermosensitivity of duplex DNA and the catalytic property of a DNAzyme. A hyperthermia induced local chemotherapy could be achieved, once the fluorescent dyes are replaced by cytotoxic drugs. Compared with either hyperthermia or chemotherapy alone, this combined chemo-hyperthermia would provide a more effective outcome of anti-tumor treatment due to the additive and synergistic effects between local hyperthermia and chemotherapy.

5.3 Outlook

One of the main challenges in cancer treatment is the administration of active doses of chemotherapeutic drugs to a tumor site while sparing the normal tissues from severe side effects. Over the past years, there has been increasing effort in developing stimuli-responsive nanosystems capable of achieving both spatial and temporal effective release of chemotherapeutic cargos at the target site. Numerous nanosystems have been developed for controlled drug release in response to a variety of endogenous or exogenous stimuli such as pH change, enzymatic activity, redox activation, photoirradiation and temperature change (Mura *et al.*, 2013).

Nanosystems in response to exogenous stimuli are considered to be more advantageous in terms of spatiotemporal control over drug release (Blum *et al.*, 2014). A thermo-responsive nanosystem based on superparamegnetic

nanoparticles holds great promise, since magnetic fluid hyperthermia (MFH) alone proved to be clinically effective against solid tumors (Thiesen and Jordan, 2008). Moreover, local hyperthermia can sensitize cancer cells to the concomitant chemotherapy (Hildebrandt *et al*., 2002).

In view of combined chemo-hyperthermia treatment of solid tumors, this DNAzyme strategy could improve the established NanoTherm® Therapy of MagForce Nanotechnology AG (Germany). Currently, the site and the size of tumors inside a patient could be determined by different *in vivo* imaging technologies that could even monitor the progress of therapy. Hence, the NP-oligonucleotide conjugates loaded with cytotoxic drugs can be directly injected into tumors guided by the cancer imaging system. The concentrated conjugates inside the tumor tissue can then be efficiently heated by an externally applied AMF leading to a concentrated local hyperthermia. More importantly, the local hyperthermia would trigger an efficient release of cytotoxic drugs leading to a concentrated local chemotherapy. Finally, the combined local hyperthermia and chemotherapy may erase the tumor in a more effective way than either hyperthermia or chemotherapy could accomplish alone.

Due to the abundant vasculatures and leaky fenestrations of the neovasculatures inside the tumor tissue, part of the injected conjugates could escape from the target site and be circulated to non-pathogenic tissue of a patient, such as liver, spleen and kidney. The two-conjugate DNAzyme strategy, however, would greatly reduce the chance of undesired drug release by anchoring the DNAzymes and the drug-loaded substrates onto separate nanoparticles. The limited amount of escaped conjugates would be quickly diluted in the circulation system away from injection site. Therefore, it is conceivable that the accumulation of two various conjugates in a same cell of non-pathogenic tissue might be unlikely. Even though there is accumulation of two various conjugates in same cells, a sufficient drug release remain impossible since the external AMF is applied specifically to tumor tissue. Therefore, the two-conjugate

DNAzyme strategy seems to be superior to other reported one-conjugate thermally controlled drug release systems in terms of sparing non-target tissues.

More importantly, this two-conjugate DNAzyme-based nanoparticle-drug release system can be further functionalized with cancer-targeting aptamers that would guide the conjugates specifically into the cancer cells. In this case, the aptamer-functionalized conjugates may even be administrated intravenously into a patient without requiring the precise location of the tumors. This strategy could be of special value to target metastatic tumors. The conjugates would accumulate at different tumor locations through blood circulation due to their targeting abilities. Hyperthermia generated by AMF, in this case, would need to be applied to larger areas to trigger the desired drug release. The chance of undesired drug release and its resultant side effects towards non-pathogenic tissues, however, would still be significantly reduced, since the release of coupled drugs from conjugates depends on both, the remotely applied hyperthermia and the local concentration of the two conjugates.

This DNAzyme-based strategy can satisfy the two most important criteria for successful therapy, *i.e.*, spatial placement and temporal delivery. Hence, I envisage that the established two-conjugate DNAzyme-based nanoparticle-drug release system presents a novel combined local chemo-hyperthermia with improved therapeutic effects against solid tumors and may be of value to fight metastatic tumors in combination with cell-specific aptamers.

6 Summary

Two approaches were designed for a thermally controlled release of drugs from nanoparticles. In the first project, a *cis*-cleavage strategy was pursued to develop a novel, self-cleaving ribozyme (termed thermozyme) that renders active upon heat. This thermozyme would be employed as a temperature-sensitive linker between nanoparticle and drug. While it should remain inactive at body temperature, the thermozyme should cleave itself at hyperthermic temperatures of 40 – 50°C releasing the attached drug. An *in vitro* selection and amplification procedure was utilized to identify thermozyme candidates from a large pool of random RNA sequences. No candidates with the pursued properties could be enriched from the starting pool. The absence of desired catalysts contrasts with successful experiments to develop novel ribozymes and suggests that other strategies may be needed to identify thermozymes.

In the second project, a *trans*-cleavage strategy was developed in combination with a catalytic DNA for the controlled release of drugs from nanoparticles. Upon heat, DNAzymes were dissociated from their complementary strands that were attached to nanoparticles. These thermally released DNAzymes could then *trans*-cleave RNA substrate strands bridging nanoparticles and drugs. Furthermore, the oligonucleotides used were replaced by their enantiomeric isomers to ensure extended *in vivo* stability. This thermally controlled drug release system was successfully investigated with a fluorescent dye as a drug substitute in human serum, establishing a more than 20-fold higher release at increased temperature than at body temperature. The results demonstrated a promising prospect towards a hyperthermia induced local chemotherapy for the treatment of solid tumors.

7 Zusammenfassung

Zwei Vorhaben wurden für eine thermisch kontrollierte Wirkstofffreisetzung von Nanopartikeln bearbeitet. Im ersten Projekt wurde eine Strategie verfolgt, um ein neuartiges Ribozym (Thermozym) zu entwickeln, das sich durch thermische Anregung selbst (in *cis*) spalten kann. Diese Thermozym würde als Temperatur-sensitiver Linker zwischen Nanopartikel und Wirkstoff eingesetzt werden. Während es bei Körpertemperatur inaktiv bleiben sollte, würde sich bei hyperthermischen Temperaturen von 40 – 50°C das Thermozym selbst spalten und den Wirkstoff freisetzen. Um Thermozyme aus einer zufälligen Bibliothek von RNA-Sequenzen zu identifizieren, wurde ein Verfahren zur *in vitro*-Selektion und Amplifikation eingesetzt. Allerdings konnten keine Kandidaten mit den angestrebten Eigenschaften angereichert werden. Die Abwesenheit möglicher Kandidaten steht im Gegensatz zu erfolgreichen Selektionen anderer Ribozyme, so dass veränderte Strategien erforderlich werden, um potentielle Thermozyme zu entwickeln.

Im zweiten Projekt wurde eine *trans*-Spaltungsstrategie in Kombination mit einer katalytischen DNA für die kontrollierte Wirkstofffreisetzung von Nanopartikeln entwickelt. Durch Wärmezufuhr wurden DNAzyme von Nanopartikel-gebundenen Komplementärsträngen dissoziiert. Diese thermisch freigesetzten DNAzyme konnten RNA-Substratstränge (in *trans*) spalten, die als Brücke zwischen Nanopartikeln und Wirkstoffen dienen. Weiterhin wurden die verwendeten Oligonukleotide durch ihre enantiomeren Isomere ersetzt, um eine verlängerte *in vivo* Stabilität zu gewährleisten. Dieses thermische gesteuerte Freisetzungssystem für Wirkstoffe konnte erfolgreich mit einem Fluoreszenzfarbstoff als Wirkstoffersatz in Humanserum getestet werden, wobei eine mehr als 20-fache Freisetzung bei erhöhter Temperatur im Vergleich zur Körpertemperatur erzielt wurde. Die Ergebnisse weisen auf einen vielversprechenden Ansatz zur Bekämpfung von soliden Tumoren durch Hyperthermie-induzierte lokale Chemotherapie.

8 References

Al-Ahmady, Z.S., W.T. Al-Jamal, J.V. Bossche, T.T. Bui, A.F. Drake, A.J. Mason, and K. Kostarelos. 2012. Lipid-peptide vesicle nanoscale hybrids for triggered drug release by mild hyperthermia in vitro and in vivo. *ACS Nano* 6:9335-9346.

Alexiou, C., W. Arnold, R.J. Klein, F.G. Parak, P. Hulin, C. Bergemann, W. Erhardt, S. Wagenpfeil, and A.S. Luebbe. 2000. Locoregional cancer treatment with magnetic drug targeting. *Cancer research* 60:6641-6648.

Arruebo, M., R. Fernández-Pacheco, M.R. Ibarra, and J. Santamaría. 2007. Magnetic nanoparticles for drug delivery. *Nano today* 2:22-32.

Ayel, E., and C. Escude. 2010. In vitro selection of oligonucleotides that bind double-stranded DNA in the presence of triplex-stabilizing agents. *Nucleic acids research* 38:e31.

Baranauskas, A., S. Paliksa, G. Alzbutas, M. Vaitkevicius, J. Lubiene, V. Letukiene, S. Burinskas, G. Sasnauskas, and R. Skirgaila. 2012. Generation and characterization of new highly thermostable and processive M-MuLV reverse transcriptase variants. *Protein engineering, design and selection* 25:657-668.

Bartel, D.P., and J.W. Szostak. 1993. Isolation of new ribozymes from a large pool of random sequences. *Science* 261:1411-1418.

Bartlett, J.M., and D. Stirling. 2003. A short history of the polymerase chain reaction. *Methods in molecular biology* 226:3-6.

Berry, C.C., and A.S. Curtis. 2003. Functionalisation of magnetic nanoparticles for applications in biomedicine. *Journal of physics D: Applied physics* 36:R198-R206.

Bhattacharyya, S., R. Bhattacharya, S. Curley, M.A. McNiven, and P. Mukherjee. 2010. Nanoconjugation modulates the trafficking and mechanism of antibody induced receptor endocytosis. *Proceedings of the national academy of sciences* 107:14541-14546.

Blank, M., T. Weinschenk, M. Priemer, and H. Schluesener. 2001. Systematic evolution of a DNA aptamer binding to rat brain tumor microvessels. selective targeting of endothelial regulatory protein pigpen. *The journal of biological chemistry* 276:16464-16468.

Blum, A.P., J.K. Kammeyer, A.M. Rush, C.E. Callmann, M.E. Hahn, and N.C. Gianneschi. 2014. Stimuli-responsive nanomaterials for biomedical applications. *Journal of the american chemical society* 137(6):2140-2154.

Bock, L.C., L.C. Griffin, J.A. Latham, E.H. Vermaas, and J.J. Toole. 1992. Selection of single-stranded DNA molecules that bind and inhibit human thrombin. *Nature* 355:564-566.

Bornstein, B.A., P.S. Zouranjian, J.L. Hansen, S.M. Fraser, L.A. Gelwan, B.A. Teicher, and G.K. Svensson. 1993. Local hyperthermia, radiation therapy, and chemotherapy in patients with local-regional recurrence of breast carcinoma. *International journal of radiation oncology biology physics* 25:79-85.

Brazel, C.S. 2009. Magnetothermally-responsive nanomaterials: combining magnetic nanostructures and thermally-sensitive polymers for triggered drug release. *Pharmaceutical research* 26:644-656.

Breaker, R.R. 1997. In Vitro Selection of Catalytic Polynucleotides. *Chemical reviews* 97:371-390.

Bruce, I.J., and T. Sen. 2005. Surface modification of magnetic nanoparticles with alkoxysilanes and their application in magnetic bioseparations. *Langmuir* 21:7029-7035.

Bruno, J.G., and J.L. Kiel. 1999. In vitro selection of DNA aptamers to anthrax spores with electrochemiluminescence detection. *Biosensors and bioelectronics* 14:457-464.

Burd, R., T.S. Dziedzic, Y. Xu, M.A. Caligiuri, J.R. Subjeck, and E.A. Repasky. 1998. Tumor cell apoptosis, lymphocyte recruitment and tumor vascular changes are induced by low temperature, long duration (fever-like) whole body hyperthermia. *Journal of cellular physiology* 177:137-147.

Cadwell, R.C., and G.F. Joyce. 1992. Randomization of genes by PCR mutagenesis. *PCR methods and applications* 2:28-33.

Caruthers, M.H. 2013. The Chemical Synthesis of DNA/RNA: Our Gift to Science. *Journal of biological chemistry* 288:1420-1427.

Chen, C., J. Geng, F. Pu, X. Yang, J. Ren, and X. Qu. 2011. Polyvalent Nucleic Acid/Mesoporous Silica Nanoparticle Conjugates: Dual Stimuli-Responsive Vehicles for Intracellular Drug Delivery. *Angewandte chemie international edition* 50:882-886.

Cheng, J., B.A. Teply, I. Sherifi, J. Sung, G. Luther, F.X. Gu, E. Levy-Nissenbaum, A.F. Radovic-Moreno, R. Langer, and O.C. Farokhzad. 2007. Formulation of functionalized PLGA-PEG nanoparticles for in vivo targeted drug delivery. *Biomaterials* 28:869-876.

Cheng, R., F. Meng, C. Deng, H.A. Klok, and Z. Zhong. 2013. Dual and multi-stimuli responsive polymeric nanoparticles for programmed site-specific drug delivery. *Biomaterials* 34:3647-3657.

Cho, B.R., and Y. Lee. 2005. Isolation of new self-cleaving ribozymes with in vitro selection. *Bulletin of the korean chemical society* 26:2033-2037.

Choi, B.R., J. Gwak, H.M. Kwon, S. Oh, K.P. Kim, W.H. Choi, Y.H. Cho, and D.E. Kim. 2010. Oligodeoxyribozymes that cleave β-catenin messenger RNA inhibit growth of colon cancer cells via reduction of β-catenin response transcription. *Molecular cancer therapeutics* 9:1894-1902.

Daniels, D.A., H. Chen, B.J. Hicke, K.M. Swiderek, and L. Gold. 2003. A tenascin-C aptamer identified by tumor cell SELEX: Systematic evolution of ligands by exponential enrichment. *Proceedings of the aational academy of sciences* 100:15416-15421.

Dewey, W., L. Hopwood, S. Sapareto, and L. Gerweck. 1977. Cellular Responses to Combinations of Hyperthermia and Radiation 1. *Radiology* 123:463-474.

Dicheva, B.M., T.L.M. ten Hagen, D. Schipper, A.L.B. Seynhaeve, G.C. van Rhoon, A.M.M. Eggermont, and G.A. Koning. 2014. Targeted and heat-triggered doxorubicin delivery to tumors by dual targeted cationic thermosensitive liposomes. *Journal of controlled release* 195:37-48.

Dobson, J. 2006b. Gene therapy progress and prospects: magnetic nanoparticle-based gene delivery. *Gene therapy* 13:283-287.

Dobson, J. 2006a. Magnetic nanoparticles for drug delivery. *Drug development research* 67:55-60.

Edelman, E., J. Kost, H. Bobeck, and R. Langer. 1985. Regulation of drug release from polymer matrices by oscillating magnetic fields. *Journal of biomedical materials research* 19:67-83.

Ellis, R.J., and S.M. Van der Vies. 1991. Molecular chaperones. *Annual review of biochemistry* 60:321-347.

Fleige, E., M.A. Quadir, and R. Haag. 2012. Stimuli-responsive polymeric nanocarriers for the controlled transport of active compounds: concepts and

applications. *Advanced drug delivery reviews* 64:866-884.

Gao, J. 2011. A novel concept for hyperthermia induced local chemotherapy. PhD Dissertation, Free Univeisity of Berlin, Germany.

Geiger, A., P. Burgstaller, H. von der Eltz, A. Roeder, and M. Famulok. 1996. RNA aptamers that bind L-arginine with sub-micromolar dissociation constants and high enantioselectivity. *Nucleic acids research* 24:1029-1036.

Gilchrist, R., R. Medal, W.D. Shorey, R.C. Hanselman, J.C. Parrott, and C.B. Taylor. 1957. Selective inductive heating of lymph nodes. *Annals of surgery* 146:596.

Gneveckow, U., A. Jordan, R. Scholz, V. BRüSS, N. Waldöfner, J. Ricke, A. Feussner, B. Hildebrandt, B. Rau, and P. Wust. 2004. Description and characterization of the novel hyperthermia-and thermoablation-system MFH® 300F for clinical magnetic fluid hyperthermia. *Medical physics* 31:1444-1451.

Goodwin, S., C. Peterson, C. Hoh, and C. Bittner. 1999. Targeting and retention of magnetic targeted carriers (MTCs) enhancing intra-arterial chemotherapy. *Journal of magnetism and magnetic materials* 194:132-139.

Goodwin, S.C., C.A. Bittner, C.L. Peterson, and G. Wong. 2001. Single-dose toxicity study of hepatic intra-arterial infusion of doxorubicin coupled to a novel magnetically targeted drug carrier. *Toxicological sciences* 60:177-183.

Gordon, R., J. Hines, and D. Gordon. 1979. Intracellular hyperthermia a biophysical approach to cancer treatment via intracellular temperature and biophysical alterations. *Medical hypotheses* 5:83-102.

Guo, W., C.Y. Yang, H.M. Lin, and F.Y. Qu. 2014. P(EO-*co*-LLA) functionalized Fe_3O_4@mSiO_2 nanocomposites for thermo/pH responsive drug controlled release and hyperthermia. *Dalton transactions* 43:18056-18065.

Gupta, A.K., and M. Gupta. 2005. Synthesis and surface engineering of iron oxide nanoparticles for biomedical applications. *Biomaterials* 26:3995-4021.

Hafner, M., E. Vianini, B. Albertoni, L. Marchetti, I. Grune, C. Gloeckner, and M. Famulok. 2008. Displacement of protein-bound aptamers with small molecules screened by fluorescence polarization. *Nature protocols* 3:579-587.

Hamula, C.L., H. Zhang, L.L. Guan, X.F. Li, and X.C. Le. 2008. Selection of aptamers against live bacterial cells. *Analytical chemistry* 80:7812-7819.

Hardiansyah, A., L.Y. Huang, M.C. Yang, T.Y. Liu, S.C. Tsai, C.Y. Yang, C.Y. Kuo, T.Y. Chan, H.M. Zou, W.N. Lian, and C.H. Lin. 2014. Magnetic liposomes for colorectal cancer cells therapy by high-frequency magnetic field treatment. *Nanoscale research letters* 9:497

He, Y.Y., P.G. Stockley, and L. Gold. 1996. In vitro evolution of the DNA binding sites of *Escherichia coli* methionine repressor, MetJ. *Journal of molecular biology* 255:55-66.

Hildebrandt, B., and P. Wust. 2007. Interactions between Hyperthermia and Cytotoxic Drugs. *In "Peritoneal carcinomatosis" Springer US*: 185-193.

Hildebrandt, B., P. Wust, O. Ahlers, A. Dieing, G. Sreenivasa, T. Kerner, R. Felix, and H. Riess. 2002. The cellular and molecular basis of hyperthermia. *Critical reviews in oncology/hematology* 43:33-56.

Hu, S.H., B.J. Liao, C.S. Chiang, P.J. Chen, I.W. Chen, and S.Y. Chen. 2012. Core-shell nanocapsules stabilized by single-component polymer and nanoparticles for magneto-chemotherapy/hyperthermia with multiple drugs. *Advanced materials* 24:3627-3632.

Hu, S.H., S.Y. Chen, D.M. Liu, and C.S. Hsiao. 2008. Core/Single-Crystal-Shell Nanospheres for Controlled Drug Release via a Magnetically Triggered Rupturing Mechanism. *Advanced materials* 20:2690-2695.

Ilium, L., S. Davis, C. Wilson, N. Thomas, M. Frier, and J. Hardy. 1982. Blood clearance and organ deposition of intravenously administered colloidal particles. The effects of particle size, nature and shape. *International journal of pharmaceutics* 12:135-146.

Isaka, Y., H. Nakamura, M. Mizui, Y. Takabatake, M. Horio, H. Kawachi, F. Shimizu, E. Imai, and M. Hori. 2004. DNAzyme for TGF-beta suppressed extracellular matrix accumulation in experimental glomerulonephritis. *Kidney international* 66:586-590.

Ising, H., F. Bertschat, T. Günther, E. Jeremias, and A. Jeremias. 1995. Measurement of free magnesium in blood, serum and plasma with an ion-sensitive electrode. *Clinical chemistry and laboratory medicine 33*(6):365-372.

Issels, R.D., S. Abdel-Rahman, C. Wendtner, M.H. Falk, V. Kurze, H. Sauer, U. Aydemir, and W. Hiddemann. 2001. Neoadjuvant chemotherapy combined with regional hyperthermia (RHT) for locally advanced primary or recurrent high-risk adult soft-tissue sarcomas (STS) of adults: long-term results of a

phase II study. *European journal of cancer* 37:1599-1608.

Ito, A., K. Tanaka, K. Kondo, M. Shinkai, H. Honda, K. Matsumoto, T. Saida, and T. Kobayashi. 2003. Tumor regression by combined immunotherapy and hyperthermia using magnetic nanoparticles in an experimental subcutaneous murine melanoma. *Cancer science* 94:308-313.

Iversen, P.O., G. Nicolaysen, and M. Sioud. 2001. DNA enzyme targeting TNF-alpha mRNA improves hemodynamic performance in rats with postinfarction heart failure. *American journal of physiology. Heart and circulatory physiology* 281:H2211-2217.

Johannsen, M., U. Gneveckow, L. Eckelt, A. Feussner, N. Waldöfner, R. Scholz, S. Deger, P. Wust, S. Loening, and A. Jordan. 2005. Clinical hyperthermia of prostate cancer using magnetic nanoparticles: presentation of a new interstitial technique. *International journal of hyperthermia* 21:637-647.

Jolma, A., T. Kivioja, J. Toivonen, L. Cheng, G. Wei, M. Enge, M. Taipale, J.M. Vaquerizas, J. Yan, M.J. Sillanpaa, M. Bonke, K. Palin, S. Talukder, T.R. Hughes, N.M. Luscombe, E. Ukkonen, and J. Taipale. 2010. Multiplexed massively parallel SELEX for characterization of human transcription factor binding specificities. *Genome research* 20:861-873.

Jordan, A., R. Scholz, K. Maier-Hauff, M. Johannsen, P. Wust, J. Nadobny, H. Schirra, H. Schmidt, S. Deger, and S. Loening. 2001. Presentation of a new magnetic field therapy system for the treatment of human solid tumors with magnetic fluid hyperthermia. *Journal of magnetism and magnetic materials* 225:118-126.

Jordan, A., R. Scholz, P. Wust, H. Fähling, and R. Felix. 1999. Magnetic fluid hyperthermia (MFH): Cancer treatment with AC magnetic field induced excitation of biocompatible superparamagnetic nanoparticles. *Journal of magnetism and magnetic materials* 201:413-419.

Jordan, A., R. Scholz, P. Wust, H. Fähling, J. Krause, W. Wlodarczyk, B. Sander, T. Vogl, and R. Felix. 1997. Effects of magnetic fluid hyperthermia (MFH) on C3H mammary carcinoma in vivo. *International journal of hyperthermia* 13:587-605.

Jordan, A., P. Wust, H. Fähling, W. John, A. Hinz, and R. Felix. 2009. Inductive heating of ferrimagnetic particles and magnetic fluids: physical evaluation of their potential for hyperthermia. *International journal of hyperthermia* 25:499-511.

Jordan, A., P. Wust, H. Fahling, W. John, A. Hinz, and R. Felix. 1993. Inductive

heating of ferrimagnetic particles and magnetic fluids: physical evaluation of their potential for hyperthermia. *International journal of hyperthermia* 9:51-68.

Joyce, G.F. 1989. Amplification, mutation and selection of catalytic RNA. *Gene* 82:83-87.

Kampinga, H. 1995. Hyperthermia, thermotolerance and topoisomerase II inhibitors. *British journal of cancer* 72:333.

Kampinga, H.H. 2006. Cell biological effects of hyperthermia alone or combined with radiation or drugs: a short introduction to newcomers in the field. *International journal of hyperthermia* 22:191-196.

Kampinga, H.H., J.F. Keij, G. van der Kruk, and A.W. Konings. 1989. Interaction of hyperthermia and radiation in tolerant and nontolerant HeLa S3 cells: role of DNA polymerase inactivation. *International journal of radiation biology* 55:423-433.

Kawai, N., A. Ito, Y. Nakahara, M. Futakuchi, T. Shirai, H. Honda, T. Kobayashi, and K. Kohri. 2005. Anticancer effect of hyperthermia on prostate cancer mediated by magnetite cationic liposomes and immune-response induction in transplanted syngeneic rats. *The prostate* 64:373-381.

Khachigian, L.M., R.G. Fahmy, G. Zhang, Y.V. Bobryshev, and A. Kaniaros. 2002. c-Jun regulates vascular smooth muscle cell growth and neointima formation after arterial injury. Inhibition by a novel DNA enzyme targeting c-Jun. *The journal of biological chemistry* 277:22985-22991.

Khvorova, A., A. Lescoute, E. Westhof, and S.D. Jayasena. 2003. Sequence elements outside the hammerhead ribozyme catalytic core enable intracellular activity. *Nature structural biology* 10:708-712.

Kievit, F.M., and M. Zhang. 2011. Surface Engineering of Iron Oxide Nanoparticles for Targeted Cancer Therapy. *Accounts of chemical research* 44:853-862.

Kim, D.H., Y. Guo, Z. Zhang, D. Procissi, J. Nicolai, R.A. Omary, and A.C. Larson. 2014. Temperature-Sensitive Magnetic Drug Carriers for Concurrent Gemcitabine Chemohyperthermia. *Advanced healthcare materials* 3:714-724.

Klussmann, S., A. Nolte, R. Bald, V.A. Erdmann, and J.P. Furste. 1996. Mirror-image RNA that binds D-adenosine. *Nature biotechnology* 14:1112-1115.

Kobayashi, D., N. Kawai, S. Sato, T. Naiki, K. Yamada, T. Yasui, K. Tozawa, T. Kobayashi, S. Takahashi, and K. Kohri. 2013. Thermotherapy using magnetic cationic liposomes powerfully suppresses prostate cancer bone metastasis in a novel rat model. *The prostate* 73:913-922.

Kohler, N., C. Sun, J. Wang, and M. Zhang. 2005. Methotrexate-modified superparamagnetic nanoparticles and their intracellular uptake into human cancer cells. *Langmuir* 21:8858-8864.

Kost, J., R. Noecker, E. Kunica, and R. Langer. 1985. Magnetically controlled release systems: effect of polymer composition. *Journal of biomedical materials research* 19:935-940.

Kost, J., J. Wolfrum, and R. Langer. 1987. Magnetically enhanced insulin release in diabetic rats. *Journal of biomedical materials research* 21:1367-1373.

Kukowska-Latallo, J.F., K.A. Candido, Z. Cao, S.S. Nigavekar, I.J. Majoros, T.P. Thomas, L.P. Balogh, M.K. Khan, and J.R. Baker, Jr. 2005. Nanoparticle targeting of anticancer drug improves therapeutic response in animal model of human epithelial cancer. *Cancer research* 65:5317-5324.

Kumar, C.S.S.R., and F. Mohammad. 2011. Magnetic nanomaterials for hyperthermia-based therapy and controlled drug delivery. *Advanced drug delivery reviews* 63:789-808.

Kurreck, J., B. Bieber, R. Jahnel, and V.A. Erdmann. 2002. Comparative study of DNA enzymes and ribozymes against the same full-length messenger RNA of the vanilloid receptor subtype I. *The journal of bological chemistry* 277:7099-7107.

Lyer, A.K., G. Khaled, J. Fang, and H. Maeda. 2006. Exploiting the enhanced permeability and retention effect for tumor targeting. *Drug discovery today* 11:812-818.

Lübbe, A., and C. Bergemann. 1997. Selected preclinical and first clinical experiences with magnetically targeted 4’-epidoxorubicin in patients with advanced solid tumors. *In "Scientific and clinical applications of magnetic carriers"*, *Springer US*: 457-480.

Lübbe, A.S., C. Bergemann, J. Brock, and D.G. McClure. 1999. Physiological aspects in magnetic drug-targeting. *Journal of magnetism and magnetic materials* 194:149-155.

Lübbe, A.S., C. Bergemann, H. Riess, F. Schriever, P. Reichardt, K. Possinger, M. Matthias, B. Dörken, F. Herrmann, and R. Gürtler. 1996. Clinical experiences

with magnetic drug targeting: a phase I study with 4′-epidoxorubicin in 14 patients with advanced solid tumors. *Cancer research* 56:4686-4693.

Laurent, S., D. Forge, M. Port, A. Roch, C. Robic, L. Vander Elst, and R.N. Muller. 2008. Magnetic iron oxide nanoparticles: synthesis, stabilization, vectorization, physicochemical characterizations, and biological applications. *Chemical reviews* 108:2064-2110.

Le, B., M. Shinkai, T. Kitade, H. Honda, J. Yoshida, T. Wakabayashi, and T. Kobayashi. 2001. Preparation of tumor-specific magnetoliposomes and their application for hyperthermia. *Journal of chemical engineering of Japan* 34:66-72.

Lepock, J. 2004. Role of nuclear protein denaturation and aggregation in thermal radiosensitization. *International journal of hyperthermia* 20:115-130.

Lepock, J.R., H.E. Frey, and K.P. Ritchie. 1993. Protein denaturation in intact hepatocytes and isolated cellular organelles during heat shock. *The journal of cell biology* 122:1267-1276.

Li, G., N. Mivechi, and G. Weitzel. 1995. Heat shock proteins, thermotolerance, and their relevance to clinical hyperthermia. *International journal of hyperthermia* 11:459-488.

Liu, J., and G.D. Stormo. 2005. Combining SELEX with quantitative assays to rapidly obtain accurate models of protein-DNA interactions. *Nucleic acids research* 33:e141.

Liu, T.Y., and T.C. Huang. 2011. A novel drug vehicle capable of ultrasound-triggered release with MRI functions. *Acta biomaterialia* 7:3927-3934.

Liu, Y., Y. Wang, C. Wan, W. Zhou, T. Peng, Z. Wang, G. Li, G. Cornelisson, and F. Halberg. 2005. The role of mPer1 in morphine dependence in mice. *Neuroscience* 130:383-388.

Lorger, M., M. Engstler, M. Homann, and H.U. Goringer. 2003. Targeting the variable surface of African trypanosomes with variant surface glycoprotein-specific, serum-stable RNA aptamers. *Eukaryotic cell* 2:84-94.

Lu, A.H., E.e.L. Salabas, and F. Schüth. 2007. Magnetic nanoparticles: synthesis, protection, functionalization, and application. *Angewandte chemie international edition* 46:1222-1244.

Lu, Z., M.D. Prouty, Z. Guo, V.O. Golub, C.S. Kumar, and Y.M. Lvov. 2005.

Magnetic switch of permeability for polyelectrolyte microcapsules embedded with Co@ Au nanoparticles. *Langmuir* 21:2042-2050.

Ma, Y., X. Liang, S. Tong, G. Bao, Q. Ren, and Z. Dai. 2013. Gold nanoshell nanomicelles for potential magnetic resonance imaging, lght-triggered drug release, and photothermal therapy. *Advanced functional materials* 23:815-822.

Maeda, H., H. Nakamura, and J. Fang. 2013. The EPR effect for macromolecular drug delivery to solid tumors: Improvement of tumor uptake, lowering of systemic toxicity, and distinct tumor imaging in vivo. *Advanced drug delivery reviews* 65:71-79.

Maier-Hauff, K., R. Rothe, R. Scholz, U. Gneveckow, P. Wust, B. Thiesen, A. Feussner, A. von Deimling, N. Waldoefner, and R. Felix. 2007. Intracranial thermotherapy using magnetic nanoparticles combined with external beam radiotherapy: results of a feasibility study on patients with glioblastoma multiforme. *Journal of neuro-oncology* 81:53-60.

Maier-Hauff, K., F. Ulrich, D. Nestler, H. Niehoff, P. Wust, B. Thiesen, H. Orawa, V. Budach, and A. Jordan. 2011. Efficacy and safety of intratumoral thermotherapy using magnetic iron-oxide nanoparticles combined with external beam radiotherapy on patients with recurrent glioblastoma multiforme. *Journal of neuro-oncology* 103:317-324.

Matsumura, Y., and H. Maeda. 1986. A new concept for macromolecular therapeutics in cancer chemotherapy: mechanism of tumoritropic accumulation of proteins and the antitumor agent smancs. *Cancer research* 46:6387-6392.

Matsuoka, F., M. Shinkai, H. Honda, T. Kubo, T. Sugita, and T. Kobayashi. 2004. Hyperthermia using magnetite cationic liposomes for hamster osteosarcoma. *BioMagnetic research and technology* 2:3.

McCauley, T.G., N. Hamaguchi, and M. Stanton. 2003. Aptamer-based biosensor arrays for detection and quantification of biological macromolecules. *Analytical biochemistry* 319:244-250.

McNamara, J.O., E.R. Andrechek, Y. Wang, K.D. Viles, R.E. Rempel, E. Gilboa, B.A. Sullenger, and P.H. Giangrande. 2006. Cell type-specific delivery of siRNAs with aptamer-siRNA chimeras. *Nature biotechnology* 24:1005-1015.

McNeil, S.E. 2005. Nanotechnology for the biologist. *Journal of leukocyte biology* 78:585-594.

Michels, A.A., V.T. Nguyen, A.W. Konings, H.H. Kampinga, and O. Bensaude. 1995. Thermostability of a nuclear-targeted luciferase expressed in mammalian cells. *European journal of biochemistry* 234:382-389.

Mitchell, A., C.R. Dass, L.Q. Sun, and L.M. Khachigian. 2004. Inhibition of human breast carcinoma proliferation, migration, chemoinvasion and solid tumour growth by DNAzymes targeting the zinc finger transcription factor EGR-1. *Nucleic acids research* 32:3065-3069.

Moroz, P., S.K. Jones, J. Winter, and B.N. Gray. 2001. Targeting liver tumors with hyperthermia: ferromagnetic embolization in a rabbit liver tumor model. *Journal of surgical oncology* 78:22-29.

Mura, S., J. Nicolas, and P. Couvreur. 2013. Stimuli-responsive nanocarriers for drug delivery. *Nature materials* 12(11):991-1003.

Nair, B.G., Y. Nagaoka, H. Morimoto, Y. Yoshida, T. Maekawa, and D.S. Kumar. 2010. Aptamer conjugated magnetic nanoparticles as nanosurgeons. *Nanotechnology* 21:455102.

Nolte, A., S. Klussmann, R. Bald, V.A. Erdmann, and J.P. Furste. 1996. Mirror-design of L-oligonucleotide ligands binding to L-arginine. *Nature biotechnology* 14:1116-1119.

Ohno, T., T. Wakabayashi, A. Takemura, J. Yoshida, A. Ito, M. Shinkai, H. Honda, and T. Kobayashi. 2002. Effective solitary hyperthermia treatment of malignant glioma using stick type CMC-magnetite. In vivo study. *Journal of neuro-oncology* 56:233-239.

Pace, N.R., and S. Spiegelman. 1966. In vitro synthesis of an infectious mutant RNA with a normal RNA replicase. *Science* 153:64-67.

Paige, J.S., K.Y. Wu, and S.R. Jaffrey. 2011. RNA mimics of green fluorescent protein. *Science* 333:642-646.

Pankhurst, Q.A., J. Connolly, S. Jones, and J. Dobson. 2003. Applications of magnetic nanoparticles in biomedicine. *Journal of physics D: Applied physics* 36:R167.

Pastor, F., D. Kolonias, J.O. McNamara, and E. Gilboa. 2011. Targeting 4-1BB costimulation to disseminated tumor lesions with bi-specific oligonucleotide aptamers. *Molecular therapy* 19:1878-1886.

Petros, R.A., and J.M. DeSimone. 2010. Strategies in the design of nanoparticles for therapeutic applications. *Nature reviews drug discovery* 9:615-627.

Pinheiro, V.B., A.I. Taylor, C. Cozens, M. Abramov, M. Renders, S. Zhang, J.C. Chaput, J. Wengel, S.Y. Peak-Chew, S.H. McLaughlin, P. Herdewijn, and P. Holliger. 2012. Synthetic genetic polymers capable of heredity and evolution. *Science* 336:341-344.

Pirrung, M.C. 2002. How to Make a DNA Chip. *Angewandte chemie international edition* 41:1276-1289.

Pradhan, L., R. Srivastava, and D. Bahadur. 2014. pH- and thermosensitive thin lipid layer coated mesoporous magnetic nanoassemblies as a dual drug delivery system towards thermochemotherapy of cancer. *Acta biomaterialia* 10:2976-2987.

Pulfer, S.K., and J.M. Gallo. 1998. Enhanced brain tumor selectivity of cationic magnetic polysaccharide microspheres. *Journal of drug targeting* 6:215-227.

Rand, R.W., H.D. Snow, D.G. Elliott, and M. Snyder. 1981. Thermomagnetic surgery for cancer. *Applied biochemistry and biotechnology* 6:265-272.

Rosensweig, R.E. 2002. Heating magnetic fluid with alternating magnetic field. *Journal of magnetism and magnetic materials* 252:370-374.

Roulet, E., S. Busso, A.A. Camargo, A.J. Simpson, N. Mermod, and P. Bucher. 2002. High-throughput SELEX SAGE method for quantitative modeling of transcription-factor binding sites. *Nature biotechnology* 20:831-835.

Ruiz-Hernández, E., A. Baeza, and M. Vallet-Regí. 2011. Smart drug delivery through DNA/magnetic nanoparticle gates. *ACS Nano* 5:1259-1266.

Saito, G., J.A. Swanson, and K.D. Lee. 2003. Drug delivery strategy utilizing conjugation via reversible disulfide linkages: role and site of cellular reducing activities. *Advanced drug delivery reviews* 55:199-215.

Salehi-Ashtiani, K., and J.W. Szostak. 2001. In vitro evolution suggests multiple origins for the hammerhead ribozyme. *Nature* 414:82-84.

Sambrook, J., E.F. Fritsh, and T. Maniates. 1989. Molecular Cloning. A Laboratory Manual. *Cold Spring Harbor Laboratory Press*: Cold Spring Harbor New York.

Santiago, F.S., H.C. Lowe, M.M. Kavurma, C.N. Chesterman, A. Baker, D.G. Atkins, and L.M. Khachigian. 1999. New DNA enzyme targeting Egr-1 mRNA inhibits vascular smooth muscle proliferation and regrowth after injury. *Nature medicine* 5:1438.

Santoro, S.W., and G.F. Joyce. 1997. A general purpose RNA-cleaving DNA enzyme. *Proceedings of the national academy of sciences* 94:4262-4266.

Santoro, S.W., and G.F. Joyce. 1998. Mechanism and utility of an RNA-cleaving DNA enzyme. *Biochemistry* 37:13330-13342.

Schärtl, W. 2010. Current directions in core-shell nanoparticle design. *Nanoscale* 2:829-843.

Schlossbauer, A., S. Warncke, P.M.E. Gramlich, J. Kecht, A. Manetto, T. Carell, and T. Bein. 2010. A programmable DNA-based molecular valve for colloidal mesoporous silica. *Angewandte chemie international edition* 49:4734-4737.

Schmid, G. 2010. Nanoparticles: From theory to application. Second edition. *In Wiley-VCH Verlag* S293.

Seelig, B., S. Keiper, F. Stuhlmann, and A. Jäschke. 2000. Enantioselective ribozyme catalysis of a bimolecular cycloaddition reaction. *Angewandte chemie international edition* 39:4576-4579.

Sefah, K., D. Shangguan, X. Xiong, M.B. O'Donoghue, and W. Tan. 2010. Development of DNA aptamers using Cell-SELEX. *Nature potocols* 5:1169-1185.

Shangguan, D., Z. Cao, L. Meng, P. Mallikaratchy, K. Sefah, H. Wang, Y. Li, and W. Tan. 2008. Cell-specific aptamer probes for membrane protein elucidation in cancer cells. *Journal of proteome research* 7:2133-2139.

Shen, R.N., L. Lu, P. Young, H. Shidnia, N.B. Hornback, and H.E. Broxmeyer. 1994. Influence of elevated temperature on natural killer cell activity, lymphokine-activated killer cell activity and lectin-dependent cytotoxicity of human umbilical cord blood and adult blood cells. *International jurnal of radiation oncology·Biology·physics* 29:821-826.

Shinkai, M., M. Yanase, M. Suzuki, H. Honda, T. Wakabayashi, J. Yoshida, and T. Kobayashi. 1999. Intracellular hyperthermia for cancer using magnetite cationic liposomes. *Journal of magnetism and magnetic materials* 194:176-184.

Silverman, S.K. 2008. Nucleic acid enzymes (ribozymes and deoxyribozymes): In Vitro Selection and Application. Wiley encyclopedia of chemical biology, John Wiley & Sons, Inc.

Sinha, R., G.J. Kim, S. Nie, and D.M. Shin. 2006. Nanotechnology in cancer therapeutics: bioconjugated nanoparticles for drug delivery. *Molecular*

cancer therapeutics 5:1909-1917.

Smyth, D.G., O. Blumenfeld, and W. Konigsberg. 1964. Reactions of N-ethylmaleimide with peptides and amino acids. *Biochemical journal* 91:589.

Song, S., L. Wang, J. Li, C. Fan, and J. Zhao. 2008. Aptamer-based biosensors. *Trends in analytical chemistry* 27:108-117.

Sun, C., C. Fang, Z. Stephen, O. Veiseh, S. Hansen, D. Lee, R.G. Ellenbogen, J. Olson, and M. Zhang. 2008. Tumor-targeted drug delivery and MRI contrast enhancement by chlorotoxin-conjugated iron oxide nanoparticles. *Nanomedicine* 3(4):495-505.

Tanaka, K., A. Ito, T. Kobayashi, T. Kawamura, S. Shimada, K. Matsumoto, T. Saida, and H. Honda. 2005. Intratumoral injection of immature dendritic cells enhances antitumor effect of hyperthermia using magnetic nanoparticles. *International journal of cancer* 116:624-633.

Tang, J., and R.R. Breaker. 1997. Examination of the catalytic fitness of the hammerhead ribozyme by in vitro selection. *RNA* 3:914-925.

Tang, J., and R.R. Breaker. 2000. Structural diversity of self-cleaving ribozymes. *Proceedings of the national academy of sciences* 97:5784-5789.

Tang, Z., P. Parekh, P. Turner, R.W. Moyer, and W. Tan. 2009. Generating aptamers for recognition of virus-infected cells. *Clinical chemistry* 55:813-822.

Thiesen, B., and A. Jordan. 2008. Clinical applications of magnetic nanoparticles for hyperthermia. *International journal of hyperthermia* 24:467-474.

Timko, B.P., T. Dvir, and D.S. Kohane. 2010. Remotely triggerable drug delivery systems. *Advanced materials* 22:4925-4943.

Torchilin, V. 2011. Tumor delivery of macromolecular drugs based on the EPR effect. *Advanced drug delivery reviews* 63:131-135.

Tuerk, C., and L. Gold. 1990. Systematic evolution of ligands by exponential enrichment: RNA ligands to bacteriophage T4 DNA polymerase. *Science* 249:505-510.

Uhlenbeck, O.C. 2003. Less isn't always more. *RNA* 9:1415-1417.

van der Zee, J. 2002. Heating the patient: a promising approach? *Annals of oncology* 13:1173-1184.

Veiseh, O., J.W. Gunn, and M. Zhang. 2010. Design and fabrication of magnetic nanoparticles for targeted drug delivery and imaging. *Advanced drug delivery reviews* 62:284-304.

Vinogradov, S.V., T.K. Bronich, and A.V. Kabanov. 2002. Nanosized cationic hydrogels for drug delivery: preparation, properties and interactions with cells. *Advanced drug delivery reviews* 54:135-147.

Wahajuddin, S.A. 2012. Superparamagnetic iron oxide nanoparticles: magnetic nanoplatforms as drug carriers. *International journal of nanomedicine* 7:3445.

Wang, X., H. Gu, and Z. Yang. 2005. The heating effect of magnetic fluids in an alternating magnetic field. *Journal of magnetism and magnetic materials* 293:334-340.

Wendtner, C., S. Abdel-Rahman, J. Baumert, M.H. Falk, M. Krych, M. Santl, W. Hiddemann, and R.D. Issels. 2001. Treatment of primary, recurrent or inadequately resected high-risk soft-tissue sarcomas (STS) of adults: results of a phase II pilot study (RHT-95) of neoadjuvant chemotherapy combined with regional hyperthermia. *European journal of cancer* 37:1609-1616.

Widder, K.J., R.M. Morris, G. Poore, D.P. Howard, and A.E. Senyei. 1981. Tumor remission in Yoshida sarcoma-bearing rts by selective targeting of magnetic albumin microspheres containing doxorubicin. *Proceedings of the national academy of sciences* 78:579-581.

Xiang, G., M.D. Schuster, T. Seki, A.A. Kocher, S. Eshghi, A. Boyle, and S. Itescu. 2004. Down-regulation of plasminogen activator inhibitor 1 expression promotes myocardial neovascularization by bone marrow progenitors. *The journal of experimental medicine* 200:1657-1666.

Yanase, M., M. Shinkai, H. Honda, T. Wakabayashi, J. Yoshida, and T. Kobayashi. 1998. Antitumor immunity induction by intracellular hyperthermia using magnetite cationic liposomes. *Cancer science* 89:775-782.

Yu, Z., N. Li, P. Zheng, W. Pan, and B. Tang. 2014. Temperature-responsive DNA-gated nanocarriers for intracellular controlled release. *Chemical communications* 50:3494-3497.

Yuanpei, L., P. Shirong, Z. Wei, and D. Zhuo. 2009. Novel thermo-sensitive core-shell nanoparticles for targeted paclitaxel delivery. *Nanotechnology* 20:065104.

Zahn, M. 2001. Magnetic fluid and nanoparticle applications to nanotechnology. *Journal of nanoparticle research* 3:73-78.

Zhang, L., W.J. Gasper, S.A. Stass, O.B. Ioffe, M.A. Davis, and A.J. Mixson. 2002b. Angiogenic inhibition mediated by a DNAzyme that targets vascular endothelial growth factor receptor 2. *Cancer research* 62:5463-5469.

Zhang, Y., N. Kohler, and M. Zhang. 2002a. Surface modification of superparamagnetic magnetite nanoparticles and their intracellular uptake. *Biomaterials* 23:1553-1561.

Zhou, J., and J.J. Rossi. 2011. Cell-specific aptamer-mediated targeted drug delivery. *Oligonucleotides* 21:1-10.

9 Appendix

9.1 Materials

9.1.1 Chemicals

[Alpha-^{32}P]GTP	Hartmann Analytic
[Gamma-^{32}P]ATP	Hartmann Analytic
Acetic acid	Rothe, Germany
Agarose	Rothe, Germany
APS	Rothe, Germany
Bromophenol blue	Serva, Heidelberg
DEPC	Sigma-Adrich, Germany
DNA ladder (20-bp)	Rothe, Germany
EDTA disodium salt dehydrate	Biomol, Germany
Ethanol	Rothe, Germany
Ethidium bromide	Fluka, France
Formamide	Promega, USA
Gelatin solution	Sigma-Adrich, Germany
HEPES	Rothe, Germany
Hydrochloric acid	Sigma-Adrich, Germany
L-Glutathione reduced	Rothe, Germany
Magnesium chloride	Sigma Aldrich, Germany
NTP set, 100 mM solutions	Fermentas, Germany
RiboLock™ Rnase inhibitor	Fermentas, Germany
Roti®-Chloroform/Isoamylalkohol (24:1)	Rothe, Germany
Roti®-Load DNA (with glycerol)	Rothe, Germany
Roti®-Mix PCR 3 (pH 7)	Rothe, Germany
Roti®-Phenol	Rothe, Germany
Rotilabo® PCR reaction tubes, 0.2 ml	Rothe, Germany
Rotiphorese® Gel 40 (19:1)	Rothe, Germany
Human serum	Sigma-Aldrich, Germany
Sodium acetate	Riedel de Häen, Germany
Sodium chloride	Rothe, Germany
Sodium hydroxide	Rothe, Germany
Standard buffer solution, pH 10.0	Sigma-Adrich, Germany
Standard buffer solution, pH 4.0	Sigma-Adrich, Germany
Standard buffer solution, pH 7.0	Sigma-Adrich, Germany
StrataClean™ Resin	Agilent Technologies, USA
Sulfo-SMCC	Sigma-Adrich, Germany
TAE buffer, 10 x	Rothe, Germany
TBE buffer, 10 x	Rothe, Germany

TCEP	Sigma-Adrich, Germany
TEMED	Rothe, Germany
Tris	Rothe, Germany
Tris hydrochloride	Rothe, Germany
Urea	Rothe, Germany
Xylencyanol	Rothe, Germany

9.1.2 Nucleic Acids

All oligonucleotides used in this work were purchased from IBA GmbH (Göttingen, Germany).

9.1.3 Enzymes

BanI, recombinant	New England Biolabs
Dnase I, Rnase-free	Fermentas, Germany
StyI-HF™	New England Biolabs
SuperScript™ III Reverse Transcriptase	Invitrogen, USA
T4 DNA ligase	New England Biolabs
T4 Polynucleotide Kinase	New England Biolabs
T7 RNA Polymerase	Fermentas, Germany
Taq DNA Polymerase	New England Biolabs

9.1.4 Buffers

Dulbecco's Phosphate-Buffered Saline (1 x DPBS) pH 6.7
137.9 mM NaCl
8.06 mM $Na_2HPO_4 \cdot 7H_2O$
2.67 mM KCl
1.47 mM KH_2PO_4

Phosphate-Buffered Saline (1 x PBS), pH 7.2
155.17 mM NaCl
2.71 mM $Na_2HPO_4 \cdot 7H_2O$
1.54 mM KH_2PO_4

Phosphate-Buffered Saline (1 x PBS), pH 7.4
155.17 mM NaCl
2.97 mM $Na_2HPO_4 \cdot 7H_2O$
1.06 mM KH_2PO_4

TAE Buffer (10 x)
400 mM Tris-Acetat (pH 8.0 at 25°C)
10 mM EDTA

TBE Buffer (10 x)
900 mM Tris–borate (pH 8.0 at 25°C)
20 mM EDTA

TE Buffer
10 mM Tris-HCl (pH 8.0 at 25°C)
1 mM EDTA

ThermoPol® Reaction Buffer
20 mM Tris-HCl (pH 8.8 at 25°C)
10 mM $(NH_4)_2SO_4$
10 mM KCl
2 mM $MgSO_4$
0.1% Triton® X-100

T4 Polynucleotide Kinase Reaction Buffer (10 x)
500 mM imidayole-HCl (pH 6.6 at 25°C)
100 mM $MgCl_2$
50 mM DTT
1 mM spermidine
1 mM EDTA

Loading Buffer for Agarose and Native Polyacrylamide Gel (6 x)
60 mM Tris-HCl (pH 7.5 at 25°C)
30 mM Na-acetate
12 mM EDTA
60% (w/v) Glycerol
0.18% (w/v) Bromphenol blue
0.12% (w/v) Xylene cyanol blue

Urea PAGE Loading Buffer (2 x)
2 x TBE
16 M Urea
0.04% (w/v) Bromphenolblue
0.04% (w/v) Xylencyanol

Reaction Buffer (release experiments of DNAzyme-based release system)
50 mM Tris-HCl (pH 7.5 at 25°C)
10 mM $MgCl_2$

In vitro Selection Buffer
50 mM HEPES (pH 7.5 at 25°C)
150 mM NaCl
2 – 10 mM $MgCl_2$
1 U/µl RiboLock™ Rnase inhibitor

9.1.5 Devices and Consumption Materials

Agarose gel chamber	Bio-Rad, USA
Amicon Ultra 30K centrifugal filter	Millipore, USA
Amicon Ultra 3K centrifugal filter	Millipore, USA
Autoclave 500-D	Sterico, AG, Switzerland
Biofuge Fresco refrigerating centrifuge	Heraeus, Germany
Clean bench	Heraeus, Germany
Contamination monitors	BERTHOLD, Germany
DNA LoBind tubes, 1.5 ml	Eppendorf, Germany
Electrophoresis constant power supply 3000/150	Pharmacia Fine Chemicals
Film processor CAWOMAT 2000R	Cawo, Germany
Fluor-coated TLC plate	Merk, Germany
Freezer -20ºC	Bosch, Germany
Freezer 4ºC	Bosch, Germany
Freezer -80ºC	Heraeus, Germany
Fuji X-ray films RX	KISKER Biotech GmbH
Gel Dol 2000	Bio-Rad, USA
Transilluminator UV reprostar	CAMAG, Switzerland
Gel electrophoresis system	Renner GmBH, Germany
Gloves	neoLab, Germany
Heracell CO_2 incubator	Thermo Scientific, USA
Horizontal electrophoresis systems	Bio-Rad, USA
Human serum	Sigma, Germany
Hypercassette film cassette	Amersham Pharmacia Biotech
Ice machine	Scotsman, USA
Kimwipes	Kimberly-Clark, UK
Laboratory balances	Sartorius, Germany
MµltiLowBinding® MµltiGuard® 1 – 20 µl	Rothe, Germany
MµltiLowBinding® MµltiGuard® 1 – 300 µl	Rothe, Germany
MµltiLowBinding®-MicroGuard® 0.1–10 µl	Rothe, Germany
Magnetic particle separator	Roche, Germany

Magnetic stirrer	IKA-Combimag RCT, Germany
Microprocessor pH meter 761	Helmut Singer Elektronik
Microwave	Daewoo Electronics, France
Milli-Q laboratory water systems	Millipore, USA
NanoDrop™ 3300 fluorospectrometer	PEQLAB, Germany
NucleoSpin® Gel and PCR Clean-up	Macherey-Nagel, Germany
NucleoSpin® Plasmid QuickPure	Macherey-Nagel, Germany
Parafilm® M	American National Can, USA
PCR apparatus	Biometra, Germany
PCR-micro-centrifuge tubes	Rothe, Germany
pGEM-T easy vector system II	Promega, USA
Phosphor screen	Molecular Dynamics, USA
Phosphorimager exposure cassette	Molecular Dynamics, USA
Phosphorimager storm 840	Molecular Dynamics, USA
Pipettes	Gilson, France
Polyacrylamide gel champer	Renner GmbH, Germany
PowerPAC 200	Bio-Rad, USA
PTC-100™ programmable thermal controller	MJ Research Inc., USA
SpeedVac SC110	Savant, USA
Syringe filter, 0.22 µm	Rothe, Germany
Table-top centrifuge	Eppendorf, Germany
Thermomixer comfort	Eppendorf, Germany
Tube rotator	VWR, Germany
Typhoon FLA 7000 multi-purpose laser scanner	GE Healthcare, Sweden
Ultrasonic bath	VWR, Germany
Ultrasonic Cleaner	BANDELIN electronic GmbH
UV-VIS sspectrophotometers	Shimadzu, USA
VARIOKLAV® steam sterilizers	Thermo Scientific, USA
Vortex-Genie 2	Scientific Industries, USA
Water bath	GFL, Germany

9.2 Abbreviations

A	absorbance
°C	degree Celsius
A.D.	Anno Domini
A_{xxx}	absorbance at xxx nm wavelength
AMF	alternating magnetic field
APS	ammonium persulfate
ATP	adenosine 5’-triphosphate
B	base
B.C.	before Christ
bp	base pairs
c	concentration
ca.	circa
cDNA	complementary DNA
Ci	curie
CPG	controlled pore glass
CT	computed tomography
Da	dalton
DEPC	diethylpyrocarbonate
DMT	4,4’-dimethoxytrityl
DNA	deoxyribonucleic acid
dNTP	deoxyribonucleotide triphosphate
DPBS	Dulbecco’s phosphate-buffered saline
ds	double-stranded
e.g.	*exempli gratia* (“for example”)
EDTA	ethylenediaminetetraacetic acid
Egr1	early growth response factors 1
EPR	enhanced permeability and retention
et al.	*et alia* (“and others”)
EtBr	ethidium bromide
f	frequency
Fig.	figure
g	gram
G	guanosine
GBM	glioblastoma multiforme
GFP	green fluorescent protein
GSH	L-Glutathione
h	hour(s)
H	amplitude
HEPES	4-(2-hydroxyethyl)-1-piperazineethanesulfonic acid
i.e.	*id est* (“it is”)
kA/m	kiloampere/meter
k_{cat}	turnover number

K_M	Michaelis constant
l	liter
M	mol/L, molar
MFH	magnetic fluid hyperthermia
Hz	hertz(s)
min	minute(s)
mM	micromolar
mol	mole(s)
mPer1	mouse period1
mRNA	messenger ribonucleic acid
NBA	nitrobenzaldehyde
NHS	*N*-hydroxysuccinimid
NK-cells	natural killer cells
nM	nanomolar
nm	nanometer(s)
nmol	nanomole
NP	nanoparticle
nt	nucleotide(s)
NTP	nucleotide triphosphate
PAA	polyacrylamide
PAGE	polyacrylamide gel electrophoresis
PAI1	plasminogen activator inhibitor 1
PBS	phosphate buffered saline
PCR	polymerase chain reaction
R^2	coefficient of determination
RFU	relative fluorescence unit
RNA	ribonucleic acid
rpm	rotations per minute
RT	room temperature or reverse transcription
RT-PCR	reverse transcription polymerase chain reaction
s	second(s)
SAR	specific absorption rate
SELEX	systematic enrichment of ligands by exponential enrichment
SMCC	succinimidyl 4-(*N*-maleimidomethyl)cyclohexane-1-carboxylate
ss	single-stranded
sulfo-SMCC	sulfosuccinimidyl-4-(*N*-maleimidomethyl)cyclohexane-1-carboxylate
t	time
Tab.	table
TAE	Tris-acetic acid-EDTA
TBE	Tris-borate-EDTA
TCA	trichloroacetic acid
TCEP	Tris(2-carboxyethyl)phosphine

TEMED	*N*,*N*,*N'*,*N'*-Tetramethylethan-1,2-diamin
Tgf-β1	transforming growth factor beta 1
TLC	thin layer chromatography
Tm	melting temperatures
Tnf-α	Tumor necrosis factor alpha
Tris	tris(hydroxymethyl)-aminomethan
U	unit(s)
UV	ultraviolet
V	volt(s)
v/v	volume per volume
VEGFR2	vascular endothelial growth factor receptor 2
w/v	weight per volume
x g	times gravity (relative centrifugal force)
XNAs	xeno-nucleic acids
ε	extinction coefficient
µl	micro liter
µM	micro molar
τ_B	Brownian relaxation time
τ_N	Néel relaxation time

Prefixes of units:

p (pico)	10^{-12}
n (nano)	10^{-9}
µ (micro)	10^{-6}
m (milli)	10^{-3}
k (kilo)	10^{3}
M (mega)	10^{6}

9.3 Curriculum Vitae

For reason of data protection, the curriculum vitae is not included in the online version.

9.4 Publication

Manuscript in preparation:

Yan, F.S., J. Gao, A. Jordan and J.P. Fürste. 2015. Design of a thermally controlled drug release system based on a catalytic DNA.

9.5 Acknowledgements

I would like to extend my sincere gratitude to Dr. Jens Peter Fürste for giving me the opportunity to perform my research under his supervision and being open for scientific discussion as well as his valuable advices. I am also indebted to Prof. Dr. Petra Knaus for being my second supervisor and for reviewing this thesis.

I own my sincere gratitude to Dr. Jiang Gao for many scientific discussions and advices. This work would not have been possible without her help introducing me into this cooperative project with MagForce Nanotechnology AG (Germany). My thanks go to MagForce Nanotechnology AG (Germany) for funding this project and for preparing the magnetic nanoparticles.

I am very grateful to Prof. Dr. Volker A. Erdmann for offering me the chance to pursue my Ph.D. degree in Germany at the first place. I also thank the China Scholarship Council for supporting my study in Free University.

Special thanks go to Dr. Werner Schröder for instructing me on DNA chemical synthesis. My special thanks also go to Dr. Christoph Weise and Dr. Murat Eravci for their valuable advices on my defense presentation. My sincere thanks should also be given to Manuela Gibson, Claudia Gallin, Andrea Senge, Gerhard Buchlow and Frank Kuppler for their support during my study here in berlin.

I own my deepest gratitude to my family and my girlfriend for their love, encouragement and support throughout my study in Germany.

9.6 Statement of Authorship

Hiermit erkläre ich, dass ich die vorliegende Arbeit selbstständig und ohne fremde Hilfe angefertigt und keine anderen als die angegebenen Hilfsmittel und Quellen verwendet habe. Außerdem versichere ich, dass ich diese Arbeit oder Teile davon in gleicher oder ähnlicher Form noch nicht als Prüfungsarbeit für eine staatliche oder andere wissenschaftlische Prüfung eingereicht habe.

Berlin, 13. August 2015 Fusheng Yan